Y3.At7:
36/14-3

Reactor Technology

1971
Quarterly
Technical
Progress
Review
Volume 14-3

A publication of the
Division of Technical Information
U.S. Atomic Energy Commission
Prepared in Cooperation
with
The American Nuclear Society

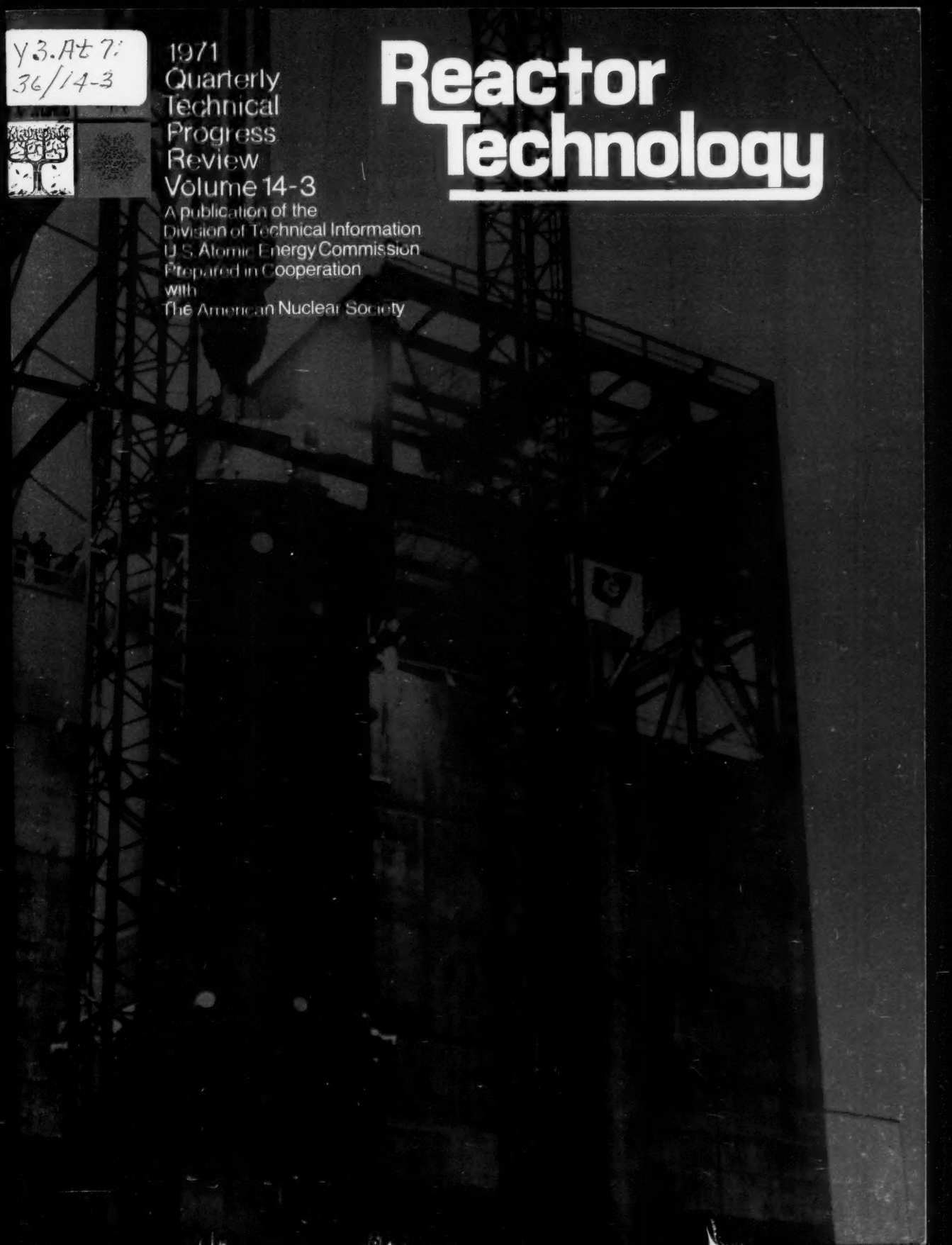

TECHNICAL PROGRESS REVIEWS

The United States Atomic Energy Commission publishes the Technical Progress Reviews to meet the needs of industry and government for concise summaries of current nuclear developments. Each journal digests and evaluates the latest findings in a specific area of nuclear technology and science. *Nuclear Safety* is a bimonthly journal; the other two are quarterly journals.

Isotopes and Radiation Technology
P. S. Baker, A. F. Rupp, and associates
Isotopes Information Center, Oak Ridge National Laboratory

Nuclear Safety
Wm. B. Cottrell, W. H. Jordan, J. P. Blakely, and associates
Nuclear Safety Information Center, Oak Ridge National Laboratory

Reactor Technology
Prepared in cooperation with the American Nuclear Society

All are available from the U. S. Government Printing Office. See the back cover for ordering instructions.

NOTICE

This journal was prepared under the sponsorship of the U. S. Atomic Energy Commission. Neither the United States nor the U. S. Atomic Energy Commission, or any of their employees, contractors, subcontractors, or their employees, makes any warranty, express or implied, or assumes any legal liability or responsibility for the accuracy, completeness, or usefulness of any information, apparatus, product, or process disclosed, or represents that its use would not infringe privately owned rights.

Availability of Reports Cited in This Review

United States Atomic Energy Commission (USAEC) reports are available at certain libraries that maintain collections of these reports. The libraries are listed on the inside front cover of each issue of *Nuclear Science Abstracts.* USAEC reports are also sold by the following governmental and international organizations: (1) National Technical Information Service (NTIS), U. S. Department of Commerce, Springfield, Va. 22151; (2) International Atomic Energy Agency (IAEA), Vienna, Austria; and (3) National Lending Library, Boston Spa, England.

Other U. S. Government agency reports identified in this journal are generally available from NTIS.

Reports from other countries are generally available at the same U. S. libraries as maintain collections of USAEC reports, and from IAEA and the originating country. **United Kingdom Atomic Energy Authority (UKAEA)** reports are sold by Her Majesty's Stationery Office, London. **Atomic Energy of Canada Limited (AECL)** reports are sold by the Scientific Document Distribution Office, Atomic Energy of Canada Limited, Chalk River, Ontario, Canada. UKAEA and AECL reports issued after March 1, 1967, are sold by NTIS to purchasers in the United States and its territories. IAEA publications are sold in the United States by UNIPUB, P. O. Box 433, New York, N. Y. 10016.

Private-organization reports should be requested from the originator.

The views expressed in this publication do not necessarily represent those of the United States Atomic Energy Commission, its divisions or offices, or of any Commission advisory committee or contractor.

Y3.At 7:
36/14-3

REACTOR TECHNOLOGY

Vol. 14, No. 3 Fall 1971

Contents

ILLINOIS STATE LIBRARY
NOV 12 1971
U. S. Supt. of Documents Deposit

COVER: Reactor vessel being installed at the Dresden 2 reactor near Morris, Ill. Commonwealth Edison Company photograph.

Superintendent of Documents, U. S. Government Printing Office, Washington, D. C. 20402, $3.00 per year.

REACTOR TECHNOLOGY

is a quarterly review of progress and developments in the reactor field including the following subject areas:

Economics	Fuel Cycles
Physics	Fluid and Thermal Technology
Mechanics	Fuel Processing
Construction	Components
Fuel Elements	Operating Performance

Prepared for reactor physicists, reactor operators, designers, fuel-cycle specialists, administrators, and others interested in the field, this journal reviews, summarizes, critically evaluates and interprets the state of the art as reflected in the current literature.

The many reports and publications referenced merit further study, and readers are urged to consult them for additional details.

Qualified authors are invited to contribute review articles for consideration for publication.

U. S. Atomic Energy Commission
Division of Technical Information
Washington, D. C. 20545

Issued quarterly by the U. S. Atomic Energy Commission. Use of funds for printing this publication approved by the Director of the Bureau of the Budget on May 12, 1969.

Minimizing Swelling and Embrittlement of Fast-Reactor Fuel Claddings

By Mihkel Kangilaski*

Abstract: *Liquid-metal-cooled fast breeder reactors (LMFBRs) are expected to produce most of the nuclear power in the near future. However, experimental results have indicated that stainless steel will undergo both swelling and embrittlement in the nuclear environment that is expected in LMFBRs. Implications of this swelling and embrittlement to the reactor design are discussed in this article. Also, the numerous variables that affect the two phenomena are considered, along with approaches to alleviate or at least minimize them.*

The economic production of electricity by nuclear means has been set as one of the nation's priorities. It is planned to achieve this goal through the use of liquid-metal-cooled fast breeder reactors (LMFBRs). These reactors will convert the ^{238}U to fissionable plutonium and thus utilize a large fraction of the uranium, rather than only the ^{235}U as the present-generation water-cooled reactors do. Present LMFBR designs call for UO_2–PuO_2 fuel, with the cladding and the main structural material being austenitic stainless steel.

Research on austenitic stainless steels has indicated that the expected nuclear environment in LMFBRs will produce serious property changes in the material. Among the most troublesome of these property changes are radiation-induced swelling of the stainless steel and drastic losses in ductility at temperatures of 600°C or above.

RADIATION-INDUCED SWELLING

The swelling of stainless steel due to irradiation at elevated temperatures was first reported by Fulton and Cawthorne.[1] This swelling occurred in the cladding of the Dounreay Fast Reactor fuel pins. These fuel pins were irradiated to a fast fluence of 4 to 7.8 x 10^{22} neutrons/cm^2 at temperatures ranging from 270 to 560°C, with a maximum observed density decrease of 7.0%. Since that time, considerable interest has been shown in this phenomenon, and many studies have been made to measure and gain an understanding of the swelling mechanism.

Radiation-induced swelling has been found in nickel,[2] nickel-base alloys,[2,3] aluminum,[4] molybdenum,[5] and vanadium,[6] as well as stainless steel. Since these materials have been the only ones which have received significant study under reactor conditions, it seems reasonable to suppose that radiation-induced swelling will be found in other materials when they are exposed to the environment expected in a fast reactor.

Radiation-induced swelling in metals is generally measured by observing thin foils of irradiated materials by transmission electron microscopy (TEM). From these observations the density and number of voids are determined. By knowing the thickness of the foil, one can calculate the total void volume of the material. A drawback to this method of measurement is the assumption that the small area that is viewed by TEM is representative of the entire sample. Also, the thicknesses of foils are not accurately known, and the void-size distribution has been shown to depend on foil thickness.[7] However, immersion results of density measurements on small pieces of irradiated material have shown remarkable agreement with density changes obtained by TEM measurements.

Attempts have also been made to determine the void size and distribution by small-angle scattering (SAS) techniques. This method has produced results in

*Deformation and Fracture Research Division, Battelle Memorial Institute, Columbus Laboratories, 505 King Avenue, Columbus, Ohio 43201.

relatively good agreement with results of density determinations by TEM.[8] The SAS technique has the advantage of averaging over a large number of voids ($\sim 10^{11}$), compared with the few hundred that are used in the TEM technique. There may, however, be unknown components of radiation damage which contribute to the scattering observed.

Implications

Any change in the dimensions of reactor components occurring during operation can be expected to complicate design. In some cases it may be possible to compensate for such changes in dimensions. However, the expected dimensional changes have to be anticipated. Since radiation-induced swelling has been found to be sensitive to many variables, the extent of swelling will not be uniform throughout the core. The greatest anticipated problem is the nonuniform swelling of fuel pins and ducts. This nonuniform swelling, if not accommodated in design, may cause bowing and twisting and eventual contact between adjacent pins or subassemblies.

Variables Affecting Swelling

Experimental results have shown that a number of interdependent variables determine the amount of swelling in irradiated austenitic stainless steel.

Instantaneous Flux. For any swelling to occur, the material must have a supersaturation of vacancies; this condition can occur only if many vacancies and interstitials are being continuously produced. Therefore a minimum flux would be required for swelling. As the instantaneous flux increases, the supersaturation of vacancies increases, and consequently the swelling rate would be expected to increase. The effect of instantaneous flux becomes more important at higher temperatures. Harkness[9] has predicted that, by increasing the instantaneous flux from 2×10^{14} neutrons/cm^2 to 2×10^{15} neutrons/cm^2 at 400°C, an equivalent fluence would double the amount of swelling. However, at 600°C a similar increase in the instantaneous flux would increase the swelling rate about 100-fold. Few experimental data are presently available on the influence of instantaneous flux on radiation-induced swelling.

Irradiation Temperature. It has been shown that at a critical temperature, the growth of voids and hence swelling is maximum. At low irradiation temperatures the recombination of vacancies and interstitials is sufficiently high to lower the void growth, whereas at high temperatures the equilibrium vacancy concentration is high enough to prevent a supersaturation of vacancies. The irradiation temperature also governs the size of voids and their density. As the irradiation temperature increases, the size of the average void increases, but the void density decreases. The maximum radiation-induced swelling in stainless steel occurs[9] at about 500°C, as illustrated in Fig. 1.

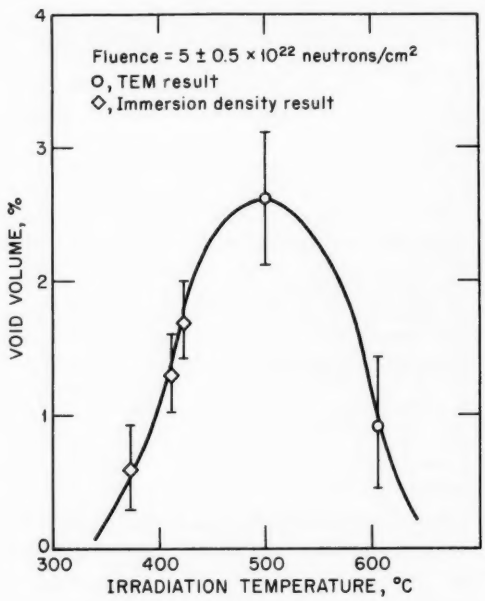

Fig. 1 Effect of irradiation temperature on swelling of 304 stainless steel.

Fluence. The radiation-induced density reduction appears to increase[10] linearly with fluence, as shown in Fig. 2. Since there is usually considerable uncertainty about the irradiation temperatures and flux levels, it is not possible to ascertain the exact dependence of swelling on total fluence.

Cold Work. Cold-worked material swells less than annealed material,[3] as illustrated in Fig. 3. The smaller density decreases in the cold-worked material are attributed to high dislocation densities. A high dislocation density is believed to annihilate the vacancies and thus prevent their supersaturation and coalescence.[11] However, it has been suggested that, once the dislocations have been removed by annihilation with vacancies, the swelling rate of cold-worked material will exceed that of annealed material. This tendency is

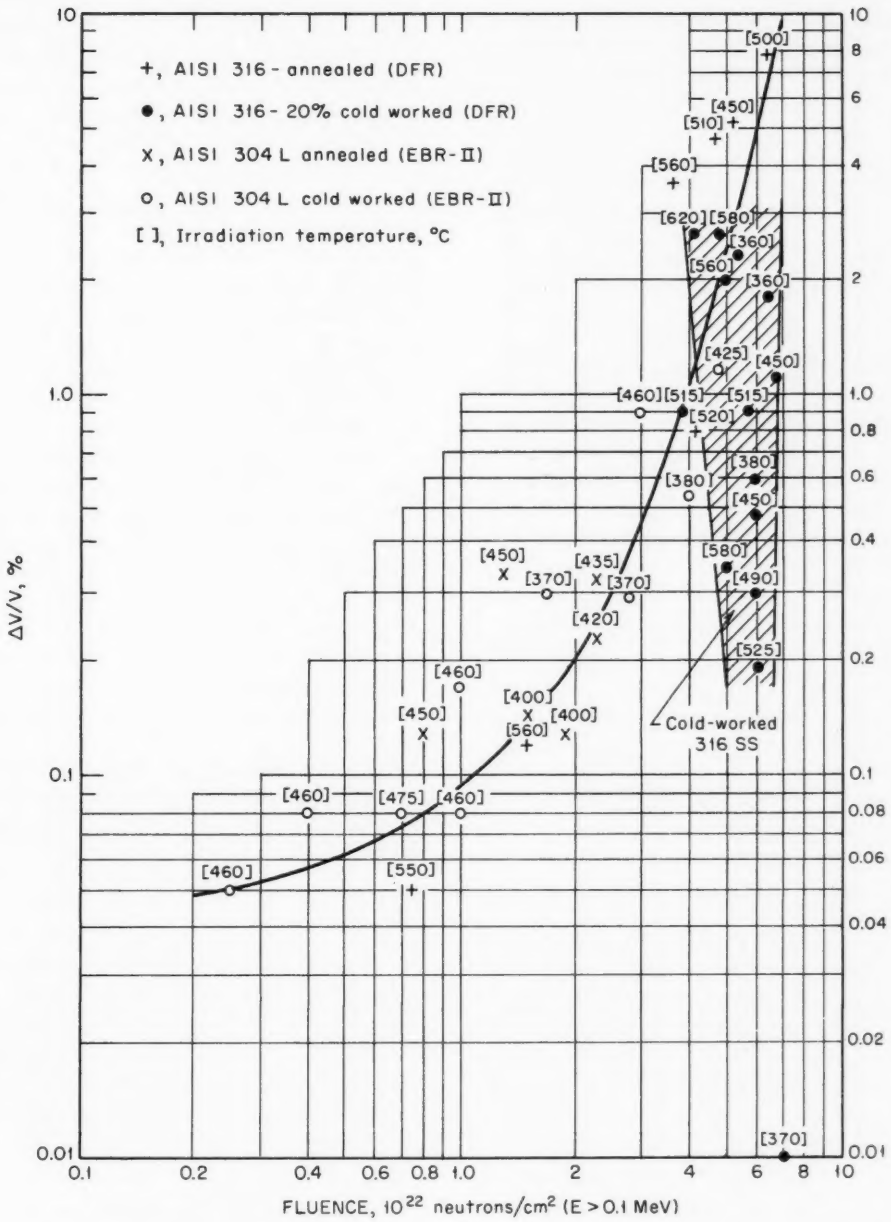

Fig. 2 Effect of fluence on swelling of austenitic stainless steel.[10]

attributed to the formation of larger voids if the dislocation density is high.[12]

Figure 3 also illustrates that the restraint of swelling due to cold work is less at higher irradiation temperatures. This is expected since the dislocations are being annealed out by the high irradiation temperature.

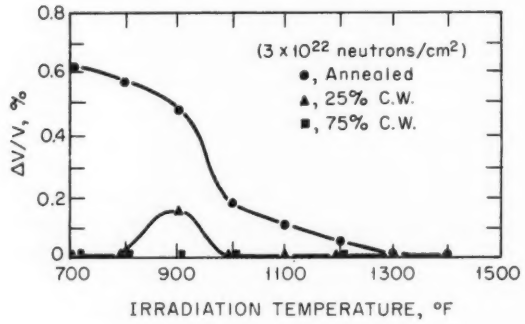

Fig. 3 Effect of cold work and irradiation temperature on swelling of austenitic stainless steel.[3]

Metal Purity. Impurity content has[3] a significant effect on the swelling rate of nickel, as shown in Fig. 4. Nickel 270, with an impurity content of 200 ppM, swells significantly; Nickel 200, with an impurity content of 1600 ppM, swells considerably less; and Inconel 600, a Ni–Fe–Cr alloy, does not swell under these conditions of flux and temperature.

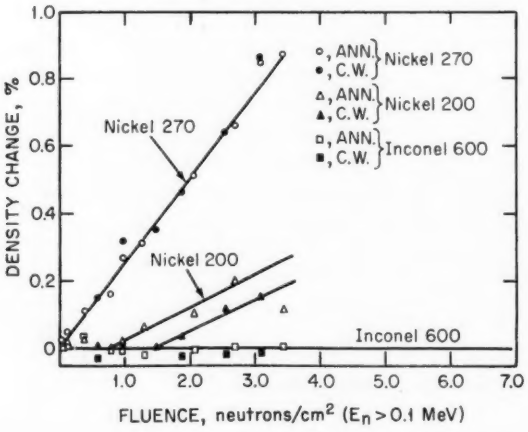

Fig. 4 Effect of purity on radiation-induced swelling in nickel.[3] (Irradiation temperature, 480°C.)

Mechanisms of Swelling

All the theories that attempt to explain the radiation-induced swelling in metals have the same physical principles.[9,12-15] The processes that best seem to describe the phenomenon are the nucleation and growth theories. Differences among the various models result from varying assumptions regarding the nucleation processes and different boundary conditions in the growth processes.

High-energy neutrons create vacancies and interstitials when they knock atoms out of their equilibrium lattice sites. These vacancies and interstitials can annihilate each other when they come into contact. Also, when vacancies or interstitials coalesce, they can form defect clusters. Thermodynamic conditions make it favorable for the supersaturated vacancies to coalesce into three-dimensional voids. The excess interstitials are favored to form interstitial dislocation loops.

Harkness[9] has suggested that the nucleation of voids occurs homogeneously, but other investigators have proposed that nucleation takes place heterogeneously at dislocations.[16] All investigators agree that helium, which is created by (n,α) reactions in metals, tends to stabilize the void and promote its growth. Experimental data have shown that stainless steel impregnated with helium by cyclotron bombardment tended to swell more during irradiation than did stainless steel that had not been injected with helium.[17]

Figure 5 illustrates the rather good agreement that is obtained between experimental and predicted swelling data using the model developed by Harkness and Li.[9]

Minimizing Swelling

Because of the large volume changes caused by radiation-induced swelling of metals, it is important that this phenomenon be minimized to facilitate the development of LMFBRs. Consequently experimental work is under way at various laboratories to develop materials which will be resistant to radiation-induced swelling and which will still be acceptable as cladding and structural materials in LMFBRs.

Fine Grain Size. Transmission electron microscopy of irradiated stainless steel has shown a lack of voids near grain boundaries.[2] The absence of voids is predicted by theory because high-angle boundaries act as good sinks for vacancies, but low-angle boundaries do not. Planetary swaging of stainless steel[18] was found to produce a structure with an average grain size

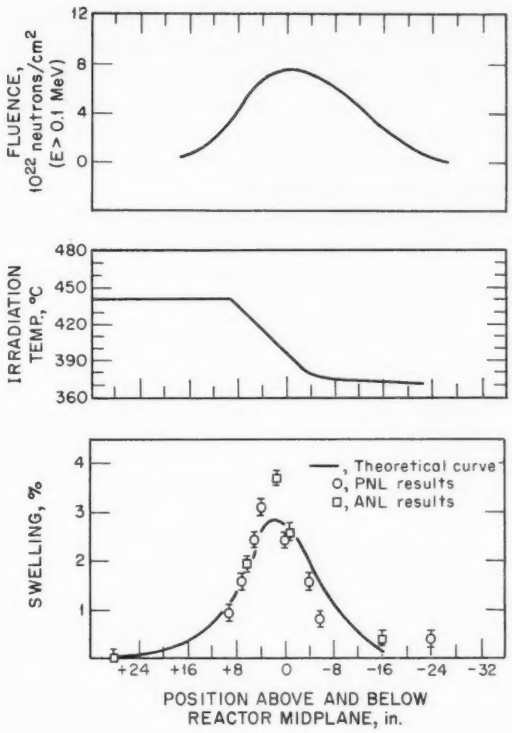

Fig. 5 A comparison of the predicted and experimental swelling profiles of an axial guide thimble irradiated[9] to a peak fluence of 5 x 10^{22} in the EBR-II.

of less than 0.002 mm. One would predict that radiation-induced swelling in such a material would be less because the large number of high-angle grain boundaries would act as sinks for the vacancies produced by radiation.

High Defect Structure. As mentioned previously, cold work induces swelling because of the interaction between dislocations and vacancies. A shock wave passing through stainless steel will also produce a large number of dislocations and mechanical twins; the defect structure is dependent on both shocking pressure and temperature.[19] Annealing studies on the shocked material indicate that the defect structure is stable to higher annealing temperatures than is the defect structure resulting from cold work. It is therefore theorized that this higher and more stable defect structure would result in less radiation-induced swelling than is experienced with cold-worked stainless steel.

Thermomechanical Treatments. A microstructure that contains stacking faults stabilized by carbide particles can be obtained with various sequences of cold work, aging, and hot working.[20] This material is expected to provide resistance to radiation-induced swelling because of the vacancy sinks in the complex defect structure. Also, these defects have shown high stability at elevated temperatures.

RADIATION-INDUCED ELEVATED-TEMPERATURE EMBRITTLEMENT

The fact that fast-neutron exposure changes mechanical properties of metals has been known for some time and has been referred to as a displacement type of radiation damage.[21] The displacement type of radiation damage occurs when energetic fast neutrons displace atoms from their equilibrium lattice sites; such displacement of atoms causes vacancies and interstitials. These vacancies and interstitials can annihilate each other if they come into contact. However, if vacancies or interstitials coalesce, they form vacancy and interstitial clusters. These clusters impede dislocation movement in metals and cause increases in strength and reductions in ductility. This displacement type of radiation damage can be removed by annealing the irradiated metal at a high enough temperature to annihilate the defect clusters. Removal of the defect clusters results in mechanical properties that are identical to the mechanical properties of the unirradiated material.

In 1963, Hughes and Caley[22] reported a new type of radiation damage which has generally been called radiation-induced elevated-temperature embrittlement or helium embrittlement. The radiation-induced elevated-temperature embrittlement has been found in austenitic stainless steels,[23-26] nickel-base alloys,[27,28] cobalt alloys,[28,29] and aluminum alloys.[30] It has not been normally found in ferritic steels,[31,32] vanadium alloys,[33] and other refractory metals.[27] The elevated-temperature embrittlement, as it occurs in austenitic stainless steels, is distinguished by the following characteristics:[34,35]

1. Drastic losses in ductility with minor changes in strength occur (Fig. 6).

2. The embrittlement cannot be removed by annealing at elevated temperatures (Fig. 6).

3. The severity of embrittlement appears to increase with increasing fluence (Fig. 7).

4. The fracture occurs intergranularly in the irradiated material, but it may occur either transgranularly or intergranularly in the unirradiated material.

Implications

The temperature range where the elevated-temperature embrittlement occurs (above 600°C) is at the expected operating temperatures of LMFBR cladding materials. Owing to the expected high burnup, the fuel is expected to undergo swelling, thereby mechanically stressing the cladding. The stainless-steel cladding is expected to have enough ductility to allow for this swelling without failure. However, if the radiation-induced embrittlement is severe enough, the ductility of the stainless steel will be reduced, and the cladding will crack rather than deform plastically when accommodating the fuel swelling. Similarly, one has to design other components in the reactor for less deformation to accommodate elevated-temperature embrittlement.

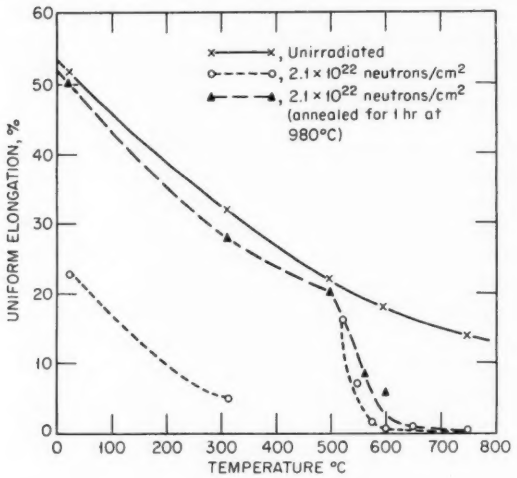

Fig. 6 Uniform elongation of unirradiated and irradiated 347 stainless steel at 50°C as a function of test temperature.[24]

Variables Affecting Embrittlement

In the discussion of the elevated-temperature embrittlement phenomenon, emphasis is placed on the austenitic stainless steels and nickel-base alloys, since almost all of the experimental work was performed on these alloys.

Irradiation Temperature. The degree of radiation-induced embrittlement is independent of irradiation temperature, provided the irradiation temperature is 700°C or below. At irradiation temperatures of 800 and 900°C, somewhat more embrittlement takes place for equivalent fast fluences.[36] This suggests that at the higher irradiation temperature, larger helium bubbles are formed at grain boundaries.

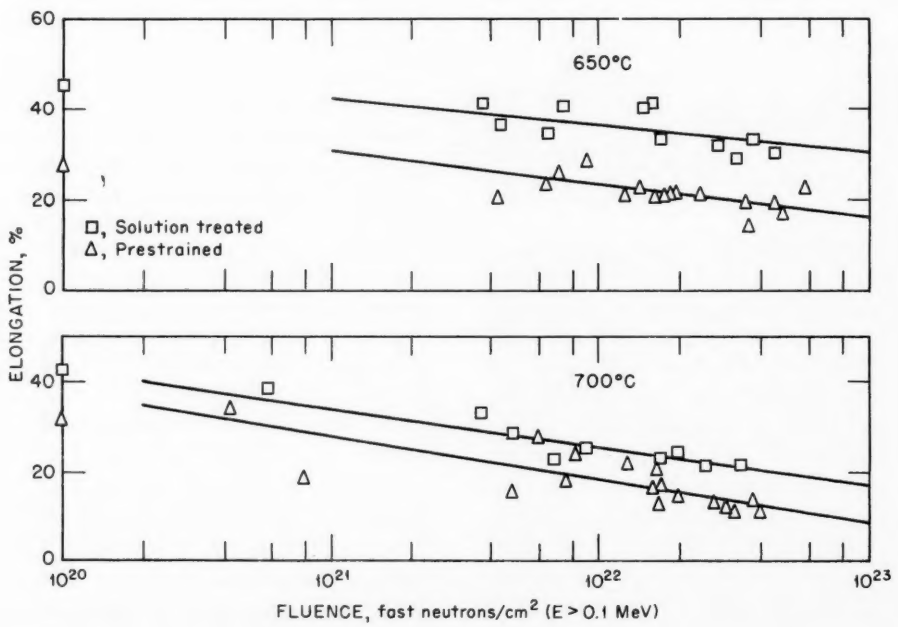

Fig. 7 Postirradiation ductility of 316 stainless steel[37] at 650 and 700°C. (Irradiation temperature, 350°C.)

Fluence. The degree of embrittlement increased[37] with increasing fluence (Fig. 7). This was probably due to increasing helium content with higher fluences,[34] as shown in Fig. 8.

Composition. It was originally believed that the degree of embrittlement increased with increasing boron content;[38] this was reasonable since helium is generated from neutron interaction with boron. However, later studies indicated that the degree of embrittlement was independent of boron content.[39] This independence of boron content was explained in terms of the dual role of boron: (1) promoting embrittlement because of helium formation and (2) improving the grain-boundary strength and thus minimizing embrittlement.[39]

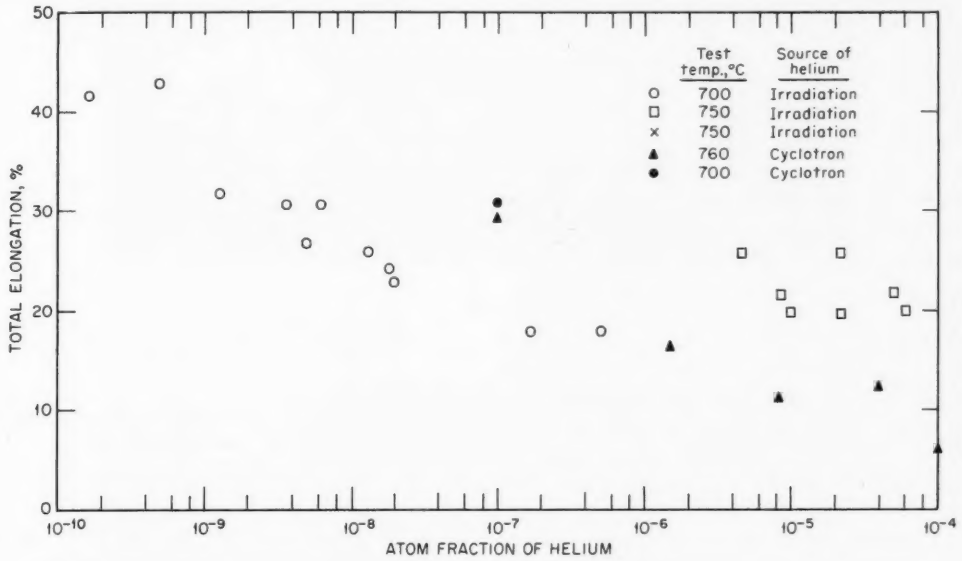

Fig. 8 Variation of total elongation of stainless steel at elevated temperature as a function of helium content (helium being either generated by neutrons or injected by cyclotron).[34]

Nickel. Numerous studies have shown that increasing nickel content results in more severe embrittlement for equivalent irradiation conditions.[34,35] This phenomenon can be explained in terms of the higher helium generation in nickel due to irradiation in comparison with that in iron.

Mechanisms of Embrittlement

Helium Embrittlement. The most widely accepted theory attributes embrittlement to helium that is generated by various neutron interactions during irradiation. The helium atoms are produced by thermal and higher energy neutrons from ^{10}B, which has a thermal-neutron (n,α) cross section of 3840 barns. Helium atoms are also produced by fast neutrons from iron, chromium, and nickel, which have reaction cross sections in the order of millibarns. Consequently, in low-energy neutrons, most of the helium will be produced from the boron impurity, provided that significant amounts of boron are present. Because of the high cross section of ^{10}B, all the ^{10}B atoms will be burned out after a thermal fluence of about 1×10^{21} neutrons/cm^2. After the ^{10}B has burned out, or in the absence of lower energy neutrons, helium will be produced by fast neutrons from iron, chromium, and nickel. Weitman[40] has recently shown that considerable amounts of helium are also produced by neutrons from ^{58}Ni. It is hypothesized that the following reactions take place:

$$^{58}Ni + \text{thermal neutrons} \rightarrow {}^{59}Ni + \gamma$$

$$^{59}Ni + \text{fast neutrons} \rightarrow {}^{56}Fe + {}^{4}He$$

Helium generated by the above mechanisms is believed to agglomerate into helium bubbles.[35] For helium generated from boron, it is expected that these

helium bubbles will be formed close to grain boundaries since boron generally segregates to grain boundaries. Helium generated by fast neutrons would be expected to be produced homogeneously throughout the material. The mechanism of helium coalescence into bubbles is not known but is assumed to be inevitable since the solubility of helium in metals is low.

Helium produced by (n,α) reactions is believed to coalesce into bubbles at grain boundaries, where it promotes intergranular fracture. The mechanism of the helium movement in metals, including bubble agglomeration, has been discussed by Barnes[41] and Hyman and Sumner.[42] These investigators hypothesize that the equilibrium internal bubble pressure is given by $p_0 = 2.28\ \gamma/r_0$, where γ is the surface tension and r_0 is the bubble radius.[35] A large uncertainty is introduced into these calculations because the surface tension is estimated to vary from 1000 to 5500 ergs/cm^2. If a tensile specimen containing these equilibrium bubbles is loaded with a tensile stress higher than the internal gas pressure and if the temperature is sufficiently high, the bubble will grow in size by acquiring vacancies from the grain boundary. When the initial stress causes the bubble to start growing, an even lower critical stress will be required to maintain bubble growth. For example, if we assume a surface tension of 1000 ergs/cm^2 and a bubble radius of 43 Å, a stress of 77,000 psi will be required for growth of the bubble. However, if the bubble has subsequently grown to 114 Å, a stress of only 29,000 psi will be required to maintain growth.[35] The final shape of the bubbles will not necessarily be spherical, and the bubbles can also be described as fissures. The bubbles (or fissures) will continue to grow with continued stress until they come together and cause fracture. Kramer suggests that moving dislocations actually sweep helium atoms from the matrix to the helium bubbles at the grain boundaries.[43]

The mechanism for embrittlement in irradiated stainless steel has been related to the ductility minimum found in most unirradiated metals and alloys at elevated temperatures.[44] In unirradiated metals and alloys, the ductility minimum occurs at a temperature somewhat below the recrystallization temperature. The ductility minimum is believed to occur when stress causes grain-boundary shearing and the formation of fissures in the grain boundaries. These grain-boundary fissures then promote intergranular fracture. Grain-boundary migration tends to minimize the effect of these fissures by continuously healing them. As the temperature is increased and the migration of the grain boundaries becomes sufficiently rapid, the fissures are healed quickly, and the ductility increases with increasing temperature. In highly irradiated stainless steel, it is believed that helium bubbles are pinning the grain boundaries and thus preventing their migration.[24] The stress–strain curves for the as-irradiated specimens, the irradiated and subsequently annealed specimen, and the unirradiated control specimen are compared in Fig. 9. Since only minimal migration occurs, the cracks

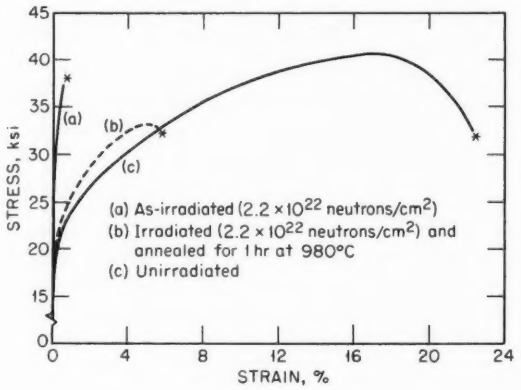

Fig. 9 Stress–strain curves for irradiated and unirradiated 347 stainless steel tested[24] in tension at 600°C.

caused by grain-boundary shearing are not healed, and consequently fracture occurs without any significant elongation taking place. As a grain-boundary crack is formed and propagates, the specimen fractures with considerably less uniform elongation and a corresponding reduction in ultimate tensile strength. The absence of wedge-type cracks at the grain boundaries of the irradiated specimen tested at 600°C (Fig. 10) indicates that fracture must propagate easily after the initial grain-boundary crack is formed.

Matrix Strengthening

Woodford et al. state that fine helium bubbles in the matrix strengthen the material. The grain boundaries themselves are not affected by irradiation, but, with the matrix strengthened, they become relatively weaker. Consequently fracture occurs at the weaker grain boundaries, and this results in intergranular fracture.[45] Observations by transmission electron microscopy have shown the pinning of dislocations by helium bubbles, which indicates that matrix strengthening is probably taking place.

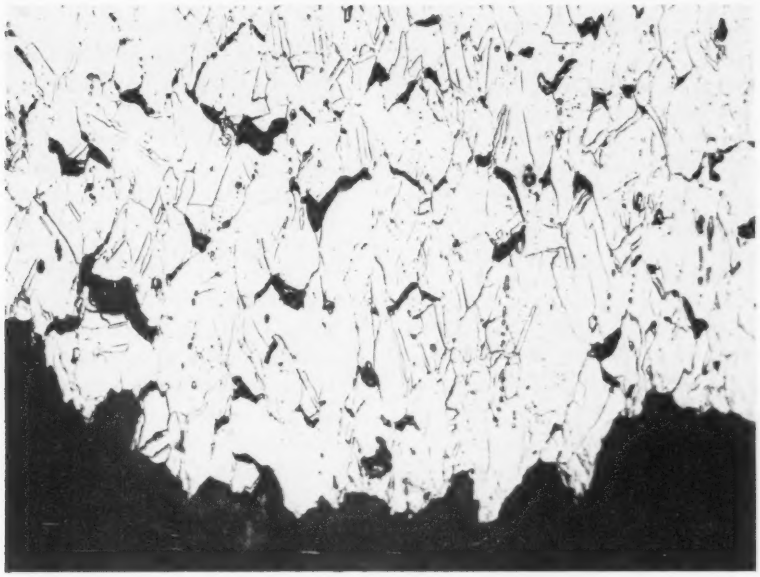

(a)

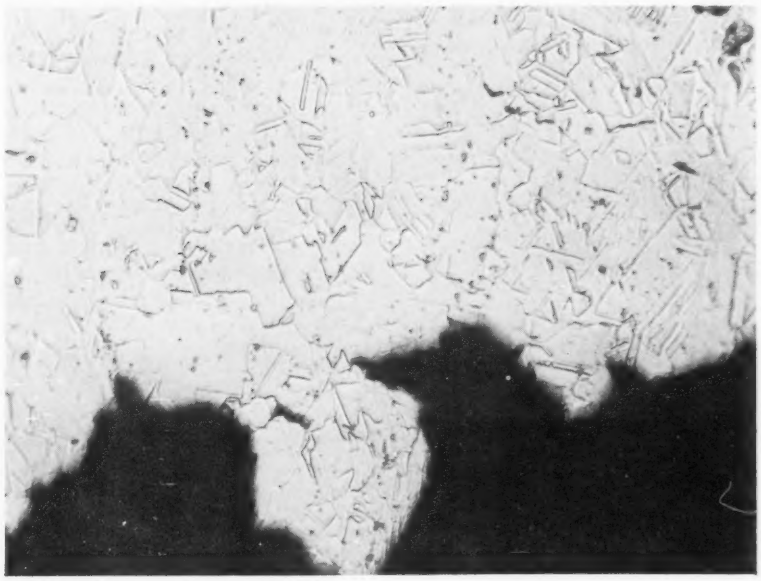

(b)

Fig. 10 Fracture area of stainless steel tested in tension at 600°C. Magnification 250 X. (*a*) Unirradiated. (*b*) Irradiated to 2.2×10^{22} neutrons/cm^2 ($E > 1$ MeV).

Other Theories. Some other theories that have been advanced to explain the radiation-induced embrittlement are:

1. Lithium, which is formed by the $^{10}B(n,\alpha)^{7}Li \rightarrow$ reaction, weakens the grain boundaries and thus causes intergranular fracture.[46]

2. Radiation-induced precipitation of carbides promotes general embrittlement, which also includes intergranular fracture.[47]

Remedies

Various approaches have been taken to eliminate radiation-induced elevated-temperature embrittlement. Although none of the techniques discussed below has completely eliminated embrittlement, all of them have minimized the degree of embrittlement.

Alloying Additions. The addition of small amounts of titanium to austenitic stainless steel considerably improved its postirradiation ductility at elevated temperatures (Fig. 11). Earlier it was thought that the improvement in ductility was due to adherence of helium bubbles to fine TiC particles.[48] However, it was subsequently concluded that the improvement was probably due to the change in fracture behavior of the material. Although unirradiated austenitic stainless steels fail by intergranular fracture at these temperatures, it was found that the titanium-modified stainless steel failed transgranularly.[49] Therefore it appears that the presence of helium bubbles at the grain boundaries does not influence the fracture behavior of titanium-modified stainless steel to such an extent, since the fracture of modified stainless steel is transgranular. The phenomenon of radiation-induced elevated-temperature embrittlement is not completely eliminated because the fracture is a mixture of transgranular and intergranular fracture.

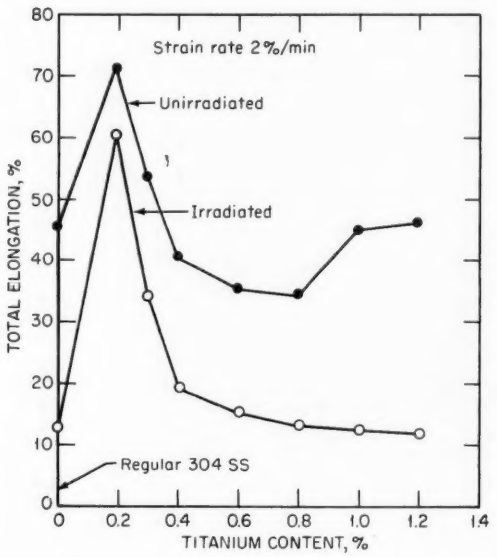

Fig. 11 Influence of titanium additions on the ductility of 304 stainless steel[48] at 842°C. Specimens irradiated[48] to 7 x 10^{20} neutrons/cm².

Heat-Treatment. Aging of unirradiated austenitic stainless steel for 24 hr at 810°C has been found to result in improved creep life.[50] This improvement in creep life is attributed to the formation of carbide particles at the grain boundaries. These carbide particles at grain boundaries stop crack propagation and consequently prevent early fracture. Preirradiation annealing of austenitic stainless steel for 24 hr at 810°C significantly improved[51] the postirradiation ductility at 700°C.

Grain Size. Decreasing the grain size resulted in significantly higher postirradiation ductility.[52] It is hypothesized that, by having a small grain size, the total grain-boundary area is increased. Thus the helium bubbles would be distributed over a larger area, and their ability to promote intergranular fracture would be decreased.

Grain Orientation. Radiation-induced embrittlement was found to be considerably less for specimens tested parallel to the rolling direction than for those tested perpendicular to the rolling direction.[53] With the grains being elongated, more grain boundaries would be parallel to the rolling direction, and thus less embrittlement would be expected in a material with oriented grains.

Although none of these remedies completely eliminates elevated-temperature embrittlement, all of them tend to minimize the phenomenon.

REFERENCES

1. C. Fulton and E. J. Cawthorne, Voids in Irradiated Stainless Steel, *Nature*, **216:** 575 (Nov. 11, 1967).
2. B. Mastel and J. L. Brimhall, Voids Produced in High Purity Nickel by Neutron Irradiation, *J. Nucl. Mater.*, **28:** 115 (1968).
3. T. T. Claudson, How Do We Solve the Swelling Problem, in *Irradiation Effects on Structural Alloys for Nuclear Reactor Applications*, American Society for Testing and Materials, Special Technical Publication No. 484, p. 400, 1971.

4. J. O. Stiegler, K. Farrell, C. K. H. Dubose, and R. T. King, *Radiation Damage in Reactor Materials,* Symposium Proceedings, Vienna, 1969, Vol. II, p. 215, International Atomic Energy Agency, Vienna, 1969 (STI/PUB/230).
5. R. C. Ran, R. L. Ladd, and J. Moteff, Neutron Damage in Molybdenum Irradiated at High Temperatures, *J. Nucl. Mater.,* **33:** 324 (1969).
6. F. W. Wiffen and J. O. Stiegler, Irradiation Damage in Vanadium at 600°C, *Trans. Amer. Nucl. Soc.,* **12**(1): 119 (June 1969).
7. H. R. Bragger, Irradiation Effects on Reactor Structural Materials, Quarterly Progress Report, May–July 1969, USAEC Report BNWL-1188, Battelle–Northwest, September 1969.
8. G. L. Kulcinski, B. Mastel, and H. E. Kissinger, Characterization and Annealing Behavior of Voids in Neutron Irradiated Nickel, *Acta Met.,* **19:** 27 (January 1971).
9. S. D. Harkness and Che-Yu Li, A Study of Void Formation in Fast-Neutron-Irradiated Metals, *Met. Trans.,* **2:** 1457 (May 1971).
10. W. Hafele, On the Development of Fast Breeders, in *Proceedings of the International Conference on Constructive Uses of Atomic Energy,* Washington, D. C., November 10–15, 1968, American Nuclear Society, Hinsdale, Ill.
11. J. J. Holmes and J. L. Straalsund, Effect of Cold Work on Irradiation-Induced Swelling, *Trans. Amer. Nucl. Soc.,* **13**(2): 559 (November 1970).
12. R. Bullough and R. C. Perrin, The Mechanism and Kinetics of Void Growth During Neutron Irradiation, in *Irradiation Effects on Structural Alloys for Nuclear Reactor Applications,* American Society for Testing and Materials, Special Technical Publication No. 484, p. 317, 1971.
13. H. R. Bragger, J. L. Straalsund, J. J. Holmes, and J. F. Bates, Irradiation Produced Defects in Austenitic Stainless Steel, Report WHAN-FR-16, WADCO Corporation, December 1970.
14. Che-Yu Li, D. G. Franklin, and S. D. Harkness, Considerations of Metal Swelling and Related Phenomena Caused by Fast Reactor Irradiation, in *Irradiation Effects on Structural Alloys for Nuclear Reactor Applications,* American Society for Testing and Materials, Special Technical Publication No. 484, p. 347, 1971.
15. J. H. Shively, *Radiation Damage in Reactor Materials,* Symposium Proceedings, Vienna, 1969, Vol. II, p. 253, International Atomic Energy Agency, Vienna, 1969 (STI/PUB/230).
16. E. E. Bloom, An Investigation of Fast Neutron Radiation Damage in an Austenitic Stainless Steel, USAEC Report ORNL-4580, Oak Ridge National Laboratory, June 1970.
17. E. E. Bloom and J. O. Stiegler, The Effect of Helium on Void Formation in Irradiated Stainless Steel, *J. Nucl. Mater.,* **36:** 331 (1970).
18. G. A. Reimann and W. R. Martin, Improved Process for the Fabrication of 316 Stainless Steel Tubing, *Trans. Amer. Nucl. Soc.,* **12**(2): 569 (December 1969).
19. M. Kangilaski and A. A. Bauer, Mechanical Properties of Shock Strengthened Austenitic Stainless Steel, Battelle–Columbus (to be published).
20. I. S. Levy, Microstructural Modifications to Stainless Steel and Nickel Base Alloys, Quarterly Progress Report on Irradiation Effects on Reactor Structural Materials, February–April 1969, p. 12.4, USAEC Report BNWL-1091, Pacific Northwest Laboratory, June 1969.
21. J. H. Crawford and D. S. Billington, *Radiation Damage in Solids,* Princeton University Press, Princeton, N. J., p. 25, 1961.
22. A. N. Hughes and J. R. Caley, The Effects of Neutron Irradiation at Elevated Temperatures on the Tensile Properties of Some Austenitic Stainless Steels, *J. Nucl. Mater.,* **10:** 60 (1963).
23. W. R. Martin and J. R. Weir, The Effect of Radiation Temperature on the Postirradiation Stress–Strain Behavior of Stainless Steel, in *Flow and Fracture of Metals and Alloys in Nuclear Environments,* American Society for Testing and Materials, Special Technical Publication No. 380, p. 251, 1965.
24. M. Kangilaski, J. S. Perrin, and R. A. Wullaert, Irradiation-Induced Embrittlement in Stainless Steel at Elevated Temperature, in *Irradiation Effects in Structural Alloys for Thermal and Fast Reactors,* American Society for Testing and Materials, Special Technical Publication No. 457, p. 67, 1969.
25. J. J. Holmes, R. E. Robbins, and J. L. Brimhall, Effect of Fast Reactor Irradiation on the Tensile Properties of 304 Stainless Steel, *J. Nucl. Mater.,* **32:** 330 (1969).
26. R. Carlander, S. D. Harkness, and F. L. Yaggee, Fast-Neutron Effects on Type 304 Stainless Steel, *Nucl. Appl Technol.,* **7:** 67 (July 1969).
27. T. T. Claudson, Effect of Neutron Irradiation on the Elevated Temperature Mechanical Properties of Nickel-Base and Refractory Metal Alloys, in *The Effects of Radiation on Structural Metals,* American Society for Testing and Materials, Special Technical Publication No. 426, p. 67, 1967.
28. M. Kangilaski, S. L. Peterson, J. S. Perrin, and R. A. Wullaert, Effect of Irradiation on the Elevated Temperature Fracture of Selected Face-Centered Cubic Alloys, *Nucl. Appl. Technol.,* **9:** 550 (October 1970).
29. J. G. Y. Chow, Effect of Irradiation on Mechanical Properties of Cobalt-Base Alloys, USAEC Report BNL-12438, Brookhaven National Laboratory, 1968.
30. R. T. King and J. R. Weir, The Effect of Irradiation on the Mechanical Properties of Aluminum Alloys, *Trans. Amer. Nucl. Soc.,* **11** (1): 146 (June 1968).
31. J. E. Irwin and A. L. Bement, Nature of Radiation Damage to Engineering Properties of Various Stainless Steel Alloys, in *The Effects of Radiation on Structural Metals,* American Society for Testing and Materials, Special Technical Publication No. 426, p. 278, 1967.
32. J. H. Frye and J. E. Cunningham, Metals and Ceramics Division Annual Progress Report for Period Ending June 30, 1966, USAEC Report ORNL-3970, Oak Ridge National Laboratory, 1966.
33. H. Böhm, W. Dienst, H. Hauck, and H. J. Laue, Irradiation Effects on the Mechanical Properties of Vanadium-Base Alloys, in *The Effects of Radiation on Structural Metals,* American Society for Testing and Materials, Special Technical Publication No. 426, p. 95, 1967.
34. J. G. Conner and S. W. Porembka, A Compendium on Properties and Characteristics for Selected LMFBR Cladding Materials, USAEC Report BMI-1900, Sec. VIII, Mechanisms of Radiation Damage, Battelle–Columbus, May 15, 1968.

35. R. S. Barnes, Embrittlement of Stainless Steel and Nickel-Base Alloys at High Temperature Induced by Neutron Irradiation, *Nature*, **206:** 1307 (June 26, 1965).
36. W. R. Martin and J. R. Weir, Irradiation Embrittlement of Low- and High-Carbon Stainless Steels at 700, 800, and 900°C, USAEC Report ORNL-TM-1516, Oak Ridge National Laboratory, June 1966.
37. I. P. Bell, J. Standring, P. C. L. Pfeil, G. H. Broomfield, K. Q. Bagley, and A. S. Fraser, The Effects of Irradiation on the High Temperature Properties of Austenitic Steels and Precipitation Hardened Nickel Alloy, presented at the Symposium on the Effects of Radiation on Structural Metals, 69th ASTM Annual Meeting, Atlantic City, N. J., June 1966.
38. P. C. L. Pfeil and P. J. Barton, The Effect of Impregnation with ^{10}B and ^{11}B on the Elevated Temperature Tensile Properties of an Irradiated Austenitic Steel, British Report AERE-R-5027, August 1965.
39. D. R. Harries and A. C. Roberts, Effects of Heat Treatment and Irradiation on the High Temperature Tensile Properties of Austenitic Stainless Steels, in *The Effects of Radiation on Structural Metals,* American Society for Testing and Materials, Special Technical Publication No. 426, p. 21, 1967.
40. J. Weitman, N. Daverhog, and S. Farvolden, Anomalous Helium Production in Nickel, *Trans. Amer. Nucl. Soc.*, **13**(2): 557 (November 1970).
41. R. S. Barnes, Mechanism of Radiation-Induced Mechanical Property Changes, in *Flow and Fracture of Metals and Alloys in Nuclear Environments,* American Society for Testing and Materials, Special Technical Publication No. 380, p. 40, 1965.
42. E. D. Hyman and G. Sumner, Irradiation Damage to Beryllium, *Radiation Damage in Solids,* Symposium Proceedings, Venice, 1962, Vol. I, p. 323, International Atomic Energy Agency, Vienna, 1962 (STI/PUB/56).
43. D. Kramer, K. R. Garr, C. G. Rhodes, and A. G. Pard, Helium Embrittlement of Type 316 Stainless Steel, *J. Iron Steel Inst., (London)*, **207:** 1141 (1969).
44. F. N. Rhines and P. J. Wray, Investigation of the Intermediate Temperature Ductility Minimum in Metals, *Trans. Amer. Soc. Metals*, **54:** 117 (1961).
45. D. A. Woodford, J. P. Smith, and J. Moteff, Observation of Helium Bubbles in an Irradiated and Annealed Austenitic Steel, *J. Iron Steel Inst. (London)*, **208:** 70 (January 1970).
46. R. B. Roy and B. Solly, Embrittlement of Neutron Irradiated 20 Cr–25 Ni–Nb Austenitic Steel at 650°C, *J. Iron Steel Inst. (London)*, **205:** 58 (1967).
47. P. R. B. Higgins and A. C. Roberts, Carbide Precipitation and Associated Tensile Behaviour in a Neutron Irradiated Stainless Steel, *J. Iron Steel Inst. (London)*, **204:** 489 (1966).
48. W. R. Martin and J. R. Weir, Solutions to the Problems of High-Temperature Irradiation Embrittlement, *The Effects of Radiation on Structural Metals,* American Society for Testing and Materials, Special Technical Publication No. 426, p. 440, 1967.
49. E. E. Bloom and J. R. Weir, Development of Austenitic Stainless Steel with Improved Resistance to Elevated-Temperature Irradiation Embrittlement, in *Irradiation Effects in Structural Alloys for Thermal and Fast Reactors,* American Society for Testing and Materials, Special Technical Publication No. 457, p. 261, 1969.
50. F. Garofalo, *Fundamentals of Creep and Creep-Rupture in Metals,* p. 223, The Macmillan Company, New York, 1965.
51. P. Patriarca, Oak Ridge National Laboratory, unpublished, March 1967.
52. W. R. Martin and J. R. Weir, Influence of Grain Size on the Irradiation Embrittlement of Stainless Steel at Elevated Temperatures, USAEC Report ORNL-TM-1043, Oak Ridge National Laboratory, March 1965.
53. H. Böhm and H. Hauck, Investigation of the Influence of Cold Working and Thermomechanical Treatment on the Radiation-Induced, High-Temperature Embrittlement of Austenitic Steels, *Trans. Amer. Nucl. Soc.*, **11**(2): 482 (November 1968).

Operating Experience at the Dresden 2 Reactor

By Myrna L. Steele*

Abstract: *The highlights of operation of Unit 2 of the Dresden Nuclear Power Station from startup through December 1970 are summarized, and maintenance and repair activities are listed.*

Unit 2 of Commonwealth Edison Company's Dresden Nuclear Power Station is an 809-MW(e) single-cycle, forced-circulation boiling-water reactor (BWR) and is located in Grundy County, Ill., about 8 miles east of Morris at the confluence of the Des Plaines and Kankakee Rivers. Subsequent to the completion of fuel loading, initial criticality[1] was achieved in Dresden 2 at 0122 hr on Jan. 7, 1970, and the turbine was first synchronized to the Commonwealth Edison grid at 2325 hr on April 13. The unit achieved 10, 25, 50, and 75% of power on April 16, April 22, April 29, and May 13, respectively. Designed power rating was achieved on October 13. By Dec. 31, 1970, Dresden 2 had produced about 9.7×10^5 MWh of electricity.

Seven hundred and twenty-four Zircaloy-2-clad UO_2 fuel assemblies[2] comprise the core, which has an equivalent diameter of 182.2 in. and an active length of 144 in. Each fuel assembly contains 49 fuel rods and is fitted with a Zircaloy-4 coolant-flow channel. The 177 movable control rods are cruciform, and each rod contains 84 stainless-steel tubes filled with B_4C granules. The control rods are the bottom-entry type and are moved vertically within the core by individual hydraulically operated locking-piston-type control-rod drives (CRDs).

The reactor coolant water enters the bottom of the core, flows upward through the fuel assemblies where boiling is produced, and the steam–water mixture is separated by steam separators and dryers that are located inside the reactor vessel. The steam passes through steam lines to the turbine, while the separated water is mixed with the incoming feedwater and returned to the core inlet by jet pumps that are located in the reactor vessel.

The turbine[3] is a tandem-compound, six-element, nonreheat type with 38-in. last-stage buckets. It has a rating of 810 MW and is designed for steam conditions of 950 psig when saturated with 0.28% moisture and of 1.5 in. Hg absolute with 0.5% makeup while extracting for four stages of feedwater heating. Steam leaving the high-pressure turbine passes through the moisture separators, where the moisture content of the steam is reduced to less than 1 wt.% before the steam enters the three low-pressure units.

The synchronous generator, which has a cooled conductor, is rated 902 MVA at 18,000 V, 0.9 power factor. The generator-exciter system is rated 2435 kVA, 400 V.

OPERATION FROM INITIAL CRITICALITY THROUGH APPROACH TO POWER

Fuel loading[4] at Dresden 2 began on Dec. 22, 1969, the day that the plant was licensed for operation, and criticality was achieved at 0122 hr on Jan. 7, 1970. Heatup with nuclear heat was begun on March 24, and primary-system design pressure and temperature were attained for the first time on March 29. The generator was synchronized to the line for the first time on April 13, and 100% of the thermal-power rating was achieved on Oct. 13, 1970.

*U. S. Atomic Energy Commission, Division of Technical Information Extension, Oak Ridge, Tenn. 37830.

A 443.5-hr shutdown was manually initiated on March 5 subsequent to the initial turbine roll and preparatory to startup testing. At 1939 hr on March 24, with the reactor just critical, a scram occurred when an idle recirculation pump was started so that it could be brought on line. The pump had added cold water to the primary system, thereby adding reactivity, and had triggered a scram from an intermediate-range (neutron flux) monitor (IRM). The reactor was returned to criticality until March 30, when it was manually shut down to locate and repair leaking tubes in the main condenser. On April 4 the reactor was restarted, and on April 6, during the process of shutdown by control-rod insertion, sufficient reactivity was added by the cooldown rate of the reactor coolant to cause a scram from the IRM trip circuit. The reactor was again brought to criticality late on April 8. On April 10 it was manually scrammed when high turbine vibration necessitated opening of the condenser vacuum breaker to reduce condenser vacuum and slow the turbine down. A manual scram was initiated because an automatic scram from a low-vacuum signal from the condenser was anticipated. At 1610 hr on that same day, the reactor was again critical and remained so until 0104 hr on April 11, when it was manually scrammed following a partial scram that occurred during surveillance testing when one group of scram solenoids in the control instrumentation failed to reset. The reactor was returned to the critical condition at 1645 hr on April 11. During system heatup on April 12, at 1545 hr, the reactor pressure was raised above 600 psi before 23 in. of vacuum had been established in the primary system, and a scram resulted. The reactor was immediately restarted after the scram. At 1716 hr the reactor was returned to critical, and heatup continued. At 2325 hr on April 13, the generator was synchronized to the line for the first time. At 0850 hr on April 14, the reactor was manually scrammed subsequent to a turbine trip to allow the breaking of condenser vacuum and consequent slowdown of the turbine. The reactor was returned to criticality at 1705 hr. After the generator was again synchronized to the line at 0725 hr on April 16, the load was increased to 40 MW(e) and was maintained at that level until 1432 hr on April 16. At this time one of the feedwater pumps was unintentionally allowed to run out while test equipment was being installed. The sudden increase in cooler feedwater flow caused an addition of reactivity and actuated a high-neutron-flux trip from the average-power-range monitor (APRM). At 1925 hr the reactor was again critical, and later that evening the 10%-of-rated-power level was reached. The loss-of-power test at 10% of rated power produced the anticipated scram at 0223 hr on April 18, and the reactor was out of service for about 54 hr for inspections preparatory to increasing the power level above 10% of rated power. The reactor was restarted for about 14 hr on April 20 and was then scrammed manually to allow testing of the high-pressure coolant-injection system (HPCIS). After the test the reactor was returned to critical at 0006 hr on April 21, and the 25%-of-rated-thermal-power level was reached on April 22. The power level was slowly increased to about 1200 MW(t), and a spurious signal was accidentally introduced into the pressure regulator at 0830 hr on April 27. The signal to the pressure regulator caused a step decrease in the set point, and the bypass valves opened automatically. The resultant high steam flow caused the main-steam-line isolation valves to close and scrammed the reactor. The plant was returned to the line, and the power level was again slowly increased. On Apr. 29, 1970, the plant first attained the 50%-of-rated-power level.

On May 8 the reactor was operating at 370 MW(t) with 100 MW(e) on the turbine. The reactor power began decreasing, and difficulty was experienced with the feedwater controls. The water level increased, and at 0353 hr a high-water-level signal tripped the turbine. When the turbine-stop valves tripped, the low-load bypass relay in the safety system, which normally picks up at 40% of power, failed to function and the reactor scrammed. The plant was off line for about 65.5 hr and was returned to service on May 10. On May 13 the 75%-of-rated-power level was achieved, and on May 14 at 2131 hr the plant was manually tripped because both operating feedwater pumps had tripped. A high differential pressure in the condensate demineralizer had caused a low suction pressure in the primary system which, in turn, had caused the feedwater pumps to trip. The reactor was scrammed to minimize the water-level transient. The plant was returned to the line in about 5 hr. On May 19, during testing of the main-steam-line isolation valves at the 75% power level, one of the valves closed and caused high flows in the other three steam lines. The resulting high steam flow in the other main steam lines initiated a main-steam-line isolation signal which resulted in closure of all main-steam-line isolation valves and tripped the reactor. The plant was returned to service 4 hr later, and it remained in service until 0336 hr on May 21. At that time an erroneous water-level signal was unintentionally fed to the feedwater-control system, and the control system raised the reactor water level to the

turbine-trip point. The turbine-stop valves closed and, since the plant load was above 45%, tripped the reactor. While the reactor was being brought back to criticality, a spurious signal from one of the IRM channels scrammed the reactor. The reactor reached criticality at 0815 hr, and the plant was returned to service, where it remained until a failure of a high-level switch in a moisture-separator tank initiated a turbine trip and caused the reactor to scram at 0307 hr on May 23. Again the plant load was above 45%, and therefore the closure of the turbine-stop valves scrammed the reactor. By 0800 hr the reactor was again critical, and the plant was back in service until May 26, when it was tripped from about 450 MW(e). A loss of the motor-generator set for the essential-power service caused the loss of the feedwater-control system, and the water level in the reactor then decreased enough to cause a reactor scram. The plant was returned to service in about 5 hr and remained in service until 1318 hr on May 28. At that time a water-level increase occurred in the reactor while the feedwater control was being transferred from automatic to manual. The increase in water level tripped the turbine, closed the turbine-stop valves, and, since the power level was greater than 45%, scrammed the reactor. The plant was returned to the line in about 4 hr, the load was increased to about 390 MW(e), and approach-to-power testing was resumed.

An inadvertent turbine trip was initiated from about 390 MW(e) at 1733 hr on June 1 while test equipment was being installed. The ensuing reactor scram resulted from closure of the turbine-stop valves. The reactor was critical again by 2323 hr, but an anticipated scram occurred the next day because of turbine-stop-valve closure during the turbine-trip startup-test procedure. By 1913 hr on June 2, the reactor was again critical, and at 0545 hr the next day an anticipated scram resulted from carrying out the startup-test procedure for closing the main-steam-line isolation valves. The reactor was returned to criticality at 1537 hr but was shut down 10 min later by control-rod insertion. The shutdown was necessitated to allow maintenance personnel to enter the dry well and make repairs on a source-range monitor (SRM). At 2000 hr on June 3, the plant was returned to the line, and the power level was increased.

On June 5 at 2128 hr, with the power level at 623 MW(e) and the plant at near-equilibrium conditions with full recirculation flow, a spurious signal occurred in the reactor pressure-control system, i.e., in the pressure regulator for the turbine-generator electro-hydraulic (EH) governor. No testing[5] was in progress and no maintenance was being performed when the spurious signal occurred. This signal opened the turbine-control valves from the 75 to the 80% reference set point for plant load and opened fully the steam-bypass valves to the condenser. The resulting turbine trip from 623 MW(e) caused the reactor to scram. During all the ensuing occurrences, the reactor was in a fully secured condition, the coolant-water level was maintained above the top of the core at all times, and there was no fuel damage.

Three seconds after the reactor scram, all four water-level sensors tripped on a low-water-level signal and initiated closure of all main-steam-line isolation valves. The two operating feedwater pumps tripped off because of low suction pressure (the third pump was out of service for maintenance). Two seconds later one of the operable pumps restarted automatically and went into and out of runout.

Since the steam-line bypass valves were still open, a depressurization occurred at 19 sec after the spurious turbine trip which allowed the swelling of the reactor-pressure-vessel water level and the probable transport of some two-phase mixture into the main steam line. The bypass valves were then automatically closed at 22 sec after the trip, and the main-steam-line isolation valves started closing at 33 sec because of a signal from the main-steam-line low-pressure switches. At about 35 to 40 sec after the turbine trip, the water level decreased rapidly when the voids collapsed after subcooled feedwater was injected into the reactor water. At about 50 sec after the turbine trip, the water level in the reactor vessel started rising again. At 1 min after the turbine trip, the operator noted that a low water level in the reactor vessel was indicated by a recorder chart. Although the water level in the reactor vessel was actually increasing, the pen on the recorder chart had stuck and continued to indicate a low water level. Reacting to the low-water-level indication, the operator switched the feedwater control from automatic to manual and increased the feedwater flow in an attempt to restore the normal water level. The actual water level apparently rose enough to flood both main steam lines and the steam lines to the isolation condenser. Within 30 sec of switching to manual feedwater-flow control, the operator discovered that the pen was stuck and that the actual water level in the reactor vessel was in excess of normal. He then adjusted the feedwater flow rate to its minimum since standard feedwater valves are not designed for positive shutoff.

A rising pressure in the reactor pressure vessel dictated the manual actuation of the isolation con-

denser about 2.5 to 3 min after reactor scram. Also, at this time the operator tried to open the main-steam-line isolation valve to the main condenser. Since the valves had not been reset from the trip on low pressure in the main steam line, they could not be opened. Within 3 min 45 sec after the reactor had scrammed, the pressure in the reactor vessel reached 1050 psig, and the operator chose to open an electromatic relief valve rather than reset and reopen the main-steam-line isolation valves. The operation of the relief valve reduced the pressure in the reactor vessel to 960 psig; the operator then closed the valve, and the pressure started rising rapidly again. At 6 min after the scram, the vessel pressure was again at 1050 psig, and the operator opened another electromatic relief valve for about 2 min. The pressure was rapidly reduced to 940 psig and then more slowly to 850 psig, at which point the relief valve was closed.

Sometime between 5 and 6 min after the reactor scram, a momentary pressure pulse in the main steam line apparently caused a safety valve to lift. At 6 min 3 sec, a 2-psig dry-well-pressure signal initiated a start of the emergency core-cooling system (ECCS), isolated the reactor-building ventilation system, and started the standby gas-treatment system. The high pressure in the dry well was attributed to the main-steam-line safety-valve operations. At 6 min 7 sec after the reactor scram, the cooling pumps for the standby diesel generator started automatically as a result of the high pressure signal from the dry well, and both recirculation pumps automatically tripped at 6 min 12 sec. The standby diesel generator started automatically at 6 min 13 sec, and core-spray systems A and B started automatically at 6 min 13 sec and 6 min 30 sec, respectively. The core-spray systems did not inject water into the reactor vessel, however, because of the high pressure in the vessel. The HPCIS auxiliary oil pump, emergency oil pump, and gland extractor started automatically, and the HPCIS turbine turned at about 6 min 30 sec; however, the system did not inject emergency core-cooling water because it had been valved out of service for repairs earlier. At 6 min 35 sec after the scram, all four low-pressure-coolant-injection-system (LPCIS) pumps started automatically but did not inject water into the reactor vessel because the vessel pressure was above the LPCIS pump-discharge pressure.

The electromatic relief valve was closed (with vessel pressure at 850 psig) about 8 min 10 sec after the reactor scram. Upon valve closure the pressure began rising at about 200 psig/min because the continued feedwater addition was greater than safety-valve leakage. Two more relief valves were opened manually at 9 min 31 sec because vessel pressure had risen to about 1097 psig. The relief valves were left open about 1 min, during which the isolation condenser was reset and brought into operation. It remained in operation for an estimated 5 to 15 min and then was manually shut off.

At 13 min 8 sec after the scram, the first erratic signal from the IRM was recorded. Since the reactor shutdown had been verified, it was assumed that steam in the containment-vessel dry well had caused some kind of damage to the cables or connections. Erratic behavior of the local power-range monitor (LPRM) was first recorded at 13 min 31 sec after scram, and this too was assumed to be caused by the steam in the dry well. Fourteen minutes after the reactor scrammed, the main-steam-line isolation valves were manually opened so that the reactor-vessel pressure could be decreased by using the bypass-valve opening jack (however, the bypass valves were not opened until about 45 min after the scram). One feedwater pump was tripped manually at about 20 min after the scram, and the reactor-vessel water level was monitored closely over the next 10 min to verify that the CRD pumps were providing the necessary flow. The pressure in the reactor vessel decreased at about 14 psi/min until 65 min after the turbine trip. This depressurization rate was attributed to the leakage through the safety valves.

In the 30- to 40-min time period, the reactor pressure decreased to less than 400 psig, and the following actions were taken to prevent injection of torus water into the core: both core-spray pumps were placed in the pull-to-lock position, three of the four LPCIS pumps were placed in the pull-to-lock position, the remaining LPCIS pump and valves were aligned for torus spraying, and the operator was prepared to restart any of the pumps if the need arose. Also, during this 30- to 40-min interval, the emergency diesels were stopped, and the standby gas-treatment system was valved open to the dry well under the following controlled, monitored conditions: a 2-in. bypass around the normal shutoff valve was opened and flow was restricted to 600 cfm for each train, a health physicist monitored the activity of the absolute filters in the standby gas-treatment system, and the stack-gas monitor was checked often and carefully.

At 45 min after the scram, the shutdown cooling was shifted to the main condenser by way of the turbine bypass valves. At 62 min the sump pump in the dry-well floor drain started automatically, pumping liquid from the dry well to the radwaste system. Five of the seven dry-well-cooling units were brought back

into service at 1 hr 15 min by valving off the high-pressure sensors in the dry well. At this point the reactor-vessel pressure was about 200 psig, and the water level in the reactor vessel was above normal.

About 1.5 hr after the scram, the power supplies for the LPRM were shut off because of indications of overheating. By that time, instrumentation personnel had established that one SRM and two IRM channels were functioning properly. At 2 hr the dry-well pressure was back on scale and reading 2.2 psig.

Over the next 22 hr, detailed analyses of particulate-filter samples from the dry well and of charcoal-filter samples from the stack were conducted. Detailed monitoring and sampling of the entire Dresden Nuclear Power Station and surrounding areas were also begun.

At 0955 hr on June 6, 1970, operations and radiation-protection personnel, equipped with Scott Air Packs and other radiation-protection apparatus, entered the dry well to obtain air samples. At this time they observed water cascading down from the upper part of the dry well in the vicinity of steam line D. Observations at the time of entry indicated that the water could be coming from one or more of the safety valves. Because of the water leakage from the main-steam-line area, the reactor water level was lowered below the main steam nozzles.

On June 6 at 2300 hr, the dry-well-purge rate was increased to facilitate iodine removal so that operations personnel could enter the dry well to assess the damage caused by the incident. The air-flow path was changed to pull air from the reactor building directly into the dry well and then through an 18-in. line to the standby gas-treatment system, and the absolute filters in the system were monitored for radiation levels.

At 1100 hr on June 7, operations and radiation-protection personnel entered the dry well for a preliminary inspection. Two safety valves on the main steam line C were cocked slightly open. The operating handles for the valves had apparently been rotated and stuck by the discharge of the safety valve on the adjacent main steam line D.

The plant[6] remained out of service until Aug. 11, 1970, when power operation was resumed subsequent to partial refueling and to repairs and cleanup of damage that resulted from the June 5 occurrence. On August 7, during the approach to power after the 2-month shutdown, a signal from the high-high-flux-level channel of the IRM scrammed the reactor. The reactor was restarted in about 39 hr but was operated at very low power levels for about 3 days. The power level was increased to about 160 MW(e) on August 11, then slowly to a nominal 400 MW(e) for about a week, and finally to about 600 MW(e) until August 28, when a turbine trip scrammed the reactor: A feedwater valve became stuck in the open position, and the resulting high water level to the turbine actuated the stop valves and scrammed the reactor. The plant was out of service for a little over 7 hr and was returned to a nominal power level of 500 MW(e) until September 11, when a faulty signal was introduced into the reactor-vessel water-level-control system and scrammed the reactor. Instrumentation personnel had inadvertently introduced the erroneous signal into the level controller while working on the water-level sensor. A high reactor-vessel water level resulted and caused a turbine trip that scrammed the reactor by closing the turbine-stop valves. The reactor was returned to the critical condition at 0010 hr on September 12, and, when the power level reached about 110 MW(e), a leak developed in the minimum flow line from the reactor feed pump to the condenser. This leak resulted in a low vacuum in the condenser which automatically shut down the reactor. The plant was returned to service and was operated between 400 and 600 MW(e) until 2123 hr on September 23, when a manual reactor shutdown was effected by control-rod insertion so that an oil leak on a low-voltage phase bushing in the main transformer could be repaired. Subsequent to these repairs, the reactor was again critical by 1746 hr on September 27, and the plant was returned to service.

On October 1 the reactor was manually shut down for 27.5 hr when the HPCIS steam-supply valve and an electromatic relief valve failed to operate properly. The HPCIS steam-supply valve was replaced and the valve stem was cleaned. After the valves were repaired, the plant was returned to service at 2307 hr on October 2 and was operated until October 10, when a turbine trip–reactor scram was initiated by a high-level signal from the moisture-separator tank. The plant was returned to service in about 4 hr and remained there until 0945 hr on October 13. One of the startup tests, calling for a manual turbine trip, was conducted at this time, and the turbine trip produced the expected reactor scram. The unit remained out of service for 243.5 hr so that condenser tube leaks could be repaired and some miscellaneous maintenance could be performed. At 1215 hr on October 23, the plant was returned to service. It was operated at a nominal 300 MW(e) until October 30, when the power level was increased to around 400 MW(e). The plant was operated at this level until 0545 hr on November 14. At that time a manual shutdown was effected so that the feedwater pumps could be repaired and five CRDs

could be replaced. Also, during the shutdown, the cause of the fast closure time[7] for one of the main-steam-line isolation valves was investigated. The main steam line in which the valve was located had been isolated on November 5 after a closure time of 2.0 sec was discovered during routine surveillance testing. When the valve was inspected, it was determined that a loose oil fitting had allowed speed-control oil to escape, and this had resulted in the short closure times. The oil was replaced, the fitting was tightened, and the valve was reset to close within a normal range of 3 to 5 sec.

At 1935 hr on November 18, the reactor was again critical but was scrammed manually at 1030 hr the next day to allow personnel to enter the dry well to investigate the cause of an electromatic-relief-valve failure in addition to a suspected leak into the dry well. The problem with the relief valve[8] was discovered at 0735 hr on November 19 during a functional test of these valves which serve the automatic blowdown system. The inspection revealed that a cotter-pin end had wedged between the solenoid guide post and the solenoid armature guide. The exposed end of the pin was bent so that it could not wedge again, and the reactor was returned to criticality at 1650 hr on November 19. The reactor was operated at power levels between 400 and 600 MW(e) for the rest of November.

A load reduction was initiated late on the evening of December 3 so that a faulty backup amplifier in the turbine-speed control system could be replaced. A return to power was interrupted at 0100 hr on December 4 for biweekly surveillance checks of the main-steam-line isolation valves. Four of the eight valves failed to close and two more exhibited high closure times of 5.7 sec. An orderly plant shutdown[9] was initiated at 0304 hr, the turbine generator was removed from the line at 0533 hr, and the reactor was shut down at 0744 hr. An investigation to ascertain the cause of the main-steam-line isolation-valve problems revealed a thin film on the pilot valves. All the pilot valves were thoroughly cleaned, and the air-supply lines and accumulators were blown down to remove any particulate material that might be in the system. The main-steam-line isolation valves were then cycled and timed in the cold condition, and functional checks were performed up to about 400 MW(e).

The reactor was restarted[6] at 0335 hr on December 6, and at 0506 hr on December 7, with the reactor generating 452 MW(e), a sudden operation of the pressure relay on the main power transformer occurred. This pressure-relay operation initiated the core-deluge system and isolated the transformer feed line, which resulted in a turbine trip–reactor scram. Subsequent investigation revealed that the lightning arresters were badly damaged on all three phase coils, the high-side taps on the windings for phases A and B had shifted slightly to one side, and an access cover plate opposite the winding of phase B was bulged upward. The transformer oil was carbonized, and an explosive air mixture existed in the transformer. The oil was drained from the transformer, and inspection of the interior revealed that a tap-changer link on the winding of phase B had burned through and the winding had flashed to ground. Links for phases A and B were also found to be loose. The transformer for Unit 3 was used to replace the failed Unit 2 transformer, and Unit 2 was returned to service on Dec. 27. On Dec. 31 the plant was removed from service for 13 hr for repair of an air-line leak in the dry well.

MAINTENANCE AND REPAIRS

January 1970 (Ref. 4)

The fine-mesh inner screens on the CRDs were replaced with 10-mil mesh screens.

February 1970 (Ref. 4)

A faulty oscillator and an amplifier in a flow indicator for the LPCIS were replaced.
A faulty sensor converter was replaced in the radiation monitor for one of the isolation condensers.

March 1970 (Ref. 4)

Damaged connector pins in one of the SRM channels were repaired.

April 1970 (Ref. 4)

The cable conduit for the SRM was insulated to prevent cable damage from high temperatures.
A faulty relay in the reactor-trip circuit was replaced.
A faulty relay in the stack-gas monitor was replaced.
The seats for leaking valves on two CRDs were replaced.

May 1970 (Ref. 4)

The internals of the pilot valves for the main-steam-line isolation valves were replaced because the pistons of the operating and test pilot valves were binding.
Damaged hangers and piping in the HPCIS steam line were repaired. A water hammer in the HPCIS had caused the damage.

June 1970 (Ref. 4)

The LPRM cables and conduit in the dry well were replaced because of heat damage to the cable insulation.
The SRM and IRM cables and conduit in the dry well were replaced because of heat damage to the cable insulation.

A pilot piston and a sleeve for a main-steam-line isolation valve were replaced because the pilot valve was sticking.
Defective components in an LPCIS valve were replaced because the valve was inoperable.
The coupling and the overload limits for a dry-well air-sampling pump were replaced.

July 1970 (Ref. 6)

The failed sampling pump in one of the stack-gas sampling systems was replaced.
The slipped gear on the inner air lock for the containment vessel was repaired.
The broken control switch on one of the ECCS valves was repaired.
The component drawer for one of the SRM channels was replaced, and a defective signal cable was repaired.

August 1970 (Ref. 6)

A defective motor on one of the ECCS valves was replaced.
A failed O ring for the accumulator on one of the CRDs was replaced.
A leaking drain valve on one of the diesel generators was replaced, and the drain line was rerouted.
The oil filters in the HPCIS were cleaned.
A defective a-c breaker on a 250-V battery was replaced.
A failed pump in the off-gas sampling system was replaced.

October 1970 (Ref. 6)

A defective control-circuit board on a 125-V battery charger was repaired.
A failed sampling pump in the stack-gas sampling system was replaced.
Leaking O rings on the accumulators for three CRDs were replaced.
One of the valves on the isolation condenser was repacked.
A shorted diode and control assembly on the 250-V charger for one bank of batteries was replaced, and the charging rate was reset.
The packing on one of the ECCS valves was replaced, and the stem was cleaned.
The entire solenoid assembly on one of the ECCS valves was replaced because of a worn guide.

November 1970 (Ref. 6)

Scale under the air-solenoid valve seat was removed, and the air system and starting solenoid for the diesel generator were cleaned.
A faulty control switch in the isolation circuitry for the primary containment system was replaced.
New solenoid kits with stainless-steel guideposts were installed on all the electromatic relief valves in the ECCS.
A leaking O ring on an accumulator for a different CRD was replaced.
The pump in the dry-well sampling system was cleaned, and a water trap was installed on the pump suction system.
The packing on a scram valve in a CRD was repaired.
A leaking fitting on an isolation valve in the primary system was repaired, and the speed-control oil was replaced.
Two CRD units were replaced with overhauled drives because of slow scram times.
The damaged relief-valve seat on one of the discharge pumps in the standby liquid-control system was relapped.
One of the valves in the ECCS was repacked.
A new accumulator was installed on one of the CRDs.
A valve seat on a relief valve for an ECCS core-spray pump was repaired, and a new spring was installed.
New setscrews were installed in a lock nut that had loosened and caused an operator for an ECCS valve to stick.

December 1970 (Ref. 6)

A plug was installed in the ECCS drain valve.
The current trip was reset on another 125-V d-c battery charger, and the lead-connection bolt was properly installed.
A new air piston was installed on the starter for the diesel generator.
The varnish-like film was cleaned from the operating and test pilot valves for the main-steam-line isolation valves, and air filters were installed on the air-supply lines.
A burned-out charging controller for a 250-V d-c battery was replaced.
A glass filter bowl was replaced in a defective air-supply filter on a core-spray valve.
A new pinion gear was installed in the air-operated starter for the diesel generator.
A valve was replaced on a starting air-receiver unit for the diesel generator.
New flange gaskets were installed on the safety valves for the main steam system, and the flange bolts were tightened.
A broken handwheel on one of the LPCIS valves was replaced.
The cracked water line to a gland on one of the LPCIS pumps was repaired.
The failed motor for the pump on the dry-well continuous air monitor was replaced.

ACKNOWLEDGMENTS

I would like to express my sincere gratitude to Mr. G. L. Diederich, Supervising Engineer of the Technical Staff of the Dresden Nuclear Power Station, and Mr. Prem Malagi, of the Generating Stations Department of Commonwealth Edison Company for their many suggestions and for providing me with many extra details to enhance the article. My appreciation goes to Mr. H. K. Hoyt, Plant Superintendent of the Dresden Nuclear Power Station, for his efforts and cooperation.

REFERENCES

1. *Hearings Before the Joint Committee on Atomic Energy, Congress of the United States, Ninety-First Congress, Second Session on Civilian Power Reactors, March 11, 1970, Part 3,* pp. 1131-1190, Superintendent of Documents, U. S. Government Printing Office, Washington, 1970.
2. Commonwealth Edison Company, Dresden Nuclear Power

Station, Units 2 and 3, Safety Analysis Report, Vol. 1, USAEC Report DOCKET-50237-17, Nov. 17, 1967.
3. Commonwealth Edison Company, Dresden Nuclear Power Station, Units 2 and 3, Safety Analysis Report, Vol. 2, USAEC Report DOCKET-50237-20, Nov. 17, 1967.
4. Commonwealth Edison Company, Dresden Nuclear Power Station, Unit 2, Semiannual Report, Dec. 22, 1969–June 30, 1970, USAEC Report DOCKET-50237-68, Aug. 28, 1970.
5. Commonwealth Edison Company, Dresden Nuclear Power Station, Unit 2, Special Report of Incident, June 5, 1970, USAEC Report DOCKET-50237-54, July 6, 1970.
6. Commonwealth Edison Company, Dresden Nuclear Power Station, Unit 2, Semiannual Report, July 1, 1970–December 31, 1970, USAEC Report DOCKET-50237-147, Mar. 3, 1971.
7. Commonwealth Edison Company, Dresden Nuclear Power Station, Unit 2, Fast Closure Time of Main Steam Isolation Valve, USAEC Report DOCKET-50237-112, Nov. 27, 1970.
8. Commonwealth Edison Company, Dresden Nuclear Power Station, Unit 2, Abnormal Occurrence Report: Failure of Electromatic Relief Valve To Open During Test, USAEC Report DOCKET-50237-118, Dec. 11, 1970.
9. Commonwealth Edison Company, Dresden Nuclear Power Station, Unit 2, Failure of Main Steam Isolation Valves To Close on Test, USAEC Report DOCKET-50237-117, Dec. 11, 1970.

Suggested Reading List

Commonwealth Edison Company, Dresden Nuclear Power Station, Unit 2, Modification to Inner Screens on Control Rod Drives, USAEC Report DOCKET-50237-40, Apr. 17, 1970.

Commonwealth Edison Company, Dresden Nuclear Power Station, Unit 2, Storage Tank Valve Malfunction, USAEC Report DOCKET-50237-41, Apr. 17, 1970.

Commonwealth Edison Company, Dresden Nuclear Power Station, Unit 2, Control Rod Insertion Time Increase, USAEC Report DOCKET-50237-44, May 14, 1970.

Commonwealth Edison Company, Dresden Nuclear Power Station, Unit 2, Main Steam Isolation Valve Failure [To Close], USAEC Report DOCKET-50237-43, May 18, 1970.

Commonwealth Edison Company, Dresden Nuclear Power Station, Unit 2, Failure of Relief Valves To Open, USAEC Report DOCKET-50237-45, May 22, 1970.

Commonwealth Edison Company, Dresden Nuclear Power Station, Unit 2, Abnormal Occurrence Report: HPCI Steam Line Displaced, USAEC Report DOCKET-50237-47, June 2, 1970.

Commonwealth Edison Company, Dresden Nuclear Power Station, Unit 2, Failure of Electromatic Relief Valve To Open, USAEC Report DOCKET-50237-49, June 8, 1970.

Commonwealth Edison Company, Dresden Nuclear Power Station, Unit 2, Excessive Control Rod Insertion Times, USAEC Report DOCKET-50237-52, June 26, 1970.

Commonwealth Edison Company, Dresden Nuclear Power Station, Unit 2, Low Pressure Coolant Injection System Inoperable, USAEC Report DOCKET-50237-57, July 17, 1970.

Commonwealth Edison Company, Dresden Nuclear Power Station, Unit 2, Excessive Closure Times for Valves 203-2B and 203-2C, USAEC Report DOCKET-50237-59, July 23, 1970.

Commonwealth Edison Company, Dresden Nuclear Power Station, Unit 2, Unexplained Fuel Failures and Excessive Control Rod Scram Times, USAEC Report DOCKET-50237-63, July 31, 1970.

Commonwealth Edison Company, Dresden Nuclear Power Station, Unit 2, Capacity Deficiency in Standby Liquid Control Pumping Circuit, USAEC Report DOCKET-50237-67, Aug. 25, 1970.

Commonwealth Edison Company, Dresden Nuclear Power Station, Unit 2, Correction in High Pressure Coolant Injection System, USAEC Report DOCKET-50237-70, Sept. 10, 1970.

Commonwealth Edison Company, Dresden Nuclear Power Station, Unit 2, Excessive Scram Times for Two Control Rods, USAEC Report DOCKET-50237-77, Sept. 25, 1970.

Commonwealth Edison Company, Dresden Nuclear Power Station, Unit 2, Welding Procedures for Primary System Piping, USAEC Report DOCKET-50237-81, Oct. 16, 1970.

Commonwealth Edison Company, Dresden Nuclear Power Station, Unit 2, Diesel-Generator No. 2/3 Found in Nonperforming Condition for Autostart, USAEC Report DOCKET-50237-100, Feb. 6, 1970.

Commonwealth Edison Company, Dresden Nuclear Power Station, Unit 2 [Excessive Control Rod Scram Times], USAEC Report DOCKET-50237-111, Nov. 27, 1970.

Commonwealth Edison Company, Dresden Nuclear Power Station, Unit 2, Failure of Sodium Pentaborate Solution To Meet Technical Specifications, USAEC Report DOCKET-50237-113, Nov. 30, 1970.

Commonwealth Edison Company, Dresden Nuclear Power Station, Unit 2, Abnormal Occurrence Report: Failure of a Control Rod To Withdraw Properly, USAEC Report DOCKET-50237-119, Dec. 18, 1970.

Commonwealth Edison Company, Dresden Nuclear Power Station, Unit 2, Control Rod Declared Inoperable [as Required by Technical Specifications], USAEC Report DOCKET-50237-120, Dec. 18, 1970.

Commonwealth Edison Company, Dresden Nuclear Power Station, Unit 2, Shutdown by Instrument Air Leak, USAEC Report DOCKET-50237-129, Jan. 8, 1971.

Commonwealth Edison Company, Dresden Nuclear Power Station, Unit 2, Secondary Containment Leak Rate Test Summary, USAEC Report DOCKET-50237-139, Jan. 25, 1971.

Commonwealth Edison Company, Dresden Nuclear Power Station, Unit 2, Abnormal Occurrence Report: Failure of Main Steam Isolation Valve 2D To Close, USAEC Report DOCKET-50237-140, Jan. 29, 1971.

Commonwealth Edison Company, Dresden Nuclear Power Station, Unit 2, High Pressure Coolant Injection Pump Flow Less Than That Specified, USAEC Report DOCKET-50237-141, Jan. 29, 1971.

Operating Experience at the Enrico Fermi Fast Breeder Reactor

By Myrna L. Steele*

Abstract: *Operations and the maintenance and repair activities for the Enrico Fermi Fast Breeder Reactor are summarized for the period from mid-July through December 1970. The material presented updates the article in* Reactor Technology, **14***(2)*.

From July 18 to Dec. 31, 1970, the Enrico Fermi Fast Breeder Reactor generated a total of 12,840 MWh. During that period the core contained the new flow-guarded subassemblies. All nuclear and plant tests of the approach-to-power program were completed on Oct. 16, 1970, with the achievement of the licensed power level of 200 MW(t) and a gross 60 MW(e). Subsequent to the completion of these tests, the plant has been operated intermittently at power levels up to 200 MW(t) to provide additional data and for demonstration purposes.

OPERATIONS SUMMARY

Subsequent to July 18, 1970, low-power physics testing began and continued[1-3] through Oct. 16, 1970. In August, criticality measurements[1] were conducted for several different primary-system temperatures in order to obtain the isothermal coefficient of reactivity. In addition, preoperational tests of the feedwater system were conducted, a cleanup program for the primary sodium system was completed for temperatures up to 700°F, and hydraulic tests were performed at 500 and 700°F to obtain additional information on the electromagnetic flowmeter in the primary sodium system. The data obtained from all these tests corresponded to the original data that were obtained during the 1963–64 startup testing with nonflow-guarded subassemblies.

Early in September the power level[2] was raised above 1 MW(t) for the first time with the core having the flow-guarded subassemblies. When the power level had been increased to about 15 MW(t), it was noted that the indicated power on one of the nuclear channels was about 20% higher than the value obtained by a rough heat balance and by temperature indications. A similar effect had been noted on the source-range channels during the loading of new fuel as old fuel was moved to storage positions at the outer row of the radial blanket. This outer row was acting as a fission plate and was increasing the neutron flux per unit reactor power at the detector. Analyses indicated that, if the detector sensitivity were increased by 2%, the needed 21% reduction in the indicated power level would be achieved. This adjustment was made and was confirmed by subsequent power operation.

A second effect was noted at the 15-MW(t) power level. The thermocouple over inner-radial-blanket (IRB) position N06–N03 indicated a higher temperature than had been predicted, and a detailed study of this position was initiated. Positions adjacent to N06–N03 were also checked. Results of the investigation showed that coolant flow to N06–N03 was not blocked, nor was flow to any adjacent subassemblies blocked. Subassemblies that had higher temperature readings in N06–N03 indicated correct temperatures when moved to other positions. Since the thermocouple readings at N06–N03 are significantly influenced by the coolant flow through the outer radial

*U. S. Atomic Energy Commission, Division of Technical Information Extension, Oak Ridge, Tenn. 37830.

blanket, it was concluded that the thermocouple does not indicate the temperature at the IRB position correctly. When the investigation of the high thermocouple readings had been completed, the approach-to-power program was continued.

The nuclear- and plant-systems-testing programs that were scheduled for two-loop 67-MW(t) operation were completed in September, and, by the end of the month, evaluations of the data that were obtained permitted three-loop 100-MW(t) operation.

Observations of steam-generator performance at the 67-MW(t) level indicated that the addition of orifices had stabilized the units and improved their heat-transfer characteristics. Also, the seal welds that were applied to the tube-to-tube-sheet welds appeared to have reduced the water-to-sodium leakage significantly.

Operation during September was interrupted unintentionally six times. Three of these interruptions occurred the same day because the trip point on the nuclear channels had been set too close to the operating point. The fourth scram resulted when the operator allowed the coolant flow to reach the low-flow trip point while he was adjusting flow values preparatory to going to higher power levels. All operators have been instructed on how to avoid allowing the coolant flow to decrease while they are adjusting pump speeds. The fifth scram resulted when a faulty transmitter gave a false low-flow signal for the secondary sodium system. The false signal caused a single-circuit shutdown and a scram because only two of the three loops were operating. A microphonic chopper in the amplifier was replaced, and the reactor was restarted. The sixth unscheduled scram resulted from a momentary low-flow signal for the secondary sodium system. Since it did not show up on the flow recorder, the signal was assumed to be spurious. After investigations revealed no causes, the plant was restarted.

During oscillator tests[3] at 133 MW(t), the automatic control system started to continuously withdraw the control rod. Control of the reactor was immediately switched to manual, and the 133-MW(t) power level was restored. The repair of a slide wire and an associated amplifier in the control system apparently eliminated the problem.

Subsequent to additional physics testing at 133 MW(t), the approach to 200 MW(t) was again resumed. The turbine was rolled when the reactor reached an indicated 155 MW(t). Most of the 200-MW(t) physics testing was conducted with the turbine on-line. On Oct. 16, 1970, the 200-MW(t) power level was achieved and maintained for 48 hr before it was reduced for further testing.

All nuclear- and plant-systems-test programs[4] were completed in November, and a 5-day full-power demonstration run was completed on November 20. The plant was operated at full power on two additional days in November.

The reactor was started[5] only twice in December 1970. One startup was for low-power testing, and the other one was for a demonstration run at 200 MW(t). Major repairs on the fission-product detector prior to the two December startups included replacing the tape, pulley, and friction block. At the end of the 200-MW(t) run, the power was held at 10 MW(t) for 2.5 hr before the reactor was scrammed from that level. Fission-product-detector response was constant for about 1 hr after the scram and then began decaying with a 3-hr half life, which is characteristic of the ^{85}Kr, ^{85}Rb chain.

MAINTENANCE, MODIFICATIONS, AND REPAIRS

August 1970 (Ref. 1)

The shaft of the No. 2 overflow pump was cleaned and lubricated because the elastomer shaft seals were bound and prevented proper functioning of the pump.

New seals, bearings, and gears were installed in the seal-oil pump for the No. 2 overflow pump.

The failed Freon compressor in the cold-trap room was sent to the vendor for rebuilding.

The suction and discharge valves and the diaphragms were replaced on the compressor for the fission-product detector.

Larger thermal-overload-trip mechanisms were installed in the power feeds to the electrolyte pump motor for the No. 1 liquid rheostat.

Overload heater elements having a higher current rating were installed in four of the safety-rod-extension drives.

A defective actuating coil for the neutron-detector cooling fan was replaced.

A shorted plug shield on the signal cable to the airborne-particulate monitor in the building was repaired.

Two faulty diode doublers were replaced in the high-voltage supply for the airborne-particulate monitor in the containment building.

Faulty resistors were replaced in the regulating-rod velocity indicator.

A defective chopper was replaced in the amplifier of the core-outlet sodium-temperature recorder.

September 1970 (Ref. 2)

The failed drive for one of the safety rods was replaced by a spare, and the failed drive was repaired so that it could be used as a spare.

The armature and field magnet in a safety-rod drive were replaced.

New diaphragms were installed on one of the compressors in the primary cover-gas system.

A burned-out shutter motor was replaced on another cover-gas-system compressor.

New stator windings and bearings were installed in the motor for a waste-gas-system vacuum pump.

New seal bearings, gears, and a key were installed in the motor of a seal-oil pump on one of the overflow pumps.

Four defective diodes and a faulty transistor in the demodulator unit of the reactor-outlet sodium-temperature-monitoring circuit were replaced.

A faulty transmitter amplifier in a secondary sodium-temperature-indicating circuit was replaced.

A defective chopper and capacitor and all the tubes in the amplifier of the primary sodium-temperature recorder were replaced to correct a low gain in the amplifier.

A defective vacuum tube and a faulty zero potentiometer were replaced in the amplifier for the level indicator for the primary sodium tank.

October 1970 (Ref. 3)

New bearings were installed in two of the safety-rod-extension drives, and six of the eight extension drives were cleaned and inspected.

A crack in the pony-motor oil reservoir on a primary sodium pump was welded closed.

A failed coil was replaced in the solenoid shutoff valve which diverts gas to storage tanks.

All valve and cask seals were replaced in the fuel-transport facility, and the drive screws were lubricated.

Teflon piston rings were installed in the actuating cylinders for the fuel-transport-facility grippers.

A damaged transistor was replaced in the reactor-outlet temperature-indicating system.

An amplifier and slide wire were replaced in the servo divider for the automatic control system, and all the connections on the Bailey connector board were resoldered.

A new alarm was installed in the reactor control room to annunciate high discharge pressure from the primary sodium pumps.

November 1970 (Ref. 4)

The motor of the No. 1 pump in the primary sodium system was removed so that the argon-seal assembly could be overhauled. Two pairs of seal faces and the U-cup seals were replaced, the seal-oil pump was replaced, and a vent line with a shutoff valve was installed in the seal cover.

The seal-oil pump on one of the overflow pumps was overhauled.

Valve-operator diaphragms and positioner O-ring seals were replaced in two of the pressure-control valves for the cover-gas system.

A defective transistor amplifier was replaced in a reactor-outlet sodium-temperature-indicating system to restore the resistance-temperature-detector (RTD) readout device to service.

A faulty amplifier in one of the primary sodium-flow transmitters was replaced, and a balanced filter was added to the flow-signal leads to eliminate a noisy flow indication and prevent low-flow shutdown.

A faulty chopper was replaced in the d-c amplifier for the flow-indication system in one of the primary sodium loops.

The control valve and control actuator for the electrolyte temperature in one of the liquid rheostats were replaced, and the temperature controller was adjusted.

December 1970 (Ref. 5)

The malfunction-detection analyzer (MDA) and associated hardware were installed in the main control room.

COLD TRAPPING

The primary sodium system[1] was intermittently cold trapped during the first week in August to maintain the saturation temperature of the sodium to <220°F and the primary-system temperature between 407 and 550°F. On August 10 the primary sodium temperature was raised to about 600°F, and the plugging temperature rose to >300°F. Primary-system temperature was held at 600°F for several days while the sodium was cold trapped to reduce the plugging temperature. When the system temperature was raised to 700°F, the plugging temperature rose to 400°F, but continuous cold trapping had reduced the primary-system plugging temperature to <250°F in 4 days. A total of about 550 hr of cold trapping was required for the primary system in August 1970.

Cold trapping of the secondary sodium loops was required in August as follows: loop No. 1, about 118 hr; loop No. 2, about 31 hr; and loop No. 3, about 28 hr.

In September, 177 hr of cold trapping[2] was required to maintain the maximum saturation temperature of the primary system at 280°F or less. Only secondary loop Nos. 1 and 2 were cold trapped in September. Loop No. 1 was cold trapped for 40.5 hr with a maximum saturation temperature of 350°F, and loop No. 2 was cold trapped for about 240 hr with a maximum saturation temperature of 460°F. The primary system[3] was cold trapped for 235 hr in October with a maximum saturation temperature of 325°F and a system temperature of 530°F. The maximum saturation temperature of 310°F was reduced to <230°F after 80 hr of continuous cold trapping of loop No. 1 of the secondary sodium system. Loop No. 2 was cold trapped intermittently for 147 hr to reduce the saturation temperature from 320 to 230°F. After the steam generator for loop No. 3 was refilled with water and returned to service, loop No. 3 was cold trapped intermittently for 63 hr, and the maximum saturation temperature was reduced from 300 to <220°F. The primary sodium system was cold trapped[4] for 192 hr

in November 1970. The saturation temperature reached a maximum of 300°F with a system temperature of 540°F. The secondary sodium system was cold trapped as follows: loop No. 1, about 91 hr to reduce the saturation temperature from 350 to <240°F; loop No. 2, about 169 hr to reduce the saturation temperature from 370 to <220°F; and loop No. 3, about 121 hr to reduce the saturation temperature from 320 to <220°F. In December 1970 the primary sodium system was cold trapped[5] for 54 hr with a maximum saturation temperature of 240°F and a system temperature of 450°F. Secondary sodium loop Nos. 1 and 3 were not cold trapped, but loop No. 2 was cold trapped for 45 hr with a maximum saturation temperature of 340°F being reduced to 210°F.

REFERENCES

1. Power Reactor Development Company, Enrico Fermi Atomic Power Plant [Operations] Report for August 1970, USAEC Report Docket-50016-88, Dec. 30, 1970.
2. Power Reactor Development Company, Enrico Fermi Atomic Power Plant [Operations] Report for September 1970, USAEC Report Docket-50016-100, Feb. 17, 1971.
3. Power Reactor Development Company, Enrico Fermi Atomic Power Plant [Operations] Report for October 1970, USAEC Report Docket-50016-104, Mar. 25, 1971.
4. Power Reactor Development Company, Enrico Fermi Atomic Power Plant [Operations] Report for November 1970, USAEC Report Docket-50016-108, Apr. 6, 1971.
5. Power Reactor Development Company, Enrico Fermi Atomic Power Plant [Operations] Report for December 1970, USAEC Report Docket-50016-109, Apr. 9, 1971.

SEMINAR ON NUMERICAL REACTOR CALCULATIONS

International Atomic Energy Agency
Vienna, Austria
Jan. 17-21, 1972

Emphasis will be on the numerical calculations that can be made on the smaller computers available in developing countries. Topics will include:

- Mathematical aspects of difference approximations to the transport equations
- Methods based on integral formulation of transport equations
- Convergence and stability of the iterative schemes
- Monte Carlo-type calculations
- Space, energy, and angular synthesis methods
- Time-dependent problems

Nominations for participation will be accepted only if presented by the government of a member state of IAEA.

For information about submission of papers and complete details about the meeting, write to:

In the United States:

Mr. John H. Kane
Special Assistant for Conferences
Division of Technical Information
U. S. Atomic Energy Commission
Washington, D. C. 20545

In other countries:

Mr. H. H. Storhaug
Division of Scientific & Technical Information
International Atomic Energy Agency
Kärntner Ring 11
P. O. Box 590
A-1011 Vienna, Austria

Operating Experience at SEFOR

By Myrna L. Steele*

Abstract: *The highlights of operation of SEFOR from August 1970 to January 1971 are summarized. Maintenance and repair activities for this period are reported. The material presented updates the SEFOR article in* Reactor Technology, **14***(2).*

The material presented below is intended to serve as a digest of events that occurred from August 1970 to January 1971. At the end of this article is a Suggested Reading List of reports pertaining to specific projects or topics. The reader who is interested in data or detailed information should consult those reports. This article reports component or system malfunctions or failures and is intended to update the operating-experience part of the article in *Reactor Technology*, **14**(2). Where available, causes and remedial actions will also be included. However, no evaluations or analyses will be attempted since the reports that contain the detailed data also contain the evaluations and analyses.

By the end of January 1971, the Southwest Experimental Fast Oxide Reactor (SEFOR)[1-4] had generated 15,476 MWh of power, of which 14,138 MWh was generated from August 1970 to January 1971. The maximum power at which the reactor was operated was 17.5 MW(t), and the longest period of continuous reactor operation, to date, was from Dec. 27, 1970, to Jan. 3, 1971. During this period the power-ascension program was conducted through 17.5 MW(t), and the static and oscillator experiments were performed as a part of the overall experimental program.

OPERATIONS SUMMARY, AUGUST 1970–JANUARY 1971

During August the power was raised to 10 MW(t) for the power-ascension program. Reactor availability was 74% for the month. On Aug. 25, 1970, difficulties were encountered with the man-entry-suit system during an operator entry into the refueling cell to remove the positioner motor for repairs. The suit became overinflated, which caused the operator to lose his balance, fall across the reactor-vessel head, and puncture the suit. The operator was immediately assisted from the refueling cell; he sustained no injuries or ill effects. Subsequent investigations revealed that there were no malfunctions of the suit but that overinflation could be produced by pinching off the exhaust hose. More extensive checks revealed that the vacuum-exhaust hoses on the suits were worn at the point where the fitting joined the hose to the backplate of the suit so that a 180° bend caused the hose to flatten and restrict the air flow. The hoses to the suits were replaced, and strain relief was added at the fitting. Forty-five-degree nipples were also added at the cell-wall–pipe-hose connection to alleviate bending at this location.

Reactor operation[1] was unintentionally interrupted five times during August: three scrams were caused by personnel errors, the fourth by a spurious noise spike in the flow controller for the main secondary-system pump, and the fifth by a low-flow signal in the main primary system during flow-oscillation tests. A sixth shutdown, which was intentional, resulted from an alarm that annunciated a primary sodium leak. The signal was spurious, however.

During September, reactor-power ascension was continued through 17.5 MW(t), and reactor availability increased to 80%. On Sept. 12, 1970, with the reactor at 5 MW(t) and Group III static tests under way, a reactor scram occurred at 1355 hr. The flow rate in the main secondary system was being increased by moving

*U. S. Atomic Energy Commission, Division of Technical Information Extension, Oak Ridge, Tenn. 37830.

the set point on the flow controller when a power setback to about 3 MW(t) and an automatic scram reset occurred. An alarm and a recorder indicated a low flow in the main secondary system. The operator initiated a manual scram immediately after the alarm was received, and the reactor was shut down from 3 MW(t). A subsequent investigation showed that the contacts on the main scram-solenoid contactor were opening before the auxiliary contacts through which the current to the coil contactor flows. This produces a relative opening of the contacts on the scram solenoid, and, if a momentary trip signal is received by the scram relay, the voltage will be removed from the scram bus, the main contacts will open, the voltage to the scram bus will be restored, and the main contacts will reclose before the auxiliary contacts open. On September 13 the contacts were adjusted so that the main and auxiliary contact sets opened simultaneously.

A manual reactor shutdown from 10 MW(t) was initiated at 0030 hr on September 20 when the auxiliary primary-system flow decreased to zero. Upon investigation of the smoke in the vicinity of the auxiliary primary-pump power supply, damage was discovered at the point of contact between the coil and brushes in the power supply. When the damage was repaired, the auxiliary primary pump was restored to service.

An alarm annunciating a high vacuum in the reactor vessel was received on September 28. Further inspection of the cover-gas system showed that the vacuum-breaker valve had cycled open as the vent valve in the cover-gas system was opened. The reactor was manually shut down so that the cover-gas pressure could be increased incrementally to determine the pressure necessary to vent the cover-gas system without causing the vacuum-breaker valve to open. The vent pressure was determined to be 9 psig. The vacuum-breaker valve was tested and found to be functioning as it should, and the problem was therefore assumed to be caused by an obstruction in the vent line. With the reactor shut down and the cover-gas pressure at ~1 psig, the high-vacuum alarm was again annunciated. Conditions for the occurrence were identical to those of September 28, and the sequence of events was monitored closely enough to determine that a partial blockage due to sodium oxide existed in the cover-gas inlet line rather than in the outlet line. The inlet line was heated, but the problem persisted; then the atmosphere in the refueling cell was changed to air, and the cover-gas inlet line was removed for cleaning. Sodium oxide was removed from the line with a plumber's snake, the line was returned to service, and the reactor cover-gas system was purged. In the search for the source of oxygen that had been introduced into the cover-gas inlet line, a small leak was noted in the monitor loop of the cover-gas line. This leak was repaired, and a routine leak-check program of the cover-gas monitor system was initiated to ensure leaktightness of the system.

Reactor operation was interrupted on five other occasions in September by unintentional scrams. Noise spikes on the coolant-flow controller were responsible for three of these scrams, another was caused by a spurious high-flux signal on a wide-range monitor (WRM) when the operator switched ranges, and the remaining scram resulted from a low reactor sodium level that occurred while the intermediate heat exchanger (IHX) was being vented.

During October, the static and balanced-oscillator test series was initiated, and oscillator experiments were conducted at power levels through 10 MW(t). Reactor availability was 58%. Subsequent to the installation of new gears to improve the characteristics of the main secondary pump for the flow-oscillation mode, reactor operation was resumed on October 23, and preparations were under way for the first balanced-oscillator tests. About 4 hr after startup, the flow from the secondary pump dropped to 1950 gpm for 10 min, then rapidly increased to 2700 gpm, and then slowly returned to normal. The reactor was shut down for an investigation of the events. The drive motor was realigned, and the system was returned to service for observation. Two shifts later the induction regulator again failed to properly respond to a flow-change signal. Since the problem appeared to be in matching the new gears, these were replaced with the old gears, and the drive motor was also replaced. On October 28, with the reactor at 10 MW(t), manual balanced-oscillator tests were in progress when the set point on the flow controller for the main primary pump was shifted from the cascade position to the remote position. A flow transient, lasting about 6 min and producing temperature changes of about 30°F for inlet and outlet sodium temperatures, resulted from the change of the set position. The reactor was shut down, and the problem was traced to an improperly wired switch. The original purpose of the switch was for selecting a signal from either the manual or the automatic balanced-oscillator equipment; however, the switch had a third, OFF, position. The position that should have been the MANUAL position actually was the OFF position. This caused the flow controller to react as it did when it was switched to the remote position. When the switch was removed and the

equipment was tested, normal flow-controller response was verified for both the remote and cascade modes of operation. The flow controller was modified by the installation of a two-position switch that allows selection of either a manual or an automatic input signal.

Two other unintentional scrams interrupted operations during October. One scram resulted when the terminals on a core-outlet thermocouple were inadvertently shorted, and the second scram occurred when the off-site power supply was lost during a thunderstorm.

On Nov. 2, 1970, the reactor was shut down for 1 month so that the NaK bubbler in the argon-purification system for the refueling cell could be replaced and for routine maintenance of equipment. During this time the ventilation-exhaust valves[3] were tested, and they failed to meet the specified limits of the license-test procedure. A disk-to-seat misalignment, which was caused by a force from the valve-operator linkage, was discovered. The valve disks on both valves were realigned, a new seat was installed on the outer ventilation-exhaust valve, and the linkage on both valves was aligned to eliminate the force that had caused the original misalignment. A subsequent check of the valves confirmed their proper functioning.

Also during the outage an investigation into the observed increase in leakage of reactor cover gas was initiated. Cover gas was leaking past the outer-vessel head seal and carrying some sodium vapor with it. About a quart of condensed sodium was removed from the top of the outer-vessel head beneath the insulation, and the tension in the outer head bolts was checked and found to be lower than expected. The bolts were retensioned, and cover-gas leakage was reduced significantly. It was hypothesized that the original tensioning had not been sufficiently tight; however, special indicators and thermocouples were installed to measure flange temperatures and rotation during a change of sodium temperatures.

Another investigation during the November outage was that of a high-temperature alarm received on October 22 from a thermocouple in the sodium-service system. A short was found between a heater connector and the insulation jacket on an adjacent pipe. The short was intermittent because of pipe movement during temperature changes in the system. At the time the alarm was received, the temperature indicated by the recorder was 875°F, but use of another readout device with the instrument showed that the actual pipe temperature was 1100°F. A malfunction of the recorder had caused a lag in the response of the instrument and prevented annunciation of the alarm at the 875° set point. An inspection of the pipe for signs of intergranular corrosion and distortion gave no indication of damage. Procedures were instituted to preclude any possibility of repetition of the occurrence in the future.

The outage for maintenance ended on Dec. 3, 1970, and the reactor was restarted for additional testing activities.

During December, reactor oscillator experiments were completed at 10 and 15 MW(t). Reactor availability for the month was 44%. On December 12, during routine surveillance tests of the undervoltage relays and of the emergency diesel-generator start and load pickup, the diesel started as it should and supplied power to bus 2A. However, power was not supplied to bus 2C because of a mechanical lockout. Although this mechanical-lockout condition is supposedly actuated only by an overcurrent condition on the bus, no indication of this condition existed. When the local reset button was pushed, power was supplied to bus 2C. Similar occurrences had occurred in the past with bus 2A, although attempts to reproduce the events or identify the cause were not successful. Through repeated testing, it was determined that the diesel did not pick up on bus 2C because the overcurrent-lockout relay was being tripped each time the breaker tripped. The cause of the relay tripping was identified as a loose mounting bolt in the breaker-trip mechanism. Subsequent inspection of the other two 480-V a-c buses, 2A and 2B, revealed that these main feeder breakers also had loose mounting bolts.

Reactor operation was interrupted unintentionally by five scrams during December 1970. On three occasions the reactor was scrammed by a low-flow signal from the main primary system during oscillator tests, the fourth scram was from a spurious signal on one of the WRM channels, and the fifth occurred when one of the instrument panels was accidentally bumped with an instrument cart.

During January 1971, reactor oscillator experiments were completed at 10 and 15 MW(t). Reactor power was increased, and 20 MW(t) operation was achieved on January 29. During this period, reactor availability increased to 93%. On Jan. 17, 1971, the reactor-vessel auxiliary-inlet resistance-temperature detector (RTD) indicated a temperature about 50°F higher than that previously observed and higher than temperatures indicated by the other sodium-temperature sensors. The RTD was judged to be malfunctioning, and the probable cause of malfunction was hypothesized to be a loose connection on the head of the RTD. Since inspection and repair of the RTD

could not be made because of its location and the reactor could be operated safely by using the auxiliary-IHX outlet thermocouple, repair of the defective RTD was scheduled for the next time that the primary sodium equipment area was purged to air.

On January 23 while the proportional band for the main primary flow was being adjusted and reset, a rapid flow increase and a corresponding power increase occurred. The reactor was shut down, and attempts were made to reproduce the flow transient without success. Since no malfunctioning or defective equipment or circuits could be found, testing activities were continued. In January 1971, two unintentional scrams occurred during oscillator testing because of improper adjustments to the oscillator.

MAINTENANCE, REPAIRS, AND MODIFICATIONS

August–October 1970 (Refs. 1 and 2)

Capacitors were added to improve the power factor of the power supply for the auxiliary primary pump.

The speed reducer for the oscillator-positioner motor was replaced.

The reactor-vessel sodium-level probes were removed, cleaned, and reinstalled.

The rectifier in the 26.5-V d-c battery charger was replaced.

The armatures in the power supply for the auxiliary primary-pump and sodium-pipe-heater circuits were replaced.

Switches were installed in the control circuits for the manual operation of valves for the Freon desuperheater.

A test fixture was fabricated for the rupture disks for the Fast Reactivity Excursion Device (FRED).

November 1970–January 1971 (Refs. 3 and 4)

The purification system for the refueling-cell argon was replaced.

Auxiliary exhaust piping was installed in the man-access-suit system, and new air-supply and exhaust hoses were installed.

A second reactor-vessel sodium-level probe was replaced with one of a new design.

A pressure switch and an isolation valve were installed on the inlet line of the cover-gas monitor loop.

A check valve was installed on the outlet line of the cover-gas monitor loop.

ACKNOWLEDGMENT

I would like to express my gratitude to Dr. G. R. Pflasterer of General Electric's Breeder Reactor Development Operation for his continuing cooperation in reviewing this series of articles and for providing many details and suggestions needed to make the articles more complete.

REFERENCES

1. General Electric Company, Southwest Experimental Fast Oxide Reactor, Quarterly Plant Operations Report No. 6, August 1–October 31, 1970, USAEC Report Docket-50231-64, Jan. 4, 1971.
2. G. R. Pflasterer and R. A. Becker (Comps.), Southwest Experimental Fast Oxide Reactor Development Program, Twenty-Sixth Quarterly Report, August–October 1970, USAEC Report GEAP-10010-26, General Electric Company, November 1970.
3. General Electric Company, Southwest Experimental Fast Oxide Reactor, Quarterly Plant Operations Report No. 7, November 1, 1970–January 31, 1971, USAEC Report Docket-50231-74, Apr. 8, 1971.
4. G. R. Pflasterer and R. A. Becker (Comps.), Southwest Experimental Fast Oxide Reactor Development Program, Twenty-Seventh Quarterly Report, November 1970–January 1971, USAEC Report GEAP-10010-27, General Electric Company, February 1971.

Suggested Reading List

D. T. Ikeuye and F. E. Young, Fabrication of Non-Fuel Core Components for SEFOR, USAEC Report GEAP-13595, General Electric Company, February 1970.

R. A. Meyer, S. L. Stewart, E. R. Craig, A. B. Reynolds, and M. L. Johnson, Design and Analysis of SEFOR Core I, USAEC Report GEAP-13598, General Electric Company, April 1970.

E. R. McKeehan, Design and Testing of the SEFOR Fast Reactivity Excursion Device, USAEC Report GEAP-13649, General Electric Company, October 1970.

General Electric Company, Southwest Experimental Fast Oxide Reactor, Malfunction of the Emergency Electrical System Tie Breakers, USAEC Report Docket-50231-52, Aug. 5, 1970.

General Electric Company, Southwest Experimental Fast Oxide Reactor, Malfunction of an Emergency Electrical System Circuit Breaker, USAEC Report Docket-50231-62, Dec. 22, 1970.

General Electric Company, Southwest Experimental Fast Oxide Reactor, Summary of Results from Testing of the Fast Reactivity Excursion Device, USAEC Report Docket-50231-77, Apr. 12, 1971.

General Electric Company, Southwest Experimental Fast Oxide Reactor, Malfunction of Reactor Vessel Overflow Line Valve and Safety System Relay, USAEC Report Docket-50231-78, Apr. 16, 1971.

Summary of Conference on Fast Reactor Fuel-Element Technology

By Myrna L. Steele*

Abstract: *Summarized are the papers and information presented at the Conference on Fast Reactor Fuel-Element Technology held in New Orleans, La., Apr. 13–15, 1971.*

The Conference on Fast Reactor Fuel-Element Technology was held in New Orleans, La., Apr. 13–15, 1971. The meeting was sponsored by the Materials Science and Technology Division of the American Nuclear Society. The summary presented below is based on the writer's notes from that meeting and from copies of some of the papers. Summaries of the papers appear in Supplement No. 1 to Vol. 14 of the *Transactions of the American Nuclear Society*. The supplement is available from the American Nuclear Society, 244 Ogden Avenue, Hinsdale, Ill. 60521. The proceedings of the meeting will be published by the end of 1971. Titles and authors of the papers are listed in Table 1.

KEYNOTE ADDRESS

The objective of the conference was to provide a basis for assessing progress and for identifying needed advances in the field. The keynote speaker, E. E. Kintner, centered his remarks around that objective and used the Nine Circles of Hell from Dante's *Inferno* as an analogy. In characterizing the problem areas of the liquid-metal-cooled fast breeder reactor (LMFBR) fuel-element design as a torment, or Circle of Hell, to be overcome, Kintner outlined clearly the tenor of data and problems to be presented in the ensuing 3 days. In addition to describing the problems, Kintner also outlined causes and proposed remedial solutions. He noted that, even though research on stainless steel–oxide fuels had been under way for at least 20 years, there was only semiarbitrary data and no design base for the design of a Fast Test Reactor (FTR) fuel element. According to Kintner, some of the problems in designing an LMFBR fuel element result from lack of the following: good data on fission-gas pressure and release, engineering definition of thermal capability, definitive data on effects of smear density on core lifetime, data on the effects of geometry of pellets, materials understanding of core-restraint effects, a concentrated program on materials swelling or behavior, good data on corrosion and on the cladding–fuel reaction, and data on transients and safety. Kintner ended his keynote address with the following suggestions as to how the program of LMFBR fuel development can be more fruitfully conducted: the program should be more cohesive and synergistic and less competitive; the important remaining questions should be defined, and efforts should be concentrated on them; bolder, broader, and better organized attacks should be conducted on key problems; design requirements should be more forcefully articulated; test environments should be more accurately defined; test conditions should be more closely delimited to power-reactor operating conditions; time and coordination of efforts and reporting are needed; and, finally, the proper leadership should be provided at all levels.

FUEL-ELEMENT DESIGN

Burgess and French, in discussing the design-to-procurement phases for an FTR fuel pin, first outlined

*U. S. Atomic Energy Commission, Division of Technical Information Extension, Oak Ridge, Tenn. 37830.

Table 1 Conference on Fast Reactor Fuel-Element Technology

Paper title	Author	Affiliation
I. KEYNOTE SESSION		
LMFBR Fuel Design—Why Can't We Do Better?	E. E. Kintner	USAEC–DRDT
II. FUEL-ELEMENT DESIGN, L. R. KELMAN, CHAIRMAN		
Evolution: FTR Fuel-Pin Design to Procurement	C. A. Burgess P. M. French	WADCO Westinghouse, Advanced Reactors Division
Fuel-Rod Design Bases for the Westinghouse Demonstration Plant	C. A. Anderson, Jr. R. A. Markley J. F. Patterson	Westinghouse, Advanced Reactors Division
Fuel Design for the AI LMFBR Demonstration Plant	L. Bernath W. B. Wolfe	Atomics International
Challenges in Development of Materials for Fast Reactors—Can We Really Do Better?	G. Karsten	Karlsruhe Nuclear Research Center
Consideration of Stabilized Stainless-Steel Alloys for LMFBR Fuel Cladding	C. N. Spalaris E. L. Zebroski	General Electric, Breeder Reactor Development Operation
III. FUEL-ELEMENT-BEHAVIOR MODELING, L. A. NEIMARK, CHAIRMAN		
Important Mechanisms in the Explanation of Cladding Diametral Increases in Mixed-Oxide Fuel Pins	S. Oldberg, Jr. D. P. Hines	General Electric, Breeder Reactor Development Operation
Mixed-Oxide Fuel-Pin Performance Analysis Using the OLYMPUS Computer Code	A. Boltax A. M. Biancheria B. L. Harbourne G. P. Soffa	Westinghouse, Advanced Reactors Division
Fine Tuning of an FBR Fuel-Modeling Code	M. E. Nathan R. N. Schweinberg	Atomics International
Practical Results on Fast Reactor Oxide Fuel-Pin Development and Modeling Activities	G. Karsten K. Kummerer D. Geithoff H. G. Kämpf	Karlsruhe Nuclear Research Center
Analysis of Mixed-Oxide Fuel-Element Irradiations Using the LIFE-I Computer Code	V. Z. Jankus R. W. Weeks	Argonne National Laboratory
Comparison of F-MODEL Predictions with EBR-II Irradiation Data	F. J. Homan W. H. Bridges W. J. Lackey C. M. Cox	Oak Ridge National Laboratory
Comparison of Measured and Predicted Performance of Stainless-Steel-Clad Mixed-Oxide Fuel Pin in a Fast Reactor	R. J. Jackson R. D. Leggett J. W. Weber L. A. Pember	WADCO
IV. FUEL MECHANISMS AND PROPERTIES, A. M. BIANCHERIA, CHAIRMAN		
1. Fuel Swelling		
Swelling and Gas-Release Models for Oxide Fuels	F. A. Nichols H. R. Warner H. Ocken S. H. Leiden	Westinghouse, Bettis Atomic Power Laboratory

Table 1 (Continued)

Paper title	Author	Affiliation
IV. FUEL MECHANISMS AND PROPERTIES (Continued)		
1. Fuel Swelling (Continued)		
Fuel Swelling—Fast Reactor Mixed-Oxide Fuels	R. N. Duncan D. A. Cantley K. J. Perry R. C. Nelson	General Electric, Breeder Reactor Development Operation
An Advanced Gas Release and Swelling Subroutine	R. B. Poeppel	Argonne National Laboratory
Swelling of Oxide Fuels at High Temperatures	W. Chubb R. F. Hilbert V. W. Storhok D. L. Keller	Battelle–Columbus Laboratories
2. Thermal Performance		
Thermal-Performance Limits for Fast Reactor Oxide Fuels	J. A. Christensen	WADCO
Effects of Burnup on Fuel-Pin Thermal Performance	A. M. Biancheria U. P. Nayak M. S. Beck	Westinghouse, Advanced Reactors Division
Thermal Performance of Fuel Rods and the Performance of LMFBRs	C. W. Sayles M. E. Nathan	Atomics International
3. Fuel–Cladding Reactions		
Fuel–Cladding Reactions in Irradiated Mixed-Oxide Fuels	C. E. Johnson C. E. Crouthamel	Argonne National Laboratory
Fuel–Cladding Reactions in Stainless-Steel-Clad Mixed-Oxide Fuel-Pin Irradiations	K. J. Perry G. F. Melde R. N. Duncan	General Electric, Breeder Reactor Development Operation
Observations of Fuel Cladding/Chemical Interactions as Applied to Gas-Cooled Fast Breeder Reactor Fuel Rods	R. B. Fitts E. L. Long, Jr. J. M. Leitnaker	Oak Ridge National Laboratory
4. Fuel–Sodium Reactions		
Reaction of Sodium with Mixed-Oxide Fuels	E. A. Aitken S. K. Evans G. F. Melde B. F. Rubin	General Electric Company
Sodium–Fuel Interactions	P. E. Blackburn A. E. Martin J. E. Battles P. A. G. O'Hare W. N. Hubbard	Argonne National Laboratory
V. MIXED-OXIDE FUEL PERFORMANCE — I, W. E. BAILY, CHAIRMAN		
FTR Driver Fuel-Development Program Status	E. E. Roake J. Hansen	WADCO
Performance of Mixed-Oxide Fuel Elements—ANL Experience	L. A. Neimark C. E. Dickerman J. D. B. Lambert W. F. Murphy	Argonne National Laboratory

(Table continues on the next page.)

Table 1 (Continued)

Paper title	Author	Affiliation
V. MIXED-OXIDE FUEL PERFORMANCE (Continued)		
Steady-State Irradiation Performance of UO_2, PuO_2 Fast Reactor Fuels	C. N. Craig K. J. Perry R. N. Duncan C. N. Spalaris	General Electric, Breeder Reactor Development Operation
In-Reactor Restructuring Temperatures and Kinetics for $(U,Pu)O_2$	A. R. Olsen R. B. Fitts W. J. Lackey	Oak Ridge National Laboratory
Spatial Distribution of Intergranular Porosity in an EBR-II-Irradiated Mixed-Oxide Fuel Element	D. C. Bullington R. D. Leggett	WADCO
Behavior of Mixed-Oxide $(U,Pu)O_2$ Fuels During Irradiation	R. M. Carroll O. Sisman	Oak Ridge National Laboratory
Distribution of Gaseous Fission Products in Irradiated Mixed-Oxide Fuels	C. E. Johnson D. V. Steidl C. E. Crouthamel	Argonne National Laboratory
VI. MIXED-OXIDE FUEL PERFORMANCE—II, G. W. CUNNINGHAM, CHAIRMAN		
Fission-Gas Release from Failed Fuel Rods in Liquid-Metal-Cooled Fast Breeder Reactors	M. D. Carelli R. D. Coffield, Jr.	Westinghouse, Advanced Reactors Division
Fuel-Dynamics Experiments on Fast Reactor Oxide Fuel Performance Under Transient Heating Conditions Using the TREAT Reactor	C. E. Dickerman L. W. Deitrich L. E. Robinson A. B. Rothman J. C. Carter	Argonne National Laboratory
Response of an EBR-II-Irradiated Mixed-Oxide Fuel Pin to an Overpower Transient in TREAT	G. E. Culley R. D. Leggett F. E. Bard	WADCO
Oxide Fuel Behavior During Transient Overpower Conditions	G. R. Thomas J. H. Field	General Electric, Breeder Reactor Development Operation
Performance of Sphere-Pac and Pelletized $(U,Pu)O_2$ During Severe Overpower Conditions	C. M. Cox D. R. Cuneo E. J. Manthos	Oak Ridge National Laboratory
Irradiation Testing of Fast Breeder Reactor $(U,Pu)O_2$ Fuels	J. R. Lindgren P. W. Flynn N. L. Baldwin	Gulf General Atomic
	R. B. Fitts A. W. Longest	Oak Ridge National Laboratory
VII. PERFORMANCE OF ADVANCED FUELS. W. K. MARTIN, CHAIRMAN		
Performance Capability of Advanced FBR Fuel	T. N. Washburn J. L. Scott	Oak Ridge National Laboratory
Swelling of UC and UN at High Temperatures	R. F. Hilbert V. W. Storhok W. Chubb D. L. Keller	Battelle–Columbus Laboratories
Unrestrained Swelling of Fission-Gas Release Experiments of Fast Reactor Fuels	C. Grando M. Montgomery A. Strasser	United Nuclear Corporation

Table 1 (Continued)

Paper title	Author	Affiliation
VII. PERFORMANCE OF ADVANCED FUELS (Continued)		
Mixed-Nitride Fuel-Irradiation Performance	A. A. Bauer J. B. Brown E. O. Fromm V. W. Storhok	Battelle–Columbus Laboratories
Thermal and Fast Irradiation of Sodium-Bonded (U,Pu)C Fuel and Fuel Elements	J. C. Clifford J. O Barner R. L. Cubitt D. C. Kirkpatrick	Los Alamos Scientific Laboratory
Effects of Irradiation on (U,Pu)C Fuel Rods to 65,000 MWd/ton Burnup	A. Strasser M. Montgomery R. Powers	United Nuclear Corporation
The Irradiation Behavior of Sodium-Bonded (U,Pu)C Fuel Pins	B. L. Harbourne P. J. Levine A. M. Biancheria	Westinghouse, Advanced Reactors Division
	T. W. Latimer L. A. Neimark	Argonne National Laboratory
VIII. WRAP-UP SESSION, A. A. BEMENT, CHAIRMAN		
Fuel-Element Design Session	L. R. Kelman	Argonne National Laboratory
Fuel-Element-Behavior Modeling Session	L. A. Neimark	Argonne National Laboratory
Fuel Mechanisms and Properties Session	A. M. Biancheria	Westinghouse, Advanced Reactors Division
Mixed-Oxide Fuel Performance—Session I	W. E. Baily	General Electric, Breeder Reactor Development Operation
Mixed-Oxide Fuel Performance—Session II	D. Moss	USAEC, Idaho
Performance of Advanced Fuels Session	W. R. Martin	Oak Ridge National Laboratory

the program for the driver assemblies. Burgess, in presenting the paper, showed the areas where the emphasis had been, and he discussed plans for future work areas. He was the first of many to emphasize *good* quality control in the fabrication of fuel pins and stated firmly that there must be rigorous control of the oxygen-to-metal (O/M) ratio. Burgess then showed some of the effects of not controlling the O/M ratio. He discussed many of the problems that had been encountered during FTR fuel-pin design and development, outlined the solutions that have evolved, and summarized some areas where efforts still need to be applied.

Anderson described the fuel-element design for the conceptual Westinghouse LMFBR Demonstration Plant. He discussed the semistatistical method used in the engineering analysis of such parameters as hot-channel and hot-spot factors, fuel-temperature profiles, and effects of cladding strain and showed how the fuel-failure probabilities were generated from these cladding-strain and rupture-strain data. Anderson then discussed the two different failure criteria that are applied: (1) cladding strain in a reactivity-insertion type of accident, where cladding strain is determined as a function of the amount of molten fuel, and (2) the loss-of-coolant-flow transient, where cladding stress is a function of cladding temperature. He then showed how calculations of this type had gone into the design of the fuel elements for the proposed Westinghouse LMFBR Demonstration Plant. Bernath, in presenting his paper on the Atomics International fuel-pin design, discussed in fairly general terms the world experience with oxide fuels and then drew on this base to describe the underlying philosophy and to present data on the fuel-element design for the Atomics International conceptual LMFBR Demonstration Plant.

Karsten discussed the fuel-element testing that has been done in the FR-1 reactor at Karlsruhe and the work that is now being done in the BR-2 reactor in Belgium. In summarizing the data from fuel-element-irradiation testing, he also noted a small amount of data on operation of a reactor having a failed fuel pin. Karsten reported some preliminary data from the German program for developing a cladding material that is better than 316 stainless steel, and he recommended the use of stabilized stainless steels as cladding materials so as to achieve greater burnups. He stressed the economic gains that are available from carbide and nitride fuels but predicted a 5- to 10-year research effort on carbide fuels before any final decision can be made relative to their utility. Spalaris of General Electric pointed out the serious carbon losses that have been noted in unstabilized stainless steel with an accompanying loss in ductility. He also said that, since the carbon-loss rate is temperature dependent, this effect is expected to be more important in end-of-life conditions.

FUEL-ELEMENT-BEHAVIOR MODELING

A paper by Oldberg and Hines described the BEHAVE codes used for determining fast reactor fuel-element behavior at General Electric. Hines, in presenting this paper, discussed the various types of data needed for the code and gave descriptions of how each physical factor was modeled mathematically. He compared some measured diametral changes for fuel pins that were irradiated in the Experimental Breeder Reactor II (EBR-II) with results from the BEHAVE codes.

Boltax, in presenting the paper by Boltax, Biancheria, Harbourne, and Soffa, described the OLYMPUS-code system used by Westinghouse for analyzing fuel-pin performance. Boltax characterized OLYMPUS as a modular code and then showed how each module was defined and how each interacted with the other modules. He described the irradiation-behavior module as being based on the WADCO–WARD theta equation for the void swelling of solution-treated cladding and the fuel-swelling module as being based on the thesis that swelling occurs from the cladding inward. Boltax attributed the cause of hydrostatic-stress-induced volume changes to irradiation creep and postulated a new phenomenon above ~550°F as "stress-induced void growth." The OLYMPUS code is normalized to high burnups, whereas the BEHAVE codes are normalized to low burnups. The PROFIT code, used at Atomics International for LMFBR fuel-element-behavior modeling, is empirically oriented and utilizes volumetric heat-generation rates as the basic input device.

Nathan presented the paper by Nathan and Schweinberg and compared results of PROFIT calculations with measured values for such parameters as equiaxed- and columnar-grain growths, fuel restructuring, and percent fission-gas release. He detailed the procedures for tuning the code to a given empirical parameter and then using the tuned code to determine the behavior of a fuel element in a given irradiation environment. The PROFIT code, like the OLYMPUS code, is normalized to high burnup.

Kummerer began the presentation of the paper by Karsten, Kummerer, Geithoff, and Kämpf by outlining the earlier fuel-pin-modeling activities and the assumptions for the SATURN-0 code, which is used at Karlsruhe. He discussed the three separate ranges of temperatures for which calculations are performed, i.e., the plastic range ($t > 1700$°C), the creep range ($750° < t < 1300$°C), and the low-temperature range. Kummerer described the SATURN-1 code as differing from SATURN-0 in that SATURN-0 does not include assumptions and calculations for fuel–cladding interactions and volume balances; SATURN-1 computes the whole time history of the fuel element, including transients. He outlined the basic assumptions and then presented some calculations for the Southwest Experimental Fast Oxide Reactor (SEFOR) fuel pins in which the thermomechanical behavior was computed as a function of time. Kummerer also reported that the effects of friction of the expanding fuel against the cladding were just now being recognized and had not been taken into consideration yet.

The LIFE-I computer code, discussed in the paper written by Jankus and Weeks of Argonne National Laboratory (ANL) and presented by Jankus, is based on mathematical representations of the parameters that affect fuel-element behavior. Jankus described LIFE-I as a code that follows the power and coolant-temperature history to determine fuel-element performance. He compared the results of LIFE-I computations with measurements for EBR-II fuel elements and discussed the effects of variation of design parameters and uncertainties on the predictions made by the code.

Homan, Bridges, Lackey, and Cox of Oak Ridge National Laboratory (ORNL) compared predictions of their FMODEL code with EBR-II experiments. The FMODEL code analytically simulates the physical parameters affecting fuel-element behavior and determines the major sources of cladding strain. Detailed comparisons of the data were presented.

Comparisons of measured and predicted diametral increases in fuel pins that were irradiated to a calculated peak burnup of 45,000 MWd/ton in the EBR-II were detailed in a paper by Jackson, Leggett, Weber, and Pember of WADCO. The WADCO–WARD theta equation was used for determining cladding swelling, and cladding temperatures were calculated from the SINTER code.

FUEL MECHANISMS AND PROPERTIES

Nichols of Bettis, in presenting the paper written by Nichols, Warner, Ocken, and Leiden, described a method for determining fuel swelling by analysis of bubble migration. BUBL-1 is based on a statistical accounting of bubble migrations, although Nichols noted that some data, basic to the program, were "guesstimates." Nichols characterized four categories of bubbles as those trapped at dislocations, those in transit from the dislocations, those trapped at grain boundaries, and those which are freed and no longer contribute to swelling. After presenting some data from calculations using BUBL-1, he then proceeded to point out its shortcomings and briefly described the remedial measures that were being taken.

Duncan described the efforts at General Electric Company's Breeder Reactor Development Operation (GE–BRDO) as taking a "macroscopic look at swelling." In presenting the paper by Duncan, Cantley, Perry, and Nelson, Duncan outlined the total approach used at GE–BRDO to simulate fuel swelling and then further discussed each concept. He stated that the calculations were based on EBR-II data and suggested the following distinctions in swelling: that attributed to fuel-density changes, that attributed to fuel-volume changes to include porosity and cracks, and that attributed to volume changes in the fuel envelope bounded by the cladding. Duncan proposed that, because of possible confusion from ambiguities in the fuel-swelling terminology, all persons who reported fuel-swelling data in the future should be very careful to define *what* they are reporting. He presented values for fission-gas release as a function of burnup and as a function of fuel density. The data were obtained from mixed-oxide fuel pins that were irradiated to 1×10^5 MWd/metric ton in the EBR-II. Duncan, like Kummerer of Karlsruhe, reported difficulties in interpreting heat-transfer data because of a friction factor. Duncan reported that 100% of the fission gas was released at about 10^5 MWd/metric ton and that there was a net volume decrease after this burnup.

In presenting his paper on a subroutine (GRASS) for calculating bubble-size distributions as a function of position in the fuel, Poeppel discussed the mechanisms of bubble production, growth, resolution, and release. He also described the LIFE computer-program input to GRASS (Gas Release And Swelling Subroutine) and the parameters which the subroutine computed for its own use.

Keller, in presenting a paper by Chubb, Hilbert, Storhok, and Keller, discussed results from high-temperature-induced fuel-swelling experiments that have been conducted by Battelle–Columbus Laboratories. He presented data from tungsten–rhenium-clad mixed-oxide fuels that had been irradiated to about 10^{20} fissions/cm^3 and whose cladding-surface temperatures ranged from 1260 to 1900°C. Keller then described not only the postulated mechanisms of the swelling but also the variations in swelling as a function of temperature. He discussed the so-called plastic core of oxide fuels that are operated at high cladding-surface temperatures and commented on the effects that this would have on the predictability of fuel behavior under reactor transient conditions.

Christensen, in discussing design and operating limits of LMFBR fuel, said that oxides were chosen as the fuel for the FTR 5 years ago because of the available experience and technology but that since then a number of factors have been discovered to have a significant effect on thermal-performance characteristics. He pointed out that the bulk of experience with oxides had been gained from light-water reactors (LWRs) and outlined the basic differences in fuel-performance demands made by the LWR and the LMFBR. Christensen then described the effects on LMFBR performance for each of the basic differences. He said that

- No significant self-shielding occurs for a fast breeder reactor (FBR), although the inward migration of the plutonium *might* reduce heat ratings.
- The thermal conductivity is very difficult to measure in an FBR environment, and data are sparse (although the understanding is adequate for most purposes).
- Structural effects resulting from preslugging of FBR fuel impose significant penalties on heat ratings.
- Although the present operating criterion is an upper limit of FBR fuel melting, operation with molten fuel might require only modified operating procedures.
- Higher burnup of FBR fuel causes a greater depression in the melting temperature.

• As compared to LWRs, FBR fuel-surface temperatures are increased because of a higher heat flux and a higher coolant temperature and are decreased because of improved (over LWRs) coolant-to-cladding heat transfer and better thermal conductivity of cladding.

• Restructuring of FBR fuels causes lower fuel densities that increase the central void size and enhance the thermal conductivity.

• Higher surface temperatures increase the fraction of fuel that is restructured, and higher thermal gradients may stimulate more restructuring.

Christensen noted a net reduction of 25 to 30% in the thermal rating for FBR fuels. He also characterized the need for better gap-conductance data as desperate.

Nayak, in presenting a paper by Biancheria, Nayak, and Beck, discussed the effects of the burnup-induced changes in chemical and physical properties on fuel-pin performance. He described the effects of gap closure at the beginning of fuel life and presented data that show the effects of dilution, gas conductance, and internal pressure on gap conductance. Sayles, who presented the paper written by Sayles and Nathan, used a different approach and considered fuel-rod thermal performance in the LMFBR plant as a whole. He established, as an example, a probability of 0.9913 that no more than 0.1% of all fuel elements in the reactor have molten centers at high-power operation and then used reliability-margin analysis to assess the amount of reactor downtime attributable to fuel-element failures and problems associated with these failures.

Crouthamel, in presenting a paper by Johnson and Crouthamel, discussed the two largest effects that have been noted in fuel–cladding reactions in stainless-steel-clad, irradiated mixed-oxide fuels. He characterized the first effect as the transport of cladding constituents into the hot fuel interior and the second effect as grain-boundary attack. He also presented probable causes of the fuel–cladding reactions and contrasted data from high- and low-density fuels.

A paper by Perry, Melde, and Duncan (presented by Perry) included additional data and analyses on fuel–cladding reactions in stainless-steel-clad, mixed-oxide fuel pins. Perry discussed effects of temperature, fuel burnup, and fission rate on the fuel–cladding reaction and showed the extent of cladding penetration by means of metallographic slides. He stated that insufficient data are available for assessing the effects of type of cladding, oxygen-to-metal (O/M) ratio in the fuel, fuel-fabrication technique, and cladding stresses and that end-of-fuel-life data are sparse and inadequate.

Fitts, in presenting a paper by Fitts, Long, and Leitnaker, gave some results of fuel–cladding reaction experiments on fuels for gas-cooled fast breeder reactors (GCFRs). He presented data on pellet, annular, and Sphere-Pac fuels having claddings of 304 and 316 stainless steels and Hastelloy X. Fitts reported three effects from the fuel–cladding reaction to be subsurface porosity, intergranular penetration, and surface reaction layers.

Aitken presented a paper that was coauthored by Aitken, Evans, Melde, and Rubin in which he discussed the reaction of sodium with mixed-oxide fuels. He said that the sodium oxide formed is generally of the hyperstoichiometric form and that the oxygen for this product can come from an O/M ratio in the fuel that either is initially too high or increases from the burnup process. He also reported that 1.91 seems to be a lower limit of O/M ratio for the formation of hyperstoichiometric sodium oxide. Aitken presented data for maximum observed fuel swelling as a function of oxygen available for the sodium reaction with the fuel and for swelling as a function of time in the reactor for failed fuel. He said that sodium-bonded fuels react more predictably and that there is an indication from fuel data from the Dounreay Fast Reactor that flowing sodium may mitigate some of the fuel swelling. He then summarized the state of knowledge of fuel–sodium reactions as follows: The form of the compound resulting from the fuel–sodium reaction is now known, and fuel swelling results from the sodium penetrating the fuel. He proposed a $(\text{time})^{1/4}$ dependence of swelling and indicated a need for experiments to determine the rate at which oxygen can be transported from the corrosion area.

A paper by Blackburn, Martin, Battles, O'Hare, and Hubbard described the research program that is under way at ANL on the interactions between sodium and $(U, Pu)O_2$ fuels. Blackburn presented the paper, showing phase diagrams and identifying the equilibrium compound as Na_3MO_4 (where the M stands for metal, i.e., uranium or plutonium). He reported that micrographs show the Na_3MO_4 compound as occurring mostly on surfaces and cracks and that UO_2–PuO_2 pellets, when reacted with sodium, show both weight and volume gains as a function of time reacted with sodium.

MIXED-OXIDE FUEL PERFORMANCE— I. STEADY-STATE BEHAVIOR

The FTR driver-fuel-development program, detailed in a paper written by Roake and Hansen and

presented by Hansen, very clearly illustrates many of Kintner's torments (see the "Keynote Address" section above). Hansen began by saying that WADCO is committed to a statistical treatment of fuel-pin data and that all the testing for their statistical analyses will be thoroughly documented. He briefly summarized the irradiation testing activities that are either planned or under way and then gave a few highlights of some of the programs. He showed slides of the fuel pins that are to be tested in the instrumented subassembly (ISA) in the EBR-II and described a new kind of fuel pin that is being fabricated for testing. Since problems have been encountered with gap-conductance data, a new test is aimed at determining these values. Hansen pointed out that WADCO's problem in testing vendor fuel for the FTR is the unavailability of an irradiation environment. He summarized the planned tests for obtaining more driver-fuel data.

The ANL experience with mixed-oxide fuel-element performance was discussed in a paper by Neimark, Dickerman, Lambert, and Murphy and was presented by Lambert. He reported on studies with both encapsulated and unencapsulated fuel elements, noting that the cladding strain is larger than predicted in some of the experimental elements. He theorized that this larger strain is caused by fission-gas pressure in addition to fuel swelling and said that the fission-gas release approaches 100% with higher burnup. He indicated that fuel melting will be mitigated by heat transfer when the fuel contacts the cladding and that this fuel–cladding contact will occur for even large diametral gaps because the fuel swells rapidly. Lambert also reported some results indicating that the swelling rate of the cladding exceeds that of the fuel for elements irradiated to 6 to 8 at.% burnup because the gap seems to increase.

A paper written by Craig, Perry, Duncan, Appleby, Spalaris, and Baily was presented by Craig and reported data on mixed-oxide fuels irradiated to over 1×10^5 MWd/metric ton. Craig discussed the plutonium redistribution observed in fuel pins where center melting occurs. He noted that a significant reduction in conductivity occurs as the O/M ratio is reduced and presented data indicating that most fission gas is released at high burnups.

Olsen, in presenting the paper by Olsen, Fitts, and Lackey, discussed the mechanisms and parameters that affect restructuring of mixed-oxide fuel while it is in the reactor. He listed the parameters and stated that, to date, no temperature limits have been established on equiaxed grain growth. Data and micrographs were shown to illustrate the processes of restructuring and the effects of temperature on the restructuring. Olsen also discussed the transport of actinides during restructuring and the probable location of their deposition. He defined vapor deposition as an early-life restructuring process and stated that this early-life restructuring has a time dependence.

Bullington, in presenting a paper by Bullington and Leggett, discussed fuel experiments with fission rates of 2.5×10^{13} to 6×10^{13} fissions/sec which are designed to measure the distribution of intergranular porosity. He presented micrographs showing pore and void concentrations and gave results of analyses of the data that were obtained in this manner.

In presenting a paper by Johnson, Steidl, and Crouthamel, Johnson gave data on the fission-product distribution and retention in mixed-oxide fuels. He described the laser-microscope sampling system used in determining the fission-product distributions and presented data obtained for both Vibrapacked- and pellet-type fuels. Johnson reported that some difficulties are involved in using this laser-microscope technique in the unrestructured and equiaxed grain regions, although very good reproducibility can be obtained in the columnar-grain region. He briefly discussed the effects of fission-gas distribution and retention on fuel behavior and fuel life.

MIXED-OXIDE FUEL PERFORMANCE— II. TRANSIENT BEHAVIOR

Coffield, who presented the Carelli–Coffield paper on fission-gas ejection, characterized fission gas as about 87% xenon, 10% krypton, and 3% helium and stated that, if the size of holes in the cladding through which this fission gas might be discharged were 10^{-4} to 10^{-5} in.^{2}, then the adjoining pins can possibly be damaged by fission-gas blanketing. He presented data on internal pressure in the pin and gas-ejection velocity from the pin as a function of time from the rupture. After about 1 min the gas ejection becomes subsonic. Coffield described what would happen when this ejected gas blanketed a surface area on an adjacent pin and discussed the temperature response of the blanketed areas. He stated that, at most, two additional pin failures would occur near the originally failed pin and that these would fail by a fission-gas jet impinging on an adjacent fuel, thus drying out the cladding and blocking heat transfer from sodium wetting.

Rothman, in presenting a paper by Dickerman, Deitrich, Robinson, Rothman, and Carter, discussed the movement and dynamics of mixed-oxide fuels under transient conditions. He briefly described the

reactor in the Transient Reactor Test Facility (TREAT), the Mark II loop in the reactor, and the associated facilities for subjecting the fuel pins to fast-reactor accident conditions. He then detailed experiments with fuel pins which had been run to failure and summarized the results as follows: The first sample showed effects of axial fuel movement in relieving cladding stresses and confirmed the ability of the cladding to freeze molten-oxide fuels without allowing melt-through of the cladding (if the cladding were properly cooled externally); in the second sample, which was run to vigorous failure, the cladding failed as a result of molten oxide melting through the wall rather than radial fuel expansion breaking open the cladding; the third sample was run to just short of failure with an energy input of about 950 J/g for about ⅓ sec; the fourth sample, an FTR-type pin, was run to just past failure (failure was indicated at 1220 J/g), an extensive loss of oxide was noted, and flow and pressure anomalies occurred, although there was no violent fuel–coolant interaction; samples five, six, and seven were small UO_2 pins that were run to vigorous failure (the maximum conversion of energy to work here was 0.02%).

Culley, in presenting a paper by Culley, Leggett, and Bard, reported results of the first transient overpower test conducted on a preirradiated mixed-oxide fuel pin. He showed the transient temperature history as a function of fuel-pin radius and reported a cladding deformation of 1.4 in. (or about 0.55%) and 24% fission-gas release from the fuel during the transient, although no melting occurred. Culley noted a total swelling of about 3% that was attributable to the transient.

Field, in presenting a paper by Thomas and Field, discussed the transient overpower performance of stainless-steel-clad, mixed-oxide fuels for LMFBRs. He showed the capsule response to irradiations in TREAT, the transient overpower failure sequence, and the fraction of fuel that was molten at the time of predicted cladding failure. Field then described the empirical model that evolved for the prediction of failure effects under overpower conditions. He compared the TREAT transients with LMFBR accident conditions and attempted to define specific transient threshold temperatures. In all the transient overpower tests, Field reported no sign of the fuel melting through the cladding and proposed that the melting of the cladding per se should not be a fuel-failure mechanism. He also noted that none of the sodium-bonded fuel pins failed when subjected to a transient which would have melted about 60% of the gas-bonded pins and that significant sodium ingress will not lower the fuel-failure threshold appreciably. Field concluded that the primary factor affecting the failure threshold is the molten-fuel volume and that the energy-input rate has a moderate effect on failure threshold. He also observed that the fuel-failure threshold varies inversely with the smear density of the fuel and nonlinearly with increasing burnup.

The performance of Sphere-Pac and pelletized $(U,Pu)O_2$ under transient overpower conditions was discussed by Cox in presenting a paper by Cox, Cuneo, and Manthos. Cox reported finding no significant change in pin diameters, although a general shortening of the pins occurred. He compared the effects of melting on both the Sphere-Pac and pelletized fuels and discussed the grain-growth processes for each type of fuel. According to Cox, pins in which fuel melting occurred showed some evidence of molten-fuel–cladding contact but, as reported by others, showed no significant damage to the cladding.

Lindgren, in presenting a paper by Lindgren, Flynn, Baldwin, Fitts, and Longest, described the irradiation testing program that is under way on fast reactor fuels for the GCFR. He contrasted the fuel elements for the LMFBR and GCFR and discussed those areas where the test conditions for the latter are in excess of those for the LMFBR. He described in detail the fission-gas trap in the test rod and showed the data collected with this kind of monitoring system. Lindgren outlined the research being done on the roughening of cladding surfaces and summarized the developmental efforts toward determining the optimum dimensions for spiral roughening ribs for the fuel-element surface.

PERFORMANCE OF ADVANCED FUELS

A paper by Washburn and Scott, presented by Washburn, characterized the most desirable features of a fuel for an FBR as high burnup, high linear heat rate, and high specific power. He said that the principal advanced fuels, the carbides and nitrides, have a thermal conductivity of about five times that of the oxides, have an upper operating boundary of ~45 kW/ft as opposed to 19 kW/ft for oxides, and an average specific power of ~350 kW/ft. Washburn identified the problems with uranium nitride (UN) and uranium carbide (UC) as fabrication costs, reactivity with air, and stoichiometry, but he stated that the marked advantages of these fuels are apparent from the LMFBR follow-on studies.

Hilbert, in presenting a paper by Hilbert, Storhok, Chubb, and Keller, discussed the swelling of UC and UN at high temperatures. He presented data which show that the swelling increases greatly as the cladding temperature rises and discussed how the swelling in UN can be controlled by the deliberate introduction of voids. After stating that UN generally behaves better than UC, Hilbert compared diffusion data for these fuels.

Grando presented a paper, written by Grando, Montgomery, and Strasser, on the measurements of unrestrained swelling and fission-gas releases of carbide and oxide fuels. He described the instrumented capsule used for the experiments and summarized the data for several operating conditions.

Bauer discussed the performance of mixed nitride fuels in presenting a paper by Bauer, Brown, Fromm, and Storhok. He showed volume changes as a function of burnup and discussed the effects of structure, sodium bonding, and high oxygen content on the swelling of (U,Pu)N. He noted that porosity occurs because of the oxygen that is present and not because of irradiation. Bauer described a fission-dissolution effect that occurs and discussed the resultant effect on swelling. With low-density mixed nitrides, Bauer reported that a central porosity starts developing at 1390°C and that swelling, caused by fission gases rather than solid fission products, begins between 1300 and 1400°C. For high-density fuel, the fission-gas release is dependent on pellet porosity up to 32×10^{20} fissions/cm^3, and larger fission-gas releases are noted at fuel exposures greater than 32×10^{20} fissions/cm^3. Bauer also reported no major problems with fuel-cladding compatibility in the high-density-pin irradiations. He described a new pin that is designed for exposures of 150,000 MWd/metric ton.

Clifford, in presenting a paper by Clifford, Barner, Cubitt, and Kirkpatrick, described results from thermal- and fast-neutron irradiation of sodium-bonded mixed monocarbide fuels. He reported essentially no changes in fuel that was irradiated in a thermal environment to about 4, 7.5, and 11.5 at.% burnup, and he summarized the results of irradiation of fuel elements in EBR-II to maximum burnups of 5.0 and 3.7 at.% at 30 kW/ft. A paper by Strasser, Montgomery, and Powers, which was presented by Grando, discussed the testing of helium-bonded carbide fuels in the EBR-II to burnups of 65,000 MWd/metric ton. Grando reported severe failures of fuel rods that were irradiated to high burnups. Claddings of 316 stainless steel, Incoloy 800, and vanadium were used. He also reported that cracking occurred in all the high-burnup carbide pellets.

Harbourne, in presenting a paper by Harbourne, Levine, Biancheria, Latimer, and Neimark, reported on tests with sodium-bonded mixed carbides. The primary purpose of the tests was to ascertain the effects of such additives as chromium or iron. Harbourne, as others before him, noted the extensive cracking and higher swelling rates for hypostoichiometric as compared with stoichiometric fuels. He theorized that a sodium-bond volume of 15% might be adequate to prevent cladding failures.

WRAP-UP SESSION

A closing session was held to assess the effectiveness and review the accomplishments of the meeting. The chairman of each preceding session gave a summary of his session, with invited additional comments from the attendees.

L. R. Kelman, chairman of the Fuel-Element Design session, pointed out the apparent controversy over making use of the swelling of stainless-steel cladding to achieve high burnup. He then turned attention to the application of existing technology to fuel-element design and analysis. He questioned whether the proper amount of effort is being applied toward fully utilizing the presently existing, although meager, technology to avoid the costly problems stemming from lack of quality control and whether sufficient effort is being expended toward evaluating the trade-offs between direct dollar costs as a function of fuel-element failures that can be tolerated and the consequences of such determinations. Kelman also posed the question of whether the utilities are sufficiently involved in fuel-element design and fuel-cycle development; his thought was that those who are developing the fast reactor fuels are not benefiting enough from the fuel-element experience being gained with the operation of thermal reactors. Kelman also described General Electric's use of 321 stainless steel as a reference cladding material as a fresh approach when compared to the common use of nonstabilized stainless steels.

L. A. Neimark, in summarizing the session on Fuel-Element-Behavior Modeling, enumerated the three items presented which he considered as new developments: (1) correlation of computer codes with a fair amount of experimental data both with and without force-fitting the data, although the codes appear to have deficiencies in analyzing pins that have been

exposed to high burnups; (2) fuel cracking can significantly affect the results obtained when fuel-element behavior is numerically simulated and consequently should be included in all models; and (3) the stainless-steel swelling correlations that are being used may be inadequate, and the concept of stress-enhanced swelling in high-burnup elements should be evaluated more closely with the idea of including these efforts in the numerical simulation models. Neimark pointed out the controversy that arises over how to distribute porosity in fuel models and expressed the thought that there is insufficient experimental evidence to support leading views. He cited as a second point of controversy the significant discrepancies in input data for codes and mentioned fission-induced creep rate and creep mechanisms for cladding deformation as examples of these discrepancies.

A. M. Biancheria, chairman of the session on Fuel Mechanisms and Properties, summarized the session by considering the areas in which papers were presented, i.e., fuel swelling, thermal performance, fuel–cladding reaction, and fuel–sodium reaction. He reported that no new, fundamental data were presented on fuel swelling, although the available data were reviewed and additional analyses were included; he suggested that what is needed is a translation of fuel-swelling theory into a working model. For thermal performance, he said that the only new data presented were those on the effect of porosity shape on thermal conductivity for a given fuel-pellet density but that new tools for analyzing and better understanding the available data were presented. His opinion was that such present criteria as "no central melting shall occur at a given overpower condition" should be reassessed to determine whether there could be other, more meaningful, possible criteria. With regard to the fuel–cladding reaction mechanisms, he noted that the data are quite scattered and that it is difficult to isolate either effects or significant parameters. These uncertainties, he said, underscored the need for additional data. In the fuel–sodium reaction mechanisms, he cited the O/M ratio as the key factor and noted that additional data are required on the kinetics of the reaction and on in-reactor tests of failed fuel rods in a flowing-sodium environment.

W. E. Baily, who chaired the first session on Mixed-Oxide Fuel Performance, reported that the present status of the mixed-oxide fuel-test program for the LMFBR was covered in detail. He said that all the recent high-burnup results were presented and told what he considered to be the high points of the session. He characterized the WADCO presentation on instrumented subassemblies as extremely important because the observed change in flow rate as a function of the number of subassemblies will have a significant effect on temperature perturbations within the subassemblies. Baily noted that the number of high-temperature subassemblies in the EBR-II is very small and that there is a very great need for more data in the cladding-temperature region of 1250°F and possibly higher. He expressed surprise that there was no presentation or discussion on methods for reducing fuel–cladding attack and cited this as an area where more work is needed. Baily voiced the opinion that development efforts should now be directed toward fuel subassemblies rather than, as in the past, toward just fuel pins. He cited the F-2 results at a burnup exceeding 100,000 MWd/metric ton as producing a clear-cut definition between cladding deformation caused by fuel swelling and that caused by swelling of the cladding. With reference to the F-2 data, he also noted that a different loading mechanism appears to be occurring at intermediate burnups and that this has not been fully evaluated. Finally, Baily observed that, although plutonium buildup in the fuel pin was given more attention in this meeting, there is a particular need to extend efforts to obtain data on the axial migration of plutonium.

DeWitt Moss (USAEC–Idaho), who substituted for the chairman of the second session on Mixed-Oxide Fuel Performance, noted that transient tests on mixed-oxide elements have been performed at 75 and 150–175 kW/ft without large-scale effects. He pointed out the fact that no violent fuel–coolant reaction has been observed, although a considerable amount of fuel has been dispersed into the sodium coolant. Moss also cited the studies of short-term gas blanketing on the mixed-oxide fuel elements as significant.

SUMMARY

The stated objective of the conference was to evaluate past progress and to identify areas where future efforts should be applied. In this, the conference was admirably successful. Session chairmen, speakers, and attendees appeared quite open, frank, and completely honest in their comments and criticisms. This healthy, self-critical attitude seemed to accomplish a great deal in contrasting the design philosophies and controversies, the available data and deficiencies, the design and materials problems and economics, and the extensions of laboratory models to operationally viable models.

ACKNOWLEDGMENTS

My appreciation is extended to Arden L. Bement, Professor of Nuclear Materials at Massachusetts Institute of Technology, for his review of this write-up; to J. E. Hard, Senior Staff Assistant to the Advisory Committee on Reactor Safeguards, for providing a copy of his notes to serve as a check on my own; and to Jack Cunningham, Associate Director of the Metals and Ceramics Division of Oak Ridge National Laboratory, for providing a complete copy of the transcript from the Wrap-Up Session. Without such assistance this article would not have been possible.

SUGGESTED READING LIST

R. J. Jackson, W. H. Sutherland, and I. L. Metcalf, Swelling and Creep Effects upon Fast Reactor Core Structural Design, *Trans. Amer. Nucl. Soc.*, **13**(1): 112 (June 1970).

C. L. Wheeler, G. C. Main, and D. C. Kolesar, COBRA-IIA—A Program for Thermal–Hydraulic Analysis in Very Large Bundles of Fuel Pins, USAEC Report BNWL-1422, Pacific Northwest Laboratory, August 1970.

S. D. Harkness, J. A. Tesk, and Che-Yu Li, An Analysis of Fast-Neutron Effects on Void Formation and Creep in Metals, *Nucl. Appl. Technol.*, 9(1): 24 (July 1970).

W. H. Sutherland and V. B. Watwood, Jr., Creep Analysis of Statically Indeterminate Beams, USAEC Report BNWL-1362, Pacific Northwest Laboratory, June 1970.

W. H. Sutherland, A Finite Element Computer Code (AXICRP) for Creep Analysis, USAEC Report BNWL-1142, Pacific Northwest Laboratory, October 1969.

A. Boltax, P. M. Murray, and A. Biancheria, Fast Reactor Fuel Performance Model Development, *Nucl. Appl. Technol.*, 9(3): 326 (September 1970).

G. W. Greenwood and M. V. Speight, An Analysis of the Diffusion of Gas Bubbles and Its Effect on the Behavior of Reactor Fuels, *J. Nucl. Mater.*, **10**(2): 140 (1963).

C. W. Sayles, A Three-Region Analytical Model for the Description of the Thermal Behavior of Low-Density Oxide Fuel Rods in a Fast Reactor Environment, *Trans. Amer. Nucl. Soc.*, **10**(2): 458 (November 1967).

H. Kämpf and G. Karsten, Effects of Different Types of Void Volumes on the Radial Temperature Distribution of Fuel Pins, *Nucl. Appl. Technol.*, 9(3): 282 (September 1970).

C. N. Craig, G. R. Hull, and W. E. Baily, Heat-Transfer Coefficients Between Fuel and Cladding in Oxide Fuel Rods, USAEC Report GEAP-5748, General Electric Company, January 1969.

V. Z. Jankus and R. W. Weeks, LIFE-I, A FORTRAN-IV Computer Code for the Prediction of Fast Reactor Fuel-Element Behavior, USAEC Report ANL-7736, Argonne National Laboratory, November 1970.

V. Z. Jankus and R. W. Weeks, LIFE-I, A History-Dependent Analysis of Fast Reactor Fuel-Element Behavior, *Trans. Amer. Nucl. Soc.*, **13**(2): 830 (November 1970).

C. M. Cox and F. J. Homan, Analysis of Mixed-Oxide Fuel-Pin Performance Using the FMODEL Computer Code, *Trans. Amer. Nucl. Soc.*, **12**(2): 536 (November 1969).

C. M. Cox and F. J. Homan, Performance Analysis of a Mixed-Oxide LMFBR Fuel Pin, *Nucl. Appl. Technol.*, 9(3): 317 (September 1970).

F. J. Homan, Fuel–Cladding Mechanical Interaction During Startup, *Trans. Amer. Nucl. Soc.*, **13**(2): 576 (November 1970).

R. C. Nelson et al., Performance of Plutonium–Uranium Mixed-Oxide Fuel Pins Irradiated in a Fast Reactor (EBR-II) to 50,000 MWd/metric ton, USAEC Report GEAP-13549, Appendix B, General Electric Company, August 1969.

W. E. Baily, Sodium-Cooled Reactors, Fast Ceramic Reactor Development Program, Quarterly Report No. 30, February–April 1969, USAEC Report GEAP-10028, General Electric Company, May 1969.

H. R. Brager, J. L. Straalsund, J. J. Holmes, and J. F. Bates, Irradiation-Produced Defects in Austenitic Stainless Steel, USAEC Report WHAN-FR-16, WADCO Corp., December 1970.

K. R. Merckx and G. L. Fox, SINTER—A Program for Calculating Radial Temperature Distribution in Oxide Fuel Pins Undergoing Sintering, USAEC Report BNWL-1241, Pacific Northwest Laboratory, January 1970.

F. A. Nichols, Behavior of Gaseous Fission Products in Oxide Fuel Elements, USAEC Report WAPD-TM-570, Westinghouse Electric Corp., October 1966.

F. A. Nichols and H. R. Warner, Interaction of Fission-Gas Bubbles with Structural Defects and Release from Nuclear Fuels, *Trans. Amer. Nucl. Soc.*, **11**(2): 489 (November 1968).

H. R. Warner and F. A. Nichols, A Statistical Fuel-Swelling and Fission-Gas Release Model, *Nucl. Appl. Technol.*, 9(2): 148 (August 1970).

F. A. Nichols and H. R. Warner, Mechanisms for the Release of Fission Gas from Oxide Fuel Rods, *Trans. Amer. Nucl. Soc.*, **13**(1): 130 (June 1970).

C. C. Dollins and H. Ocken, A Fission-Gas Swelling Model Incorporating Re-Solution Effects, *Nucl. Appl. Technol.*, 9(2): 141 (August 1970).

D. L. Keller and W. Chubb, Progress on High-Temperature Fuels Technology During November 1969–January 1970, USAEC Report BMI-1879, Battelle Memorial Institute, February 1970.

E. Duncombe, CYGRO-3—An Improved Model for Prediction of Oxide Fuel Rod Performance, *Trans. Amer. Nucl. Soc.*, **13**(1): 349 (June 1970).

E. E. Gruber, Calculated Size Distributions for Gas-Bubble Migration and Coalescence in Solids, *J. Appl. Phys.*, **38**: 238 (1967).

Che-Yu Li, S. Pati, R. B. Poeppel, R. O. Scattergood, and R. W. Weeks, Some Considerations of the Behavior of Fission-Gas Bubbles in Mixed-Oxide Fuels, *Trans. Amer. Nucl. Soc.*, **12**(2): 531 (November 1969).

E. M. Baroody, Calculations on the Collisional Coalescence of Gas Bubbles in Solids, *J. Appl. Phys.*, **38**: 4893 (1967).

M. August, On the Theory of Swelling, *Kernenergie*, **11**: 186 (1968).

B. R. T. Frost, Theories of Swelling and Gas Retention in Ceramic Fuels, *Nucl. Appl. Technol.*, 9(2): 128 (August 1970).

R. W. Weeks, R. O. Scattergood, and S. R. Pati, Migration Velocities of Bubble-Defect Configurations in Nuclear Fuels, *J. Nucl. Mater.*, **36**(2): 223-229 (August 1970).

F. A. Nichols, Kinetics of Diffusional Motion of Pores in Solids, *J. Nucl. Mater.*, **30**(1/2): 143-165 (April 1969).

R. L. Ritzman, A. J. Markworth, W. Oldfield, and W. Chubb, Interpretations of Fission-Gas Behavior in Refractory Fuels, *Nucl. Appl. Technol.*, **9**(2): 167 (August 1970).

D. L. Keller, Progress on Development of Fuels and Technology for Advanced Reactors During July 1969–June 1970, USAEC Report BMI-1886, Battelle Memorial Institute, July 1970.

K. J. Perry and C. N. Craig, Austenitic Stainless-Steel Compatibility with Mixed-Oxide Fuel, *Trans. Amer. Nucl. Soc.*, **12**(2): 564 (November 1969).

C. Johnson, C. Crouthamel, H. Chen, and P. Blackburn, Studies in Mixed-Oxide Irradiated Fuels Transport of Cladding Components, *Trans. Amer. Nucl. Soc.*, **12**(2): 565 (November 1969).

General Electric Company, Sodium-Cooled Reactors, Fast Ceramic Reactor Development Program, Quarterly Report No. 35, May 1970–July 1970, USAEC Report GEAP-10028-35, September 1970.

General Electric Company, Sodium-Cooled Reactors, Fast Ceramic Reactor Development Program, Quarterly Report No. 34, February 1970–April 1970, USAEC Report GEAP-10028-34, June 1970.

S. F. Bartram and R. E. Fryxell, Preparation and Crystal Structure of $NaUO_3$ and $Na_{1.1}U_3O_{1.6}$, USAEC Report GEMP-733, General Electric Company, April 1970.

F. J. Homan, W. H. Bridges, W. J. Lackey, and C. M. Cox, Comparison of FMODEL Predictions with EBR-II Irradiation Data, *Trans. Amer. Nucl. Soc.*, **14**(Suppl.): 8 (1971).

R. B. Fitts, V. A. DeCarlo, E. L. Long, Jr., and A. R. Olsen, Thermal Performance and Restructuring of Pellet and Sphere-Pac Fuels, *Trans. Amer. Nucl. Soc.*, **13**(2): 549 (November 1970).

A. R. Olsen, C. M. Cox, and R. B. Fitts, Low-Burnup Irradiation Tests of Sphere-Pac Sol-Gel $(U,Pu)O_2$ Fuels, *Trans. Amer. Nucl. Soc.*, **13**(1): 32 (June 1970).

A. R. Olsen, Intermediate-Burnup Irradiation Tests of Sphere-Pac Sol-Gel Fuels, *Trans. Amer. Nucl. Soc.*, **13**(1): 32 (June 1970).

A. R. Olsen, R. B. Fitts, and C. M. Cox, Analysis of the Validity of Fast Reactor Fuel Tests in Existing Test Reactors, in National Symposium on Developments in Irradiation Testing Technology, September 9–11, 1969, NASA Lewis Research Center, Sandusky, Ohio, USAEC Report CONF-690910, pp. 127-150, National Aeronautics and Space Administration, 1969.

F. A. Nichols, Theory of Columnar Grain Growth and Central Void Formation in Oxide Fuel Rods, *J. Nucl. Mater.*, **22**: 214 (1967).

A. DeVolpi, C. E. Dickerman, and J. F. Boland, Preliminary Performance Data from Fast-Neutron Hodoscope at TREAT, *Trans. Amer. Nucl. Soc.*, **12**(2): 868 (November 1969).

C. E. Dickerman, L. E. Robinson, A. K. Agrawal, and J. F. Boland, First TREAT Loop Experiment on Oxide Fuel Meltdown, *Trans. Amer. Nucl. Soc.*, **12**(2): 867 (November 1969).

C. E. Dickerman, L. E. Robinson, J. F. Boland, R. Purviance, and K. Schmidt, First TREAT Experiment on High-Energy Fuel Failure of an Unirradiated Oxide Fast Reactor Fuel Pin in Flowing Sodium, *Trans. Amer. Nucl. Soc.*, **13**(1): 370 (June 1970).

D. R. MacFarlane, SAS1A—A Computer Code for the Analysis of Fast Reactor Power and Flow Transients, USAEC Report ANL-7607, Argonne National Laboratory, October 1970.

A. B. Rothman, A. K. Agrawal, R. T. Purviance, K. J. Schmidt, J. F. Boland, and R. D. Leggett, Failure Threshold TREAT Experiment with an Unirradiated Prototypical Fuel Element, *Trans. Amer. Nucl. Soc.*, **13**(2): 652 (November 1970).

L. W. Deitrich, F. L. Willis, R. T. Purviance, K. J. Schmidt, C. E. Dickerman, and J. F. Boland, High-Energy Transient Meltdown of Irradiated UO_2 in a TREAT MARK II Loop, *Trans. Amer. Nucl. Soc.*, **13**(2): 652 (November 1970).

D. F. Schoeberle et al., A Method of Calculating Transient Temperatures in a Multiregion, Axisymmetric, Cylindrical Configuration. The ARGUS Program, 1089/RE248, Written in FORTRAN-II, USAEC Report ANL-6654, Argonne National Laboratory, November 1963.

F. E. Bard, Jr., PECT-I: A FORTRAN-IV Computer Program To Determine the Plastic-Elastic Creep and Thermal Deformation in Thick-Walled Cylinders, USAEC Report BNWL-1171, Pacific Northwest Laboratory, December 1969.

G. R. Thomas and J. H. Field, Transient Overpower Irradiation of Axially Restrained, Zero-Burnup Fast Reactor Fuel Specimens, USAEC Report GEAP-13562, General Electric Company, September 1969.

T. Hikido and J. H. Field, Molten-Fuel Movement in Transient Overpower Tests of Irradiated Oxide Fuel, USAEC Report GEAP-13543, General Electric Company, September 1969.

R. G. Stuart and G. R. Thomas, Effects of Fission Gas on Transient Overpower Fuel-Rod Failure, *Trans. Amer. Nucl. Soc.*, **13**(2): 654 (November 1970).

General Electric Company, Sodium-Cooled Reactors, Fast Ceramic Reactor Development Program, Quarterly Report No. 29, November 1968–January 1969, USAEC Report GEAP-5753, February 1969.

G. R. Thomas and J. H. Field, Transient Performance of Mixed-Oxide Powder Fuel with Up to 60% Melting, *Trans. Amer. Nucl. Soc.*, **12**(1): 343 (June 1969).

J. F. Fletcher and J. Greenborg, Nitride Fuels for Fast Breeder Reactors: Fuel-Cycle Considerations, USAEC Report BNWL-606, Pacific Northwest Laboratory, February 1968.

T. W. Latimer, L. A. Neimark, C. E. Johnson, and C. E. Crouthamel, Compatibility of Carbide Fuels with Potential LMFBR Claddings, *Trans. Amer. Nucl. Soc.*, **12**(2): 594 (November 1969).

C. A. Alexander, J. S. Ogden, and W. M. Pardue, Vaporization of Nitride and Carbide Fuels, *Trans. Amer. Nucl. Soc.*, **12**(2): 581 (November 1969).

A. A. Bauer and V. W. Storhok, Irradiation Studies of (U,Pu)N, *Nucl. Met., Met. Soc. AIME*, **17**(Pt.1): 532-544 (1970).

A. Strasser and M. Montgomery, Irradiation of Uranium–Plutonium Carbides, *Trans. Amer. Nucl. Soc.*, **12**(2): 597 (November 1969).

P. J. Levine, B. L. Harbourne, A. Biancheria, T. W. Latimer, and L. A. Neimark, Postirradiation Observations of Sodium-Bonded (U,Pu)C Fuels, *Trans. Amer. Nucl. Soc.*, **13**(2): 606 (November 1970).

R. F. Hilbert, V. W. Storhok, and W. Chubb, Irradiation Behavior of UO_2 at Surface Temperatures from 1300 to 1900°C, *Trans. Amer. Nucl. Soc.*, **13**(1): 130 (June 1970).

R. F. Hilbert, V. W. Storhok, and W. Chubb, The Role of Grain Boundaries in the Swelling of UN at 1600 to 1700°C, *Trans. Amer. Nucl. Soc.*, **13**(2): 564 (November 1970).

R. F. Hilbert, V. W. Storhok, and W. Chubb, Irradiation Behavior of UN at High Temperatures, *Trans. Amer. Nucl. Soc.*, **12**(2): 547 (November 1969).

A. A. Bauer, E. O. Fromm, J. H. Saling, and V. W. Storhok, Irradiation of Mixed-Nitride Fuel, *Trans. Amer. Nucl. Soc.*, **11**(2): 523 (November 1968).

A. A. Bauer, J. H. Saling, and V. W. Storhok, Irradiation Performance of (U,Pu)N, *Trans. Amer. Nucl. Soc.*, **12**(2): 598 (November 1969).

Los Alamos Scientific Laboratory, Advanced Plutonium Fuels Program, Quarterly Status Report, April 1–June 30, 1970, USAEC Report LA-4494, August 1970.

D. N. Dunning, Loading of Sodium-Bonded Fuel Capsules, USAEC Report LA-4393, Los Alamos Scientific Laboratory, Feb. 24, 1970.

United Nuclear Corp., Fast Reactor Mixed-Carbide Fuel-Element Development Program, Eleventh Quarterly Progress Report, January–March 1970, USAEC Report UNC-5259, May 1970.

AMERICAN NUCLEAR SOCIETY—CRITICAL REVIEWS

The Atomic Energy Commission has contracted with the American Nuclear Society to prepare for publication on a regular basis detailed Critical Review articles written by experts selected from the ANS membership and reviewed by an advisory committee of top leaders and scientists in the field. In this issue the articles are on pages 258–311.

Members of the Critical Review Advisory Committee are:

Sidney Siegel, *Chairman*	Atomics International
William Chittenden	Sargent & Lundy Engineers
Don E. Ferguson	Oak Ridge National Laboratory
Paul Lottes	Argonne National Laboratory
Peter Murray	Westinghouse Electric Corporation
David Okrent	University of Arizona
Herbert Parker	Battelle–Northwest
Joseph Prestele	New York Consolidated Edison
W. C. Redman	Argonne National Laboratory
Charles Stevenson	Argonne National Laboratory
Bertram Wolfe	Battelle–Northwest

ANS Critical Review Editor, *Norman H. Jacobson*

ANS Officers:

President, *John W. Landis*

Vice President/President-Elect, *James R. Lilienthal*

Treasurer, *J. Ernest Wilkins, Jr.*

Executive Secretary, *Octave J. Du Temple*

Comments on the articles should be communicated directly to the ANS Critical Review Advisory Committee or Editor, 244 E. Ogden Avenue, Hinsdale, Ill. 60521.

ANS GUIDELINES FOR PREPARING CRITICAL REVIEWS FOR *REACTOR TECHNOLOGY*

One interpretation of the words "Critical Review" emphasizes the word *critical.* That type of article would have as its purpose the discussion of a single subject, which has been uncertain and perhaps controversial, in considerable depth. An example might be a critical review of the values of alpha for plutonium, assessing all the work done and arriving at a best current estimate. This paper is primarily addressed to specialists on the particular subject, and serves as an authoritative source for the information they use.

In the second interpretation of a Critical Review, the emphasis is on the word *review,* in the sense of survey. Such a paper would be broader and probably more descriptive in scope. A paper on "Solubility of Metallic Elements in Liquid Sodium" is an example of this category. Such a paper would be addressed to a much broader group of readers and written in a fashion that would be of interest to the majority of reactor technologists. It would provide enough of an introduction that the specialist from another field could immediately appreciate why the subject is important.

The criteria for these two types of articles may not be very different:

1. The paper should be based on a thorough coverage of relevant work on the subject from many sources. A review based on the work of only one individual or group is better suited for publication in one of the regular society journals. The review should be critically selective, reporting only the most valid results and indicating why some prior results have a questionable status. The review should call attention to significant gaps where more work is required in the subject of the article.

2. The paper should be timely, on a subject of active current interest.

3. The scope of articles acceptable as Critical Reviews includes all the subject areas identified for *Reactor Technology* (Economics, Physics, Mechanics, Construction, Fuel Elements, Fuel Cycles, Fluid and Thermal Technology, Fuel Processing, Components, Operating Performance), as well as Materials (including Source and Special Nuclear), Environmental Effects, and Effluent Management. Not desired are (1) reports of original research proposed for first publication and (2) review articles directed toward the specialist in the field of nuclear safety (which is covered by the AEC's bimonthly review *Nuclear Safety*).

4. The paper should be organized so that it is of immediate practical use to the readers. Such organization requires: attention to consistent use of units, presentation of important data in summary curves or tables, and a fully adequate bibliography to the original literature. Details on size, honorarium, style, etc., can be obtained from ANS.

In-Reactor Creep of Reactor Materials

By E. R. Gilbert*

Abstract: *Irradiation creep is an important phenomenon in fast reactors. It affects the diameter changes and stress distributions in the cladding and in the nuclear fuel. It can also ameliorate distortions in structural components by allowing stress relaxation. Deformations that would lead to failure in postirradiation tests can be achieved by irradiation creep. Models are reviewed whereby irradiation either enhances creep or induces new mechanisms. The relative importance of these models is estimated. Data do not cover a sufficient range of temperature, flux, time, and stress to permit reliable prediction of materials behavior for the design goals of future liquid-metal-cooled fast breeder reactors (LMFBRs). Studies in progress in the United States, United Kingdom, and other nations are expected to provide important data in the near future.*

INTRODUCTION

Irradiation in a nuclear reactor increases the creep rate of stainless steels and other materials. Such increased creep, in conjunction with other irradiation-induced effects, can lead to increases in fuel-pin diameter, axial warpage of fuel pins, changes in the dimensions and geometry of coolant passages between pins, and modifications in properties of materials. These effects, in turn, may alter reactivity (particularly in fast reactors) and affect fuel life. Hence the study of irradiation-induced creep and similar phenomena is an important element in the Liquid Metal Cooled Fast Breeder Reactor (LMFBR) Program sponsored by the U. S. Atomic Energy Commission (AEC), Division of Reactor Development and Technology.

As pointed out by Wensch[1] in 1963, core structural materials must possess sufficient strength and ductility to withstand stresses and strain associated with fast reactor operations, even after irradiation to fluences of 10^{24} neutrons/cm^2. Fuel cladding must maintain integrity despite neutron fluxes in excess of 5×10^{15} neutrons/(cm^2)(sec) ($E > 0.1$ MeV), exposures in excess of 10^{23} neutrons/cm^2, temperatures up to 700°C, and pressures of several thousand psi from fission products released from the fuel.

In 1968 Cunningham[2] described the AEC program on development of fast reactor fuel cladding. Thin-walled type 316 stainless-steel cladding for service up to 800°C with retention of 3 to 5% ductility at neutron fluences up to 3×10^{23} neutrons/cm^2 was established as a program goal. High-priority research programs were designated to define the effects of irradiation-induced swelling and creep. Swelling and irradiation creep were not necessarily expected to be detrimental to material properties, since they might actually serve to improve ductility.

In 1970 Weber[3] stressed the need for the development of analytical models of fuel and cladding behavior under fast-neutron-flux irradiation. These models must include cladding swelling and creep and must be suitable for incorporation into integral fuel-element models describing total fuel-element performance.

The objectives of the experimental and theoretical investigations on creep in the AEC program[2] are: (1) to develop a description of irradiation creep for engineering applications and (2) to achieve a fundamental understanding of the nature of irradiation creep so that existing and future data can be extrapolated to prototypical conditions. This article contains a brief section entitled Engineering Design Considerations, followed by a more detailed section titled Mechanisms of Irradiation Creep. Attempts are made to point out experiments that should be performed and to discuss major questions and problems. Emphasis is placed on stainless steels because of the high level of interest in these materials. Much of

*Hanford Engineering Development Laboratory, WADCO Corporation, a subsidiary of Westinghouse Electric Corporation, Richland, Wash. 99352.

the theory and many of the data reported in the literature are based on zirconium and other metals, and this information is also included because of its application to the basic mechanisms of irradiation creep.

ENGINEERING DESIGN CONSIDERATIONS

The reactor engineering designer must consider not only irradiation creep but also the related factors of hardening, embrittlement, swelling, and ductility changes resulting from neutron irradiation. Because of this interaction, all these factors are briefly reviewed in this section.

Austenitic Stainless Steels

Hardening and Embrittlement. It has long been recognized that irradiation produces hardening and embrittlement in stainless steels. The hardening results in increases in yield and tensile strength and changes in related mechanical properties. Embrittlement associated with hardening and grain-boundary weakening reduces fracture strength and rupture life. The hardening and embrittlement depend on irradiation temperature as well as on many other experimental and material variables. The fundamental aspects of hardening and fracture problems in nuclear reactors have recently been reviewed by Bement.[4]

Swelling. In 1967 Cawthorne and Fulton[5] announced that stainless steels undergo swelling when irradiated and reported as much as 7% void-volume increase in type 316 stainless steel when irradiated to 7.8×10^{22} neutrons/ cm^2 total fluence. Since that time considerable effort to characterize this important phenomenon has been in progress. Efforts to describe swelling in terms of radiation-damage theory, thermodynamics, kinetics, microstructure, and reactor environmental variables have not yet been completely successful.[6-11] The controversial question of how much swelling can occur before saturation is of critical engineering significance.

Empirical equations have been developed[12-14] to provide a description of swelling which can be applied to reactor design studies. The latest equation that represents swelling of annealed 304 stainless steel in EBR-II in the temperature range of 370 to 500°C is[14]

$$\Delta V/V = [(T - 40) \times 10^{-10}] \exp (32.6 - 0.015T - 5100/T)\, \phi t^{[2.05 - (27/\theta) + (78/\theta^2)]} \quad (1)$$

where $\Delta V/V$ = volume increase, %
$\theta = T - 623.0$
ϕt = neutron fluence in units of 10^{22} neutrons/ cm^2 ($E > 0.1$ MeV)
T = temperature, °K

This equation was developed from a set of three mutually consistent empirical equations describing void concentration, void diameter, and void volume and is recommended for design studies and analyses until better equations are available. A comparison of Eq. 1 with data at ~420 to 440°C is shown in Fig. 1. Cold-worked stainless steels show less swelling than is described by Eq. 1, which is for solution-treated stainless steel.

Diameter Changes in Stainless-Steel Fuel Cladding. The changes in diameter of a fuel cladding at high burnups result from several contributing factors.[15] The total diameter increase can be measured by a profilometer as shown by curve A in Fig. 2*a*. Another measurement that can be made on the cladding is the change in bulk density represented by curve B. The difference between curves A and B is due to constant-volume deformation processes, such as thermal creep (curve F, Fig. 2*b*), and constant-volume irradiation creep (curve E, Fig. 2*b*).

The contributions to change in bulk density, curve B, are: zero-stress swelling, curve D; "volume creep," curve C;* and densification due to microstructural instabilities, curve G. Division of volume change by 3 provides the conversion to diameter change.

The shapes of the curves in Fig. 2 result from the dependence of swelling and creep on axial distributions of temperature, neutron flux, spectrum, and stress. For example, at a neutron fluence of 10^{23} neutrons/ cm^2, Eq. 1 predicts a maximum in volume increase at ~450°C. Maximum diameter increases in fuel pins are observed near the center, typically around 450°C. Less swelling is observed at the cooler lower end and at the hotter upper end of the fuel pin. The neutron flux and average energy both decrease from the fuel-pin center to the ends and contribute toward a maximum in the diameter increase somewhere near the center. Maximum diameter increases at fluences approaching 10^{23} neutrons/ cm^2 are typically several percent.

Irradiation Creep. Irradiation creep is defined as excess time-dependent deformation (above that found

*Volume creep is unique since plastic deformation usually results in no change in total volume. Volume creep is synonymous with stress-assisted swelling.

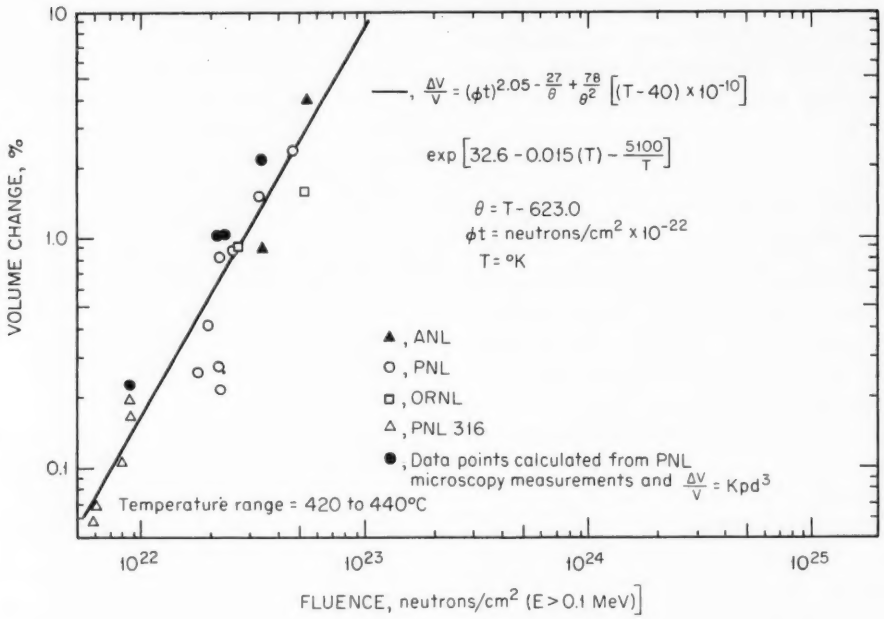

Fig. 1 Swelling in AISI type 304 stainless steel.[14]

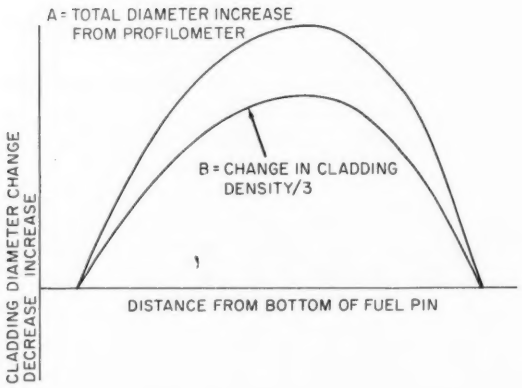

Fig. 2*a* Fuel-cladding diameter increase as measured by profilometer (curve A) and by change in bulk density (curve B).

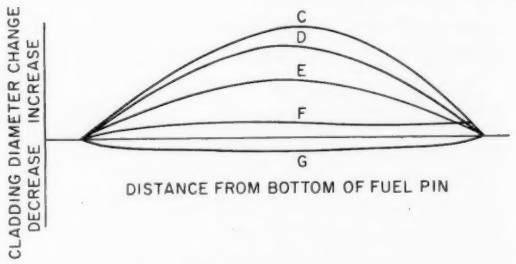

Fig. 2*b* Effect of irradiation-volume creep (curve C), zero-stress swelling (curve D), constant-volume irradiation creep (curve E), thermal creep (curve F), and densification (curve G) on fuel-cladding diameter increase.

in the absence of irradiation) under an applied stress resulting from irradiation. Usually during plastic deformation the specimen volume is constant, so that, in a uniaxial tensile test as the specimen elongates, the specimen cross section reduces correspondingly. During irradiation creep when volume is not constant but is increasing, the specimen cross section may not decrease as the tensile specimen elongates. This behavior is a consequence of volume creep, which (shown in Fig. 2) contributes toward increase in diameter of fuel pins at high burnup.

Volume creep is attributed to the hydrostatic stress component and is therefore important in tensile creep results and in pressurized tube specimens where the hydrostatic stress component is large. In shear tests the hydrostatic stress component is zero, and the

contribution of volume creep is expected to be negligible. During constant-volume creep, shear causes more creep for an equivalent effective stress than tensile or biaxial stress states. However, correlation of irradiation-induced creep data on austenitic stainless steels[16] showed a reversal in the effect of stress state. As a result of volume creep, tensile creep data showed more creep than shear data.

To account for volume creep under different stress states, the investigators[16] defined the ratio of effective strain $\bar{\epsilon}$ to effective stress $\bar{\sigma}$ as

$$\bar{\epsilon}/\bar{\sigma} = \gamma/3\tau = \epsilon/6\sigma = 4\epsilon_h/33\sigma_h \qquad (2)$$

where γ/τ is the shear strain per unit shear stress, ϵ/σ is the tensile strain per unit tensile stress, and ϵ_h/σ_h is the diametral strain per unit diametral stress in a pressurized tube. This definition of strain under different states of stress and the incorporation of a damage function to account for the different neutron spectra in various irradiation-test facilities has been used to derive an equation for irradiation-induced creep of annealed austenitic 304, 316, and EN58B stainless steels.[17] This equation is based primarily on torsion data generated at 250°C on annealed 316 stainless-steel helical springs in the Dounreay Fast Reactor (DFR).[18] Creep as a linear function of stress is defined by the equation

$$\bar{\epsilon}/\bar{\sigma} = 2 \times 10^{-9}[1 - \exp(-T\phi t)] + 4.5 \times 10^{-7}\bar{E}\phi t \exp(1.41 - 0.0027T) \qquad (3)$$

where $\bar{\epsilon}/\bar{\sigma}$ = effective strain to effective stress ratio in psi^{-1} as defined in Eq. 2
T = temperature, °K
ϕt = total neutron fluence in units of 10^{23} neutrons/cm^2 ($E > 10^{-10}$ MeV)
$\bar{E}$ = average neutron energy in MeV for provision of an approximate damage function

This equation is used in design and creep studies at Hanford Engineering Development Laboratory.

A model of irradiation creep based on microstructural features and void generation properties of the specimen has been developed for austenitic stainless steels for moderate to high stress levels by Tesk and Li[19] and by Harkness, Tesk, and Li[20] at Argonne National Laboratory. This model predicts an irradiation-creep rate dependent on stress to the second power in contrast to the linear dependence described by Eq. 3.

Fuel–Duct Bowing. The equations for irradiation-induced swelling and creep of stainless steel have been applied to the Fast Test Reactor (FTR) ducts to evaluate the resultant combined effect of thermal strain, swelling, and creep on duct deflection.[21] Figure 3 shows the deflections evaluated for a duct operated for 275 days and then unrestrained during refueling. The original straight configuration of the duct is shown in Fig. 3*a*. Figure 3*b* shows the deformed shape after experiencing only swelling strains due to flux and temperature gradients and then the shape being unrestrained. A pronounced outward bow is shown. The deflections calculated by addition of the creep equation are shown in Fig. 3*c*. For the conditions of fluence and transverse temperature gradients used, an inward bow results, but with significantly less magnitude, because the predicted creep strains almost entirely relax the thermal stress prior to the onset of swelling and greatly reduce the magnitude of swelling deformation. This study concludes that irradiation creep may greatly ameliorate the bending distortions of core components.

Ductility. Distinct differences are commonly found between thermally activated and irradiation-induced creep behavior. Theories usually predict a low dependence of strain rate on stress during irradiation creep. In this respect, theory and experiment are in agreement. This feature is very significant because it leads to the expectation of superplastic ductility during irradiation-enhanced deformation. Ductile in-pile

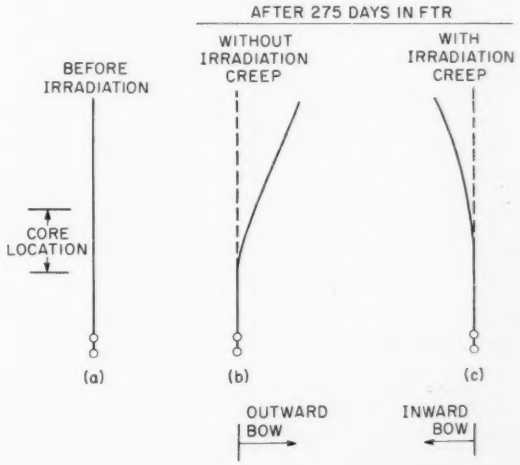

Fig. 3 Comparison of unrestrained duct deflection curves before (*a*) and after 275 days in the Fast Test Reactor, (*b*) without irradiation creep, and (*c*) with irradiation creep.[21]

behavior observed in materials that are less ductile in postirradiation tests has been rationalized by this feature. Such has been the case for zirconium alloys[22] and graphite.[23,24] Evidence for enhanced ductility as a result of irradiation creep has recently been reviewed by Nichols.[25]

Cladding strains approaching 2% in excess of swelling observed in Mark IA fuel pins clad with 304 stainless steel[26] in EBR-II appear to be evidence for irradiation-enhanced ductility since postirradiation tests on specimens irradiated to similar fluence levels fail at diametral strains below 1%.[27] For design considerations, a steady-state strain limit of 0.2% is used for thermal-creep strains with no similar design limit specified for swelling and irradiation-creep strains, even though they also contribute to the total strain.[28]

Nuclear Fuel

Irradiation causes nuclear fuels to swell. If the fuel swells and contacts the cladding, the amount of stress exerted on the cladding depends on the relative compressive creep strength of the fuel and the cladding and on the fuel swelling rate. Compressive creep of UO_2 during neutron irradiation has been measured by Perrin, Robinson, and Basham.[29] At high temperatures, above 1000°C, in a fission flux of 1.2×10^{13} fissions/(cm^3)(sec), the creep rate was about 10 times the thermal-creep rate. The irradiation-enhanced creep rate appears to be nearly a linear function of fission rate and applied stress. It is strongly dependent on temperature. Irradiation creep is also observed at low temperatures in UO_2.[30] Here it is also linear with stress but is only weakly dependent on temperature. Routbort and Solomon[31] have summarized irradiation creep in UO_2 in terms of temperature as shown in Fig. 4. As a result of considering irradiation-enhanced creep in nuclear fuels, the fuel-cladding interface pressure will be considerably lower than predicted when only thermal creep is considered. Fuel-cladding interaction is a complex problem being studied in integrated fuel-element-performance models.[3]

Zirconium Alloys

Since void formation has not been observed in zirconium alloys,[32] swelling is not believed to be a serious problem. The irradiation-induced creep rate in zirconium alloys at low stresses in the region of design applications has been measured on cold-worked pressurized tubes by Ross-Ross and Hunt.[33] The creep rate of cold-worked Zircaloy-2 is described by

$$\dot{\epsilon}_h = 4 \times 10^{-27} \sigma_h \phi (T - 433) \qquad (4)$$

where $\dot{\epsilon}_h$ = tangential strain rate, hr^{-1}
σ_h = tangential stress, psia
ϕ = neutron flux ($E > 1$ MeV)
T = temperature, °K

For cold-worked Zr-2.5 Nb, Eq. 4 is divided by 3. This equation was derived from data obtained from 250 to 350°C in neutron fluxes from 1 to 3×10^{13} neutrons/(cm^2)(sec) ($E > 1$ MeV).

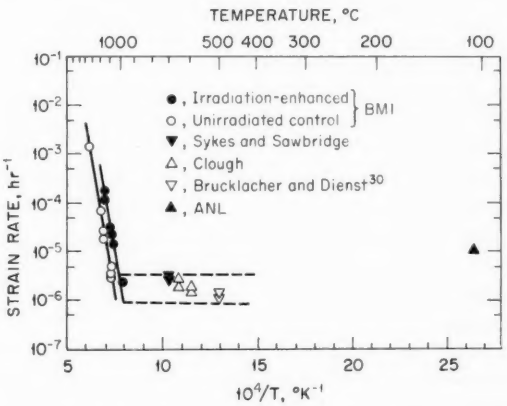

Fig. 4 Irradiation creep in UO_2.[31] All data are normalized to a stress of 3500 psi and a fission rate of 1.2×10^{13} fissions/(cm^3)(sec).

MECHANISMS OF IRRADIATION CREEP

In this discussion of mechanisms of irradiation creep, for convenience in separating effects found during in-pile irradiation, in contrast to those found in postirradiation creep tests, the mechanisms are separated into two categories, dynamic and structural.

The dynamic mechanisms (Table 1) establish the format of this article. A dynamic mechanism may include the effect of irradiation on enhancement of thermal-creep mechanisms, as is the case in Eqs. 6,8, 18, 19, and 21 in Table 1, or the inducement of new mechanisms not operating in the absence of irradiation, as in Eqs. 5, 9-11, 14, 16, and 23. Structural mechanisms affect thermally activated creep as a result of the influence of the irradiation-altered structure. The more common structural mechanisms are given in Table 2. Structural mechanisms may produce either softening (higher creep rate) or hardening (lower creep rate).

This article does not exhaustively delve into the basic physics of the mechanisms. For greater detail on the fundamentals, the reader is referred to an excellent article on mechanisms for in-reactor creep by Piercy[34] and the original articles listed in the references. This list of references is not complete but will be helpful to the reader requiring more detail.

Dynamic Mechanisms

Dynamic mechanisms are defined as those in which a change in creep rate occurs upon removal or application of an irradiation field. Dynamic irradiation-creep mechanisms are based on the common feature of Frenkel-pair generation from neutron-atom interactions and the separation of these into clusters through neutron- and fission-produced displacement spikes, and diffusion. Mechanistic details of these processes are controversial. The supersaturation of irradiation-produced defects above thermal-equilibrium concentrations may cause defects to condense into clusters, which then interact with other defect structures and chemical inhomogeneities so as to alter their role in creep. Supersaturation may also cause dislocations to climb.

Spike Mechanisms. The first reported study on the influence of irradiation on creep was conducted by Andrade,[35] who observed increases in the transient creep rate of cadmium single-crystal wires during alpha-particle bombardment with a polonium source. He attributed this effect to microscopic hot spots initiating glide at the surface. Although subsequent attempts by other investigators to confirm his results met with failure, a recent study[36] showed that the transient creep rate of zinc single crystals was increased by gamma irradiation from a ^{60}Co source, whereas the steady-state rate showed practically no change.

Early irradiation-creep mechanisms did not invoke the microstructural details now found in the more developed mechanisms. An example is the above-mentioned description by Andrade of enhanced primary creep in cadmium by microscopic hot spots. A later concept[37] (Fig. 5) described irradiation creep in terms of relaxation of elastic strains by hot spots (neutron or fission-fragment spikes). The predicted creep strain by this model is

$$\epsilon_{sp} \simeq \epsilon_{el} V_{sp} \alpha_1 N_1 \chi_1 \phi t \qquad (5)$$

where ϵ_{sp} = strain induced by spikes
ϵ_{el} = elastic strain taken as σ/E
V_{sp} = spike volume
α_1 = average number of spikes per neutron collision
N_1 = number of atoms per unit volume
χ_1 = neutron cross section per atom
ϕt = fast-neutron fluence

Creep by this mechanism is linear in stress and rather insensitive to temperature. It would be difficult to demonstrate that this mechanism is actually responsible for irradiation creep, but Eq. 5 provides a reasonable prediction of the level of irradiation creep observed in some experiments. Similar mechanisms[38,39] discussed consider only partial relaxation in the spike volume and therefore predict lower and reasonable creep rates.

Perrin described an irradiation-creep mechanism for ceramic fuels that have low thermal conductivity.[40] The mechanism incorporates continuous annealing from fission spikes. As a result, strain hardening is prevented, and the specimen creeps continuously only in the primary stage as described in Eq. 6.

$$\epsilon = \dot{\epsilon}^{p}_{th}\, t \qquad (6)$$

where $\dot{\epsilon}^{p}_{th}$ is the primary-stage creep rate. A flux dependence exists because the creep rate is enhanced with respect to a slower steady-state rate in thermal creep after strain hardening has occurred. The higher the flux, the earlier the stage of creep and the higher the resulting creep rate. The creep rate appears steady and is characterized by the same temperature dependence as thermal creep. High-temperature irradiation creep in UO_2 is strongly temperature dependent in accord with Eq. 6 (Fig. 4).

Irradiation Growth. Irradiation growth occurs in anisotropic materials as a result of a preferred orientation of dislocation loops generated by irradiation on certain crystallographic planes (Fig. 6*a*). Growth strains in zirconium alloys have been described[41] by the following equations for low and high fluences:

$$\epsilon_g = -G\chi_2\phi t \qquad \phi t < 10^{20} \text{ neutrons/cm}^2\ (E > 1 \text{ MeV}) \qquad (7a)$$

$$\epsilon_g = A_1 G \chi_2 (\phi t)^{1/2} + A_2 \qquad \phi t > 10^{20} \text{ neutrons/cm}^2\ (E > 1 \text{ MeV}) \qquad (7b)$$

where G is the growth coefficient, χ_2 is the cross section for elastic collisions with an atom, and A_1 and A_2 are constants.

Table 1 Mechanisms of Dynamic Irradiation Creep

Equation No.	Author	Equation	Mechanism
5	Brinkman and Wiedersich[37]	$\epsilon_{sp} \simeq \epsilon_{el} V_{sp} \alpha_1 N_1 \chi_1 \phi t$	Spike relaxation
6	Perrin[40]	$\epsilon = \dot{\epsilon}^{p}_{th}\, t$	Spike annealing
8	Roberts and Cottrell[43]	$\dot{\epsilon} = \sigma \dot{\epsilon}_g / \sigma_y$	Yielding creep
9	Hesketh[51]	$\gamma = \tau/8\mu\ [1 - \exp(-\phi t/B)]$	Transient dislocation climb
10*a*	Hesketh[55]	$\dot{\epsilon} = C\sigma\phi$	Loop orientation (isotropic)
10*b*	Hesketh[39]	$\dot{\epsilon} \simeq A_3 \dot{\epsilon}_g \sigma / T$	Loop orientation (anisotropic)
11	Gilbert and Straalsund[64]	$\dot{\epsilon}_{mn} = \alpha(\phi,t,T)\sigma_{mn} + [\beta(\phi,t,T)W + \kappa(\phi,t,T)]\,\delta_{mn}$	Constant volume creep, volume creep, and swelling strain
14	McElroy, Dahl, and Gilbert[17]	$\bar{\epsilon}/\bar{\sigma} = 2 \times 10^{-9}\ [1 - \exp(-T\phi t)] + 4.5 \times 10^{-7}\, E\phi t \exp(1.14 - 0.0027T)$	Transient climb, loop orientation, and volume creep
16	Gilbert and Holmes[71]	$\dot{\epsilon} = b\pi(r_p^2 - r_c^2)\, \partial N_2 / \partial(\phi t)\, \phi f(\sigma,T) + N_2 \pi r_p^2 / \rho\ \dot{\epsilon}_{th}$	Loop unfaulting
17	Schoeck[73]	$\dot{\epsilon} = \dot{\epsilon}_{th}(1 + a^2 \alpha_2 \phi / D_{th} S_1)$	Dislocation climb enhanced by vacancy diffusion
18	Brinkman and Wiedersich[37]	$\dot{\epsilon} = \dot{\epsilon}_{th}(D_{th} + \dot{N}\,\overline{X^2})/D_{th}$	Dislocation climb enhanced by vacancy diffusion
19	Nichols[74,75]	$\dot{\epsilon} = A_5 \sigma^4 L^2 (D_{th} + \dot{N}\,\overline{X^2})$	Dislocation climb over obstacles enhanced by vacancy diffusion
21	Harkness, Tesk, and Li[20]	$\dot{\epsilon} = A_6 \sigma^2 L / \mu^2 bd\ (2D_{th}\, \sigma^2 bL / \mu kT + Q_{i,\mathrm{dis}} - Q_{v,\mathrm{dis}} / \mathrm{L\ b^2})$	Dislocation climb over obstacles enhanced by interstitial diffusion
22	Nichols[25,74,75]	$\dot{\epsilon} = \dot{\epsilon}_g + \dot{\epsilon}_L + (1/\dot{\epsilon}_{\mathrm{int}} + 1/\dot{\epsilon}_{\mathrm{climb}} + \dot{\epsilon}_{\mathrm{cut}})^{-1}$	Composite mechanism: growth, loop orientation, glide, climb, and cutting
23	Ashby[97]	$\gamma = (N_i \Omega / \mu_R)\sigma\Omega$	Loop diffusion creep

Explanation of Symbols Used in Equations

ϵ_{sp} = strain induced by spikes
ϵ_{el} = elastic strain
V_{sp} = spike volume
α_1 = average number of spikes per neutron collision
N_1 = number of atoms per unit volume
χ_1 = neutron cross section per atom
ϕ = fast-neutron flux
t = time
ϵ = creep strain
$\dot{\epsilon}^{p}_{th}$ = primary stage of thermal creep
$\dot{\epsilon}$ = creep rate
σ = applied stress
$\dot{\epsilon}_g$ = growth strain rate
σ_y = yield stress
χ_2 = cross section for elastic collision with an atom
A_i = constant, where i = 1 to 6
T = absolute temperature, °K
C = irradiation-induced creep-rate coefficient
b = Burgers vector
$\dot{\epsilon}_{mn}$ = strain-rate tensor
σ_{mn} = stress tensor
α = coefficient to constant-volume irradiation creep
β = coefficient of the hydrostatic stress, W
κ = strain due to zero-stress swelling
$\bar{\epsilon}$ = effective strain for nonconservative volume creep
$\bar{\sigma}$ = effective stress
$\overline{E}$ = average neutron energy, MeV
δ_{mn} = Kronecker delta

Table 1 (Continued)

Explanation of Symbols Used in Equations (Continued)

r_p = radius at which unfaulted loops are pinned
r_c = critical radius for loop unfaulting
N_2 = number of loops per unit volume
$\dot{\epsilon}_{th}$ = thermal-creep rate
ρ = dislocation density
D_{th} = thermal-diffusion coefficient
a = lattice parameter
α_2 = atom fraction of vacancies produced per unit fluence
S_1 = atomic fraction of places where vacancies and interstitials anneal out
$\dot{N}$ = atomic fraction of vacancies produced per time unit
$\overline{X^2}$ = mean-squared distance a vacancy must move to reach a sink
L = spacing between obstacles
$D^* \simeq D_{th} + \dot{N}\overline{X^2}$
μ = elastic shear modulus
d = obstacle height
$Q_{i,\mathrm{dis}}$ = interstitial flux to dislocations
$Q_{v,\mathrm{dis}}$ = vacancy flux to dislocations
B = decay constant
$\gamma, \dot{\gamma}$ = shear strain and shear-strain rate
N_i = number of interstitials/(cm^3)(sec) absorbed by loops
μ_R = chemical potential of defects midway between dislocations
Ω = atomic volume of the defect

Table 2 Irradiation-Induced Microstructures Affecting Creep

Softening
- Dissolution of solution-strengthening elements
- Obstacle coarsening (overaging)
- Suppression of strain aging
- Increased mobile dislocation density
- Loops unfaulting
- Point-defect cluster decomposition
  - Enhanced climb
  - Obstacle removal
- Nabarro–Herring diffusion creep of loops
- Cold-work recovery

Hardening
- Obstacle generation (point-defect clusters, loops and voids)
- Precipitation strengthening

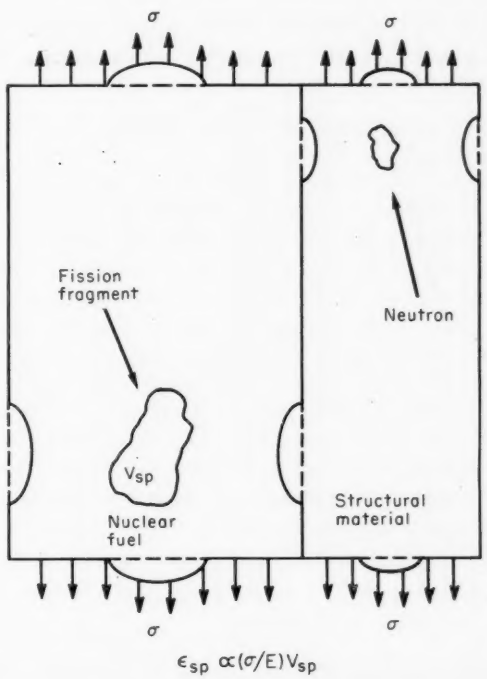

Fig. 5 Spike relaxation. Key: arrows indicate stress (sigma); solid lines indicate final specimen shape; broken lines indicate initial specimen shape.

Irradiation growth also occurs in face-centered cubic (fcc) and body-centered cubic (bcc) metals if the specimens have been cold worked. This was a significant discovery[42] since growth had previously been regarded as a peculiarity of anisotropic crystal structures. An explanation was that a preferred dislocation Burgers vector orientation (Fig. 6*b*) developed during cold work because of the asymmetry of the deformation and because the active glide planes were rotated toward the axis of deformation. This direction consequently elongated faster than others as the dislocations climbed by absorbing interstitials. Since the experiments were conducted between one-fourth and one-third of the Tm, vacancies were immobilized by clustering. During irradiation creep, directions most susceptible to acceleration by irradiation were those suffering the greatest deformations during prestraining. Also, since less acceleration was observed in annealed metals, it was inferred that clustering merely immobilizes vacancies. Dislocations climb past obstacles, which otherwise

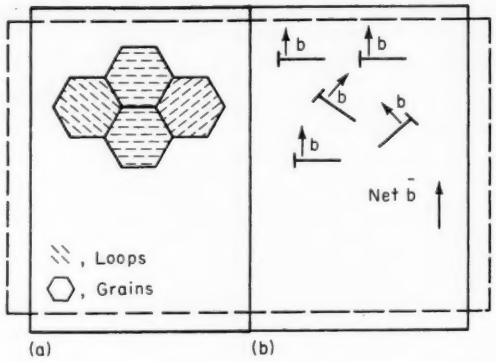

Fig. 6 Irradiation growth: (*a*) anisotropic material, (*b*) cold-worked isotropic material.

impede glide, by consuming excess interstitials. On the basis of these results, it is reasonable to expect irradiation growth to occur in cold-worked stainless steels.

Yielding Creep. Irradiation creep in uranium was described in terms of an irradiation-growth phenomenon by Roberts and Cottrell[43] who envisioned internal stresses building up between grains (Fig. 7) as a result of irradiation growth. When this growth stress reached the yield stress, the polycrystalline specimen gave way plastically to an externally applied stress which is small compared to the yield strength of a uniformly stressed sample. The mechanism is referred to as the mechanism of yielding creep. During plastic deformation most of the work is done by the internal stresses, and the external stress merely guides the local deformations so that their average has a nonvanishing component in the direction of the external stress. This model was described by

$$\dot{\epsilon} = \frac{\sigma \dot{\epsilon}_g}{\sigma_y} \tag{8}$$

where $\dot{\epsilon}_g$ is the growth strain rate and σ_y is the yield stress. The dependence on neutron flux and temperature is contained in the growth strain rate. This mechanism did a remarkably good job of describing the experimental results obtained[43] for uranium during irradiation.

Later theories for yielding creep appropriate to large applied stresses[44] and appropriate to small stresses[45] were combined[46] to provide a comprehensive description of yielding creep in zirconium alloys. Since the variables stress, neutron flux, time, and temperature are interdependent in this model, a simple equation expressing the irradiation-creep strain as a product of these variables does not exist. Hesketh's[46] yielding creep model requires considerable analytical effort and understanding to apply to data analysis or

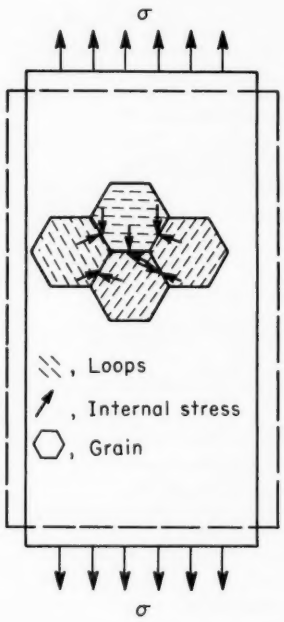

Fig. 7 Yielding creep.

design problems. Figure 8 gives an example of the complexity of this model. The effect of neutron flux on the creep rate is a function of the ratio of applied to internal stress. At low stress ratios the creep is not quite linear in flux, but at moderate stress levels the creep rate varies with the square root of flux. From studies by Fidleris,[47] Hesketh computed an internal stress of 25,000 psi for Zircaloy-2.[46] At an applied

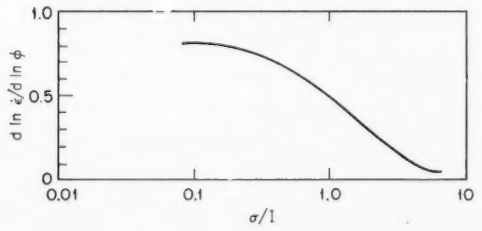

Fig. 8 Index of the flux dependence[46] as a function of σ/I.

stress of 20,000 psi, the ratio of applied to internal stress is ~0.8 (Fig. 8). Therefore a plot of creep rate vs. neutron flux for data generated in different reactors under an applied stress of 20,000 psi should have a slope of 0.5 on log-log graph paper. This plot is shown in Fig. 9, and the data are in good agreement with the prediction by the yielding-creep theory.

Figure 10 is a comparison of irradiation creep at 300°C in cold-worked Zircaloy-2 and quenched-and-aged Zr-2.5 Nb with the yielding-creep model. Good agreement is found, and the internal stresses computed by the model, 25,000 psi for Zircaloy-2 and 43,000 psi for Zr-2.5 Nb, have the same ratio as the microscopically measured yield strengths of the alloys.[48,49]

The yielding-creep model described by Hesketh predicts that the flux dependence becomes stronger as the stress and temperature are lowered, the stress dependence becomes less strong as the temperature is lowered or as the neutron flux is increased, and the temperature dependence is lowered as the flux is increased or as the stress is decreased. The main inconsistency is this last prediction. Data show that the temperature dependence is increased as the stress is decreased.[33,47]

Piercy[34] criticized Hesketh's yielding-creep model on the basis that the internal stress is relaxed during creep and therefore is not as large as the values calculated by the model. This would lead to an overprediction of irradiation creep by the yielding-creep model. Furthermore, the calculated time for the internal stress to relax after the irradiation field is removed is longer than that required for the irradiation-creep rate to decrease after reactor shutdown in the tests[47] on Zircaloy-2. Piercy's objection to the yielding-creep model, based on the failure of a preirradiated Zircaloy-2 specimen to show more enhancement than a specimen without preirradiation, did not take into account possible retardation of thermal creep due to irradiation hardening.

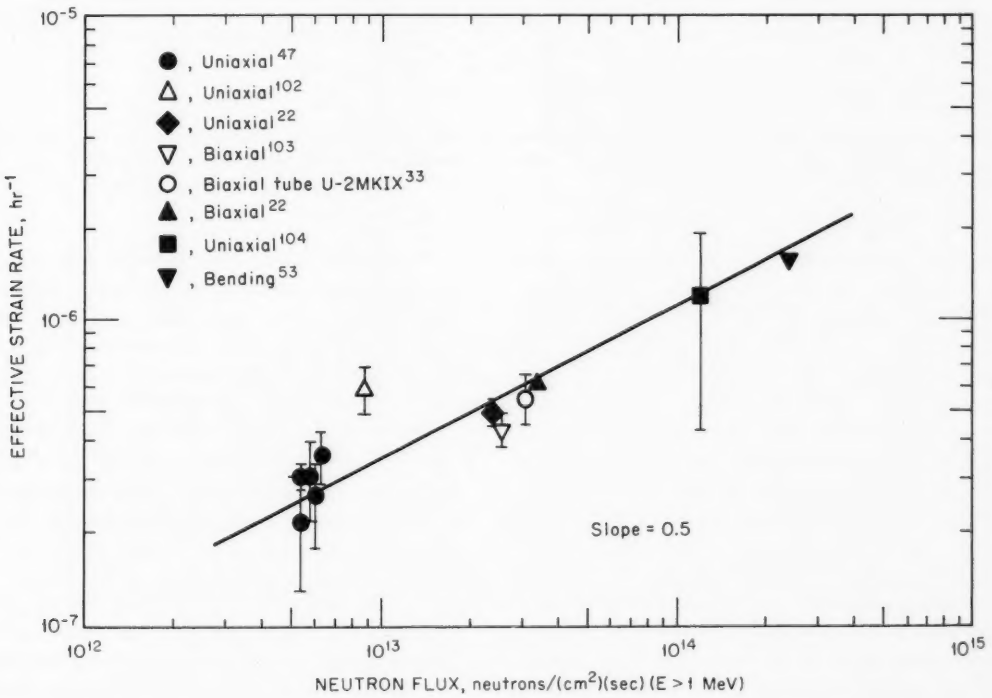

Fig. 9 Effect of neutron flux on irradiation effective creep rate (computed by Eq. 13*a*) of cold-worked Zircaloy normalized to an effective stress of 20,000 psi (Eq. 12) and 300°C. Data from Ref. 104 were extrapolated to a flow stress of 20,000 psi. The creep rates plotted represent the total effective creep rate less the effective creep rate measured in tests on unirradiated specimens. This correlation between uniaxial and biaxial creep implies that there is not a strong anisotropy effect at these low strain rates.

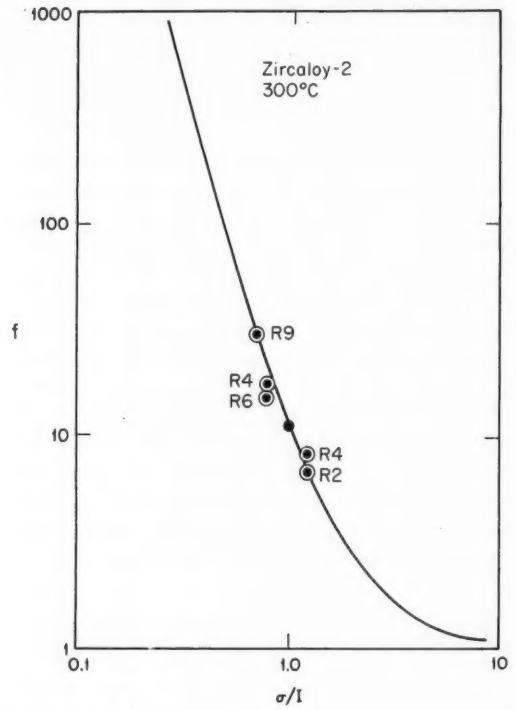

Fig. 10*a* Creep-rate enhancement factor f vs. ratio of applied to internal stress for cold-worked Zircaloy-2 with I = 25,000 psi.[46,47]

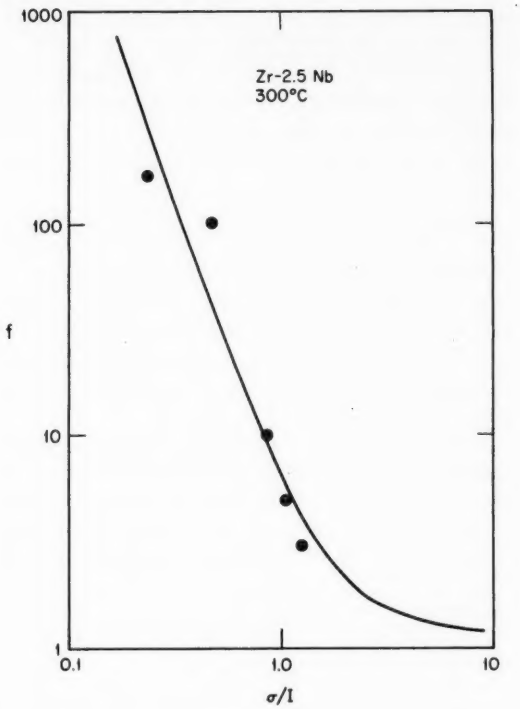

Fig. 10*b* Creep-rate enhancement factor f vs. ratio of applied to internal stress for quenched and aged Zr–2.5 Nb with I = 43,000 psi.[48,49]

Hesketh suggested that irradiation–creep predictions be based on decreasing values of the irradiation growth coefficient G[49] with increasing neutron fluence. Growth strains are described[41] by Eq. 7 for low and high fluences. He indicated that extrapolations based on linear or steady-state irradiation creep would overestimate the actual creep since the growth coefficient decreases from about 10 to 1 as neutron fluence increases from 10^{17} to 10^{20} neutrons/cm^2 ($E > 1$ MeV). However, irradiation–creep data for Zircaloy-2 have been extended to a neutron fluence of 7×10^{20} neutrons/cm^2 ($E > 1$ MeV) (Fig. 11).[22] Since the irradiation-induced creep appears steady beyond a fluence of 1×10^{20} neutrons/cm^2 ($E > 1$ MeV), one could conclude from the creep data that the growth coefficient does not decrease to values below 1 after a neutron fluence of 10^{20} neutrons/cm^2 ($E > 1$ MeV) is achieved. Until higher fluence growth data, at least as high as the fluence for which irradiation–creep data now exist, are reported, it does not seem advantageous to base high-neutron-fluence extrapolation of irradiation creep on extrapolated values of decreasing G.

Transient Irradiation-Induced Climb. In-pile creep studies conducted in the 1950s were usually performed at rather high stresses or temperatures so that thermal creep could be measured easily. Although searching for an enhancement of thermal creep, these investigators usually found either no effect or a slight reduction in creep rate due to irradiation hardening.[50] The strongest evidence that irradiation indeed enhances or induces creep was found in stress-relaxation experiments. A greater amount of stress relaxation under constant strain was found in tests conducted in-pile rather than in control tests. The in-pile stress-relaxation tests were usually carried out to low levels of neutron fluence, and relaxation apparently ceased after a strain on the order of a tenth of an elastic deflection. On the basis of these results, Hesketh[51] developed a model for transient irradiation creep by dislocation climb. The model involves the bowing of dislocation segments (Fig. 12) by climb under the combined forces due to line tension, applied stress, and chemical stress from the supersaturation of irradiation-produced defects. An equilibrium position is

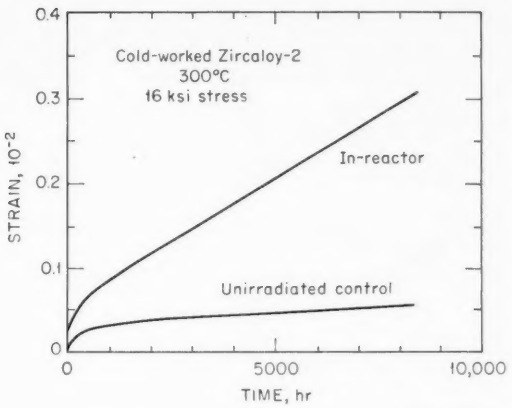

Fig. 11 Transient and steady-state irradiation creep in cold-worked Zircaloy-2.[22]

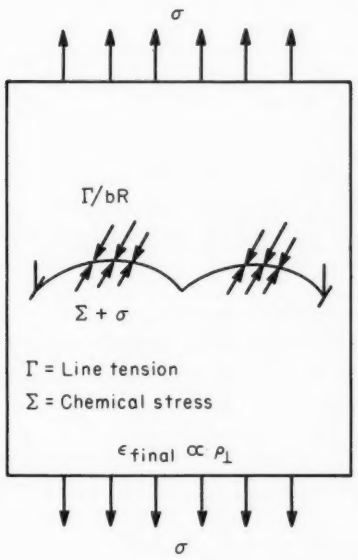

Fig. 12 Transient dislocation climb.

reached when the flow of vacancies and interstitials into each dislocation becomes equal. The strain rate decreases with increasing fluence until a final strain is achieved at the equilibrium position according to

$$\gamma = \frac{\tau}{8\mu}\left[1 - \exp\left(-\phi t/B\right)\right] \qquad (9)$$

where μ is the elastic shear modulus and B is a decay constant. The final strain is dependent upon dislocation density.[16,51-53] The amplitude of the final strain in Eq. 9 corresponds to the dislocation density of an annealed specimen.

Loop Orientation (Steady-State Irradiation Creep). With the advent of precision in-pile extensometers and advanced capsule technology in the 1960s, irradiation-enhanced or -induced creep was measured in a variety of materials. Results obtained to high fluence levels approaching 10^{22} neutrons/cm^2 ($E > 1$ MeV) on martensitic steels show that the transient stress relaxation is followed by a slower steady-state relaxation (Fig. 13).[54] Hesketh reported

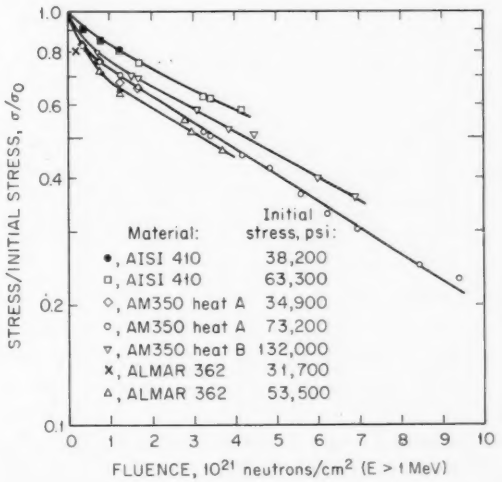

Fig. 13 In-pile transient and steady-state stress relaxation of martensitic iron-base alloys[54] at 310°C.

steady-state creep operating independently of transient creep in a wide variety of materials representing fcc, bcc, and hexagonal close-packed crystal systems.[55,56] He attributed this steady-state creep to a mechanism whereby clusters of irradiation-produced defects (vacancy cascades) collapse into dislocation loops aligned preferentially on the available crystallographic planes under the influence of applied stress (Fig. 14). Stress does not provide sufficient energy to change the type of plane onto which the dislocation loop is formed,[34] but stress can decrease the critical size a cluster must attain for the loop to be stable. This mechanism led to the following equations:

$$\epsilon = C\sigma\phi \qquad \text{isotropic material} \qquad (10a)$$

$$\dot{\epsilon} \simeq A_3 \dot{\epsilon}_g \sigma / T \qquad \text{anisotropic material} \qquad (10b)$$

where C and A_3 are creep-rate coefficients, and $\dot{\epsilon}_g$ is the growth strain rate. Steady-state creep is predicted for isotropic materials,[55] but the time dependence of irradiation creep in an anisotropic material[39] depends on the time dependence of the growth strain rate.

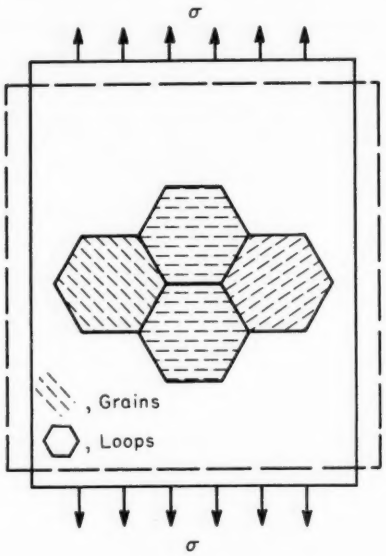

Fig. 14 Loop orientation.

Volume Creep. Although many authors have acknowledged an effect of irradiation on specimen volume,[5-14] very little attention has been given[49,57] to possible effects of stress on these volume increases. The effect of stress on volume is referred to as volume creep. Volume creep is synonymous with stress-assisted swelling. Dividing the volume increase by 3 yields the corresponding linear strain if the volume increases are isotropic.

Graphite undergoes volume creep in addition to irradiation growth and irradiation creep.[23,24,58,59] Deformation of graphite is a nonconservative volume process even in the absence of irradiation[60,61] with volume creep an important part of irradiation creep in pyrolytic graphite,[24,57,62]

At high temperatures in austenitic stainless steels, where voids grow during irradiation, a tensile stress reduces the effectiveness of the surface energy to suppress void growth. If this effect is sufficiently large, volume creep will occur (Fig. 15) and can influence the diameter increase in fuel elements (Fig. 2). Volume creep appears as swelling in excess of the zero-stress swelling.

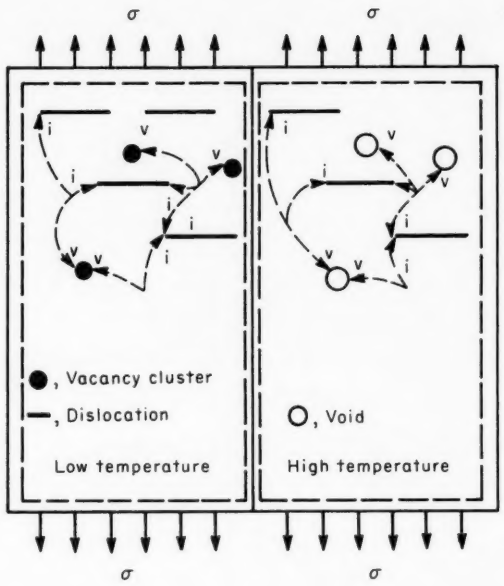

Fig. 15 Volume creep.

At low temperatures, vacancies are immobile and do not form large voids. Instead, as shown in Fig. 15, they cause swelling due to the dilatations associated with accumulation of single vacancies and small vacancy clusters (Fig. 16) for molybdenum.[63] Again, volume creep may occur but by a different mechanism than at high temperatures. Applied stress increases the effective capture radius of a dislocation for interstitials and thereby may reduce the number of interstitials that annihilate at vacancy sites. More vacancies are allowed to survive in the presence of stress and contribute to swelling and low-temperature volume creep.

A relation for nonconservative volume creep under different states of stress was developed by Gilbert and Straalsund.[64] The contribution of volume changes on strain rate was expressed as

$$\dot{\epsilon}_{mn} = \alpha(\phi,t,T)\sigma_{mn} + [\beta(\phi,t,T)W + \kappa(\phi,t,T)]\delta_{mn} \quad (11)$$

where α = stress coefficient
β = coefficient of the hydrostatic stress, W
κ = strain due to zero swelling
δ_{mn} = Kronecker delta equal to unity for normal strains and equal to zero for shear

The stress coefficients and the zero-stress swelling coefficient are functions of neutron flux, time, and temperature. The contribution of volume creep is greater for larger ratios of β/α. For shear strain rates δ_{mn} is zero, and volume creep does not contribute to shear deformation. A typical description of the fluence and temperature dependence of 3κ for 304 stainless steel at high temperatures is given by Eq. 1. Figure 16 shows 3κ for both low and high temperatures in molybdenum. The temperature and fluence dependences of α and β are not clearly defined over a wide temperature and fluence range, but as a first approximation the temperature dependence of β might be expected to be similar to the temperature dependence of κ.

In relating Eq. 11 to Fig. 2, curve B represents the sum of β and κ, and curve E represents α; curve C represents β, and κ is represented by curve D. Experiments are needed to clearly demonstrate the extent of volume creep over a temperature, stress, and fluence range of concern to LMFBRs.

Irradiation-Creep in Stainless Steels at Low Temperature. Mosedale et al.[18] studied creep of several metals and alloys in the form of weighted helical springs in the DFR and found behavior similar to that reported by Hesketh for the Herald Reactor,[55] a transient strain followed by steady-state creep continuing to neutron fluence levels of 10^{21} neutrons/cm^2 ($E > 0.82$ MeV). These results and some results obtained in the Dounreay Materials Test Reactor (DMTR)[52] are shown in Fig. 17. Type 316 stainless steel displayed entirely transient creep in the DMTR, in contrast to both transient and steady-state creep in the DFR. Cold work increased the irradiation-induced transient-creep strain in 316 stainless steel in accord with Hesketh's[51] transient-climb model, Eq. 9. Less irradiation creep was observed in alloys than in unalloyed metals. Of particular significance is the very small amount of irradiation creep observed in solution-treated PE16. If the steady-state creep component is due to the stress orientation of loops as described by Hesketh[55] in Eq. 10*a*, then the unique structure of solution-treated PE16 either suppresses loop formation or reduces the effectiveness of stress on orientation. This indicates that it may be feasible to design alloys with the desired irradiation-creep properties through control of the microstructure.

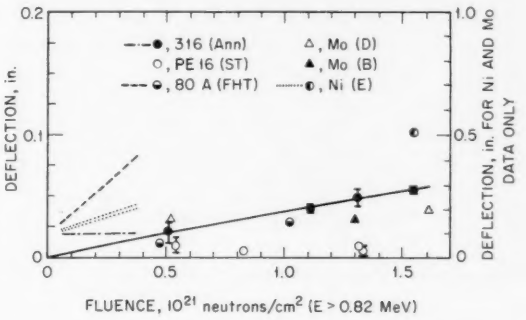

Fig. 17 Deflection in helical springs due to irradiation creep. Deflection is normalized to 25 turns and a stress of 1890 psi. Solid lines and data points represent irradiation in DFR and broken lines represent irradiation in DMTR. Note the change in scale for molybdenum and nickel data.[18]

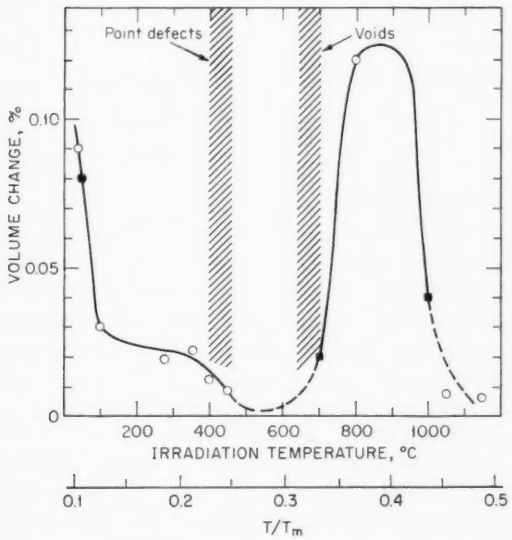

Fig. 16 Volume change in irradiated molybdenum as a function of irradiation temperature normalized to 2.5×10^{19} neutrons/cm^2 ($E > 1$ MeV).[63]

Measurement of tensile-irradiation creep of annealed 304 and 20% cold-worked 316 stainless steels in a Hanford reactor[16] showed more transient strain in the cold-worked 316 stainless steel in accord with results of Lewthwaite, Mosedale, and Ward[52] and Hesketh's transient climb model. The creep strain for annealed 304 stainless steel was described by the sum of Eqs. 9 and 10*a* as plotted in Fig. 18 with other data on annealed stainless steels. Whereas these data appear to provide reasonable agreement, a nonconventional definition of effective strain was used for the tensile data. The tensile data showed ~ six times more strain

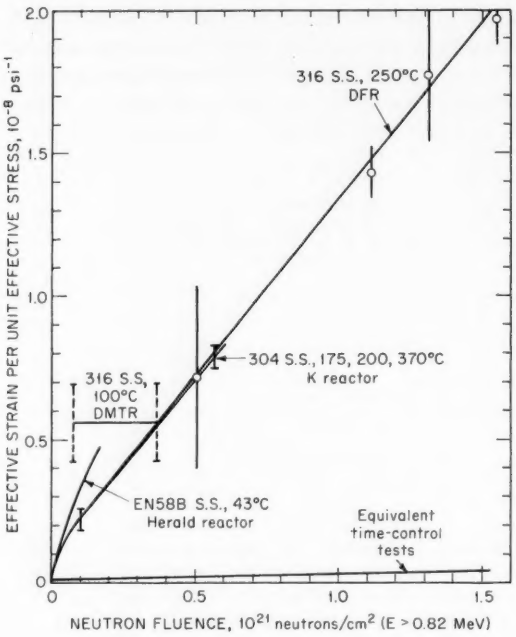

Fig. 18 Irradiation-induced creep[55] in annealed austenitic stainless steels type 316 (Refs. 18 and 52), 304 (Ref. 16), and EN58B.

than needed to correlate with the torsional-spring data using the sum of Eqs. 9 and 10*a* and the effective strain and effective stress for constant-volume deformation[65] defined in Eqs. 12 and 13*a*. The discrepancy was attributed to volume creep occurring under the hydrostatic stress component of the tensile stress. A ratio of 9 for β/α in Eq. 11 allowed redefinition of the effective strain under conditions of nonconservative volume as described in Eq. 13*b*.

$$\bar{\sigma} = \sqrt{3}\tau = \sigma = 0.866\sigma_h \qquad (12)$$

$$\bar{\epsilon} = \gamma/\sqrt{3} = \epsilon = 1.154\epsilon_h \qquad \text{constant volume} \quad (13a)$$

$$\bar{\epsilon} = \gamma/\sqrt{3} = \epsilon/6 = 0.105\epsilon_h$$

$$\text{nonconservative volume} \quad (13b)$$

where $\bar{\sigma}$ = effective stress
τ = shear stress
σ = tensile stress
σ_h = tangential stress in a pressurized tube
$\bar{\epsilon}$ = effective strain
γ = shear strain
ϵ = tensile strain
ϵ_h = tangential strain in a pressurized tube

As a first approximation it was assumed that the ratio $\beta/\alpha = 9$ was independent of fluence, temperature, and stress level, although it is realized that α and β probably have separate functional relations. The ratio of β/α does not affect the definition of effective stress, and therefore Eq. 12 is valid for both conservative and nonconservative volume deformation.

Figure 19 shows the creep-rate constant C of Eq. 10*a* determined from the slopes of the curves in Fig. 18 plotted vs. temperature. The data from the DMTR were not included since steady-state creep was not observed. The creep rate decreases as temperature increases, much like the effect of temperature on point-defect annealing as observed for swelling in molybdenum[63] (Fig. 16) at low temperatures.

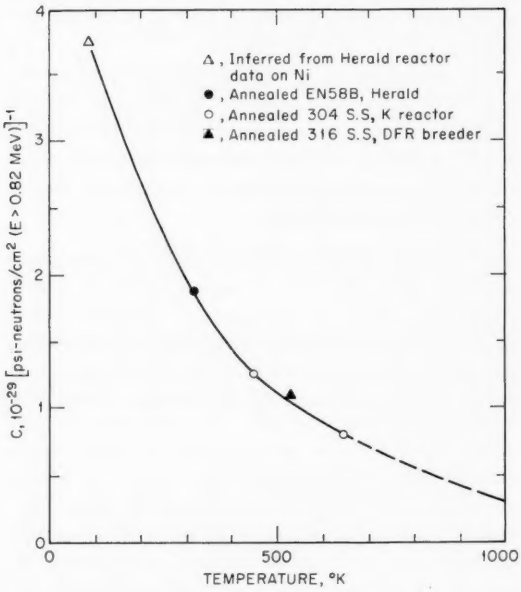

Fig. 19 Temperature dependence of the irradiation-induced creep-rate coefficient, *C*.[16]

The combined expression for the results shown in Fig. 18, which incorporates the state-of-stress correlation for nonconservative volume deformation by Eqs. 12 and 13*b*, the temperature dependence of Fig. 19, and the average neutron energy to compensate for the different neutron spectra of the irradiation-test facilities, is given as[17]

$$\bar{\epsilon}/\bar{\sigma} = 2 \times 10^{-9} [1 - \exp(-T\phi t)] + 4.5 \times 10^{-7} \bar{E}\phi t \exp(1.14 - 0.0027T) \quad (14)$$

where $\bar{\epsilon}/\bar{\sigma}$ = effective strain to effective stress ratio in psi^{-1} as defined by Eqs. 12 and 13*b*
T = temperature, °K
ϕt = total neutron fluence in units of 10^{23} neutrons/cm^2 ($E > 10^{-10}$ MeV)
$\bar{E}$ = average neutron energy in MeV

Stress-relaxation results on annealed 304 stainless steel tested in tension[66] and in torsion[67] in a common irradiation-test facility show consistency with the creep results in that more stress relaxation was observed in tension than in torsion. These low stress results are shown in Fig. 20. The solid curves were computed from Eq. 15 which was adapted to describe stress relaxation by differentiation of Eq. 14 with respect to time, separating stress and time, and integrating over stress and time under constant strain. Total strain is maintained constant by allowing the elastic strain to be replaced by the irradiation-induced strain.

$$\ln \sigma/\sigma_0 = -A_4 \left(\frac{E}{\mu}\right) [1 - \exp(-\phi t/B)] - C \left(\frac{E}{\mu}\right) \phi t \quad (15)$$

where σ_0 = initial stress
σ = stress at fluence ϕt
A_4 = related to the amplitude of the transient strain from Eq. 9
C = rate constant from Eq. 10*a*
E or μ = elastic modulus in tension or in shear

When the values of A_4 and C from the constant-load creep data (Eq. 14) are adjusted for the state of stress by Eq. 13*b*, agreement is found between the creep and stress-relaxation data for nonconservative volume deformation as shown by the curves computed from the creep data and the stress-relaxation data points in Fig. 20.

Since a component undergoing irradiation creep in bending is composed of mixed tensile and compressive stresses, its stress relaxation is expected to be less than that observed in tension but greater than that observed in torsion. This is because compressive stresses are not expected to produce volume creep and may even reduce the extent of swelling. The resulting stress-relaxation curve for bending composed of mixed tensile and compressive stresses is expected to be intermediate to the two curves (Fig. 20) for shear and tension.

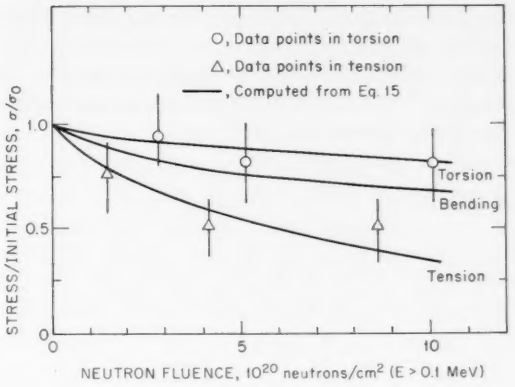

Fig. 20 Irradiation-induced stress relaxation in annealed 304 stainless steel at 100°C.[16,66,67]

Irradiation Creep in EBR-II. Diametral strain data generated[68] on annealed 304 stainless-steel tubes pressurized with helium in EBR-II show a creep rate in fair agreement with Eq. 14 using the relations of Eqs. 12 and 13*b* and nonconservative volume creep. Subsequent higher fluence data,[69] however, show strains less than those predicted by Eq. 14. This discrepancy is most likely due to Eq. 14 being an oversimplification of the problem of describing irradiation creep. The 370°C test temperature used in these studies places the tests just slightly to the right of the minimum in zero-stress swelling for stainless steel as shown typically for molybdenum in Fig. 16, whereas data used in developing Eq. 14 were obtained primarily to the left of this minimum. The coefficients in Eq. 11 may vary differently with temperature such that the ratio of β/α or the relative contribution of volume creep may depend on temperature.

Comparison of modeling-code predictions and observed performance of EBR-II driver fuel led to the conclusion that above 2 at.% burnup, irradiation-induced cladding creep is an important factor that becomes dominant above about 2.5 at.% burnup (fluence 2.6×10^{22} neutrons/cm^2, $E > 0.1$ MeV).[26] A study[70] of experimental mixed-oxide pins irradiated in EBR-II has consistently shown cladding-diameter increases greater than can be accounted for by zero-stress swelling. Considering the limited compressive strength in the fuel due to irradiation creep[30,31] as discussed under the heading "Nuclear Fuel," the stresses exerted on the cladding by the fuel could be

too low to activate considerable thermal creep. These cladding deformations may be due to irradiation creep in the cladding. The origin of cladding stresses and the extent of fuel-cladding interaction are complex problems receiving much attention.[3]

Loop Unfaulting. Dislocation loops are generated by the collapse of defect clusters produced by irradiation. If these dislocations can glide, they will contribute to the creep rate. In close-packed structures these loops are faulted and cannot glide. At high temperatures these dislocations grow by absorbing point defects (Fig. 21) until they reach a critical radius

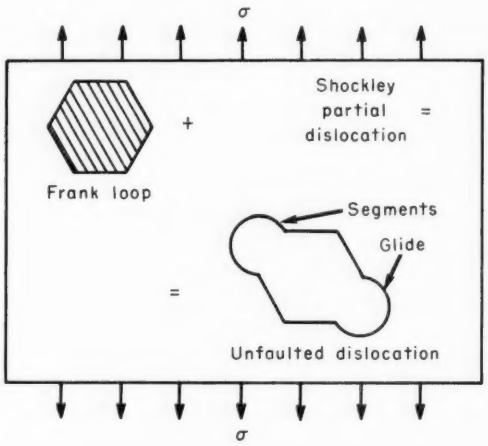

Fig. 21 Loop unfaulting.

above which it is energetically favorable for them to unfault and transform into loops capable of gliding. A mechanism based on loop unfaulting, suggested by Gilbert and Holmes,[71] is described by

$$\dot{\epsilon} = b\pi\,(r_p^2 - r_c^2)\,\frac{\partial N_2}{\partial \phi t}\phi f(\sigma,T) + \frac{N_2 \pi r_p^2}{\rho}\,\dot{\epsilon}_{th} \qquad (16)$$

where r_p = radius at which unfaulted loops are pinned
r_c = critical radius for loop unfaulting
N_2 = number of loops per unit volume
ρ = the dislocation density

Other terms are as previously defined.

The first term arises from the nucleation rate of dislocations or the rate at which irradiation-induced Frank partial loops become unfaulted and their subsequent glide until stopped by obstacles. Stress and temperature assist in the bowing of loop segments from which a stress and temperature dependence arise. The second term arises from the rate of motion of unfaulted loop segments beyond the radius where dislocations become pinned. The stress and temperature dependence of the second term are similar to that for thermal creep.

This mechanism is a possible source of irradiation creep at temperatures above 500°C and would contribute to constant volume deformation (curve E, Fig. 2). If the critical radius for unfaulting were achieved by the coalescence of faulted loops, then this mechanism would not be dependent on high-temperature diffusion for growth, and loop unfaulting could occur at low temperatures.

Dislocation Climb. Irradiation-enhanced dislocation climb has been a suspected mechanism for irradiation creep for many years,[43] but only recently has the problem received careful attention. Nabarro[72] pointed out in 1948 that irradiation should not directly enhance diffusion creep, commonly referred to as Nabarro-Herring creep involving mass transfer between grain boundaries parallel to and normal to a tensile-stress axis. Since irradiation-produced defect concentrations are assumed to not be increased or decreased by stress, stress cannot set up concentration or chemical potential gradients of these defects. Therefore stress cannot directly influence mass transfer or diffusion of irradiation-produced defects.

Schoeck[73] later described a dislocation-climb model for irradiation creep by enhanced vacancy diffusion. His treatment resulted in the following equation:

$$\dot{\epsilon} = \dot{\epsilon}_{th}\left(1 + \frac{a^2 \alpha_2 \phi}{D_{th} S_1}\right) \qquad (17)$$

where a is the lattice parameter, α_2 is the atom fraction of vacancies produced per unit fluence, and S_1 is the atomic fraction of places where vacancies and interstitials anneal out. Other terms are as previously defined. Equation 17 involves thermal creep plus a flux-dependent contribution due to irradiation-enhanced climb.

Brinkman and Wiedersich[37] described a similar model given in Eq. 18:

$$\dot{\epsilon} = \dot{\epsilon}_{th}(D_{th} + \dot{N}\,\overline{X^2})/D_{th} \qquad (18)$$

where $\dot{N}$ is the atomic fraction of vacancies produced per time unit, and $\overline{X^2}$ is the mean-squared distance a vacancy must move to reach a sink. Nichols[74,75] used a description similar to that given by Brinkman and

Wiedersich for the enhancement of the diffusion coefficient and applied it to a specific model[76] for climb over obstacles. Nichols' result is

$$\dot{\epsilon} = A_5 \sigma^4 L^2 (D_{th} + \dot{N}\overline{X^2}) \qquad (19)$$

where A_5 is a constant, L is the average spacing of obstacles, and the other terms are as previously defined.

These models have been criticized by Mosedale[77,78] and Hesketh[46,79,80] on arguments similar to the concepts given by Nabarro for diffusion creep. These are typically based on the assumption that stress does not produce a chemical potential gradient for diffusion of irradiation-produced defects, and hence, diffusion of defects produced by irradiation is entirely independent of stress.

More specifically applied to the problem of dislocation climb, local deviations from detailed balancing of vacancies and interstitials produced by neutron flux[77] may permit a climbing segment to attain the critical height and slip sooner than in the absence of the neutron flux. If the reverse process occurs as frequently, in which a segment almost ready to slip suffers a reverse when a burst of defects of the wrong kind arrives, irradiation should, therefore, not affect creep by a climb mechanism. On the other hand, Buckley[42] asserted that vacancies are immobilized by clustering, and dislocation climb occurs predominantly by consumption of excess interstitials. As a result, the probability of climb releasing dislocations from obstacles greatly exceeds the probability of causing them to encounter obstacles.

Hesketh's transient-climb model[51] involves the bowing of dislocation segments under the combined forces due to line tension, applied stress, and chemical stress from irradiation-produced defects. The chemical stress was expressed as

$$\Sigma = kTb^{-3} \ln \frac{C_{ve} C_i}{C_v C_{ie}} \qquad (20)$$

where Σ = chemical stress
k = Boltzmann constant
T = temperature
b = Burgers vector
C_{ve} = thermal equilibrium concentration of vacancies
C_v = actual vacancy concentration
C_i = interstitial concentration
C_{ie} = thermal equilibrium concentration of interstitials

Since interstitials and vacancies move independently to cause a void to shrink or to grow as well as to cause a jog to climb up or down, the chemical stress is valid only when considering defects of only one type.[81] Equation 20 is meaningless when there are large supersaturations of both interstitials and vacancies. Under these conditions the defect behavior is controlled by kinetic rather than thermodynamic factors. Hesketh's climb model led to a transient creep rate, Eq. 9, which ceased when the flow of vacancies and interstitials into each dislocation became equal and an equilibrium position was reached.

Lewthwaite and Mosedale,[82] in discussing problems of determining the stress dependence of irradiation creep in specimens with a complex stress state, suggested the possibility that segments which have climbed by Hesketh's transient mechanism[51] in Eq. 9 and Fig. 12 may be able to bow out further in their slip planes and that the number climbing far enough to do this significantly will depend on stress, as will the area of plane swept by the bowed segments. The stress dependences will be compounded, leading to a stronger stress dependence.

Experiments conducted[42] on a variety of fcc and bcc metals have shown irradiation creep in excess of the transient strain described by Eq. 9. The excess strain was attributed to dislocation glide in addition to climb. Thermal- or displacement-spike stresses may literally knock short segments of dislocation forward past local pinning points, with the barriers being surmounted by direct intersection or by cross slip. Another possibility is that the excess interstitial flux may permit dislocations to climb past barriers in the glide plane.

If there is a small difference in interstitial and vacancy sink concentrations, the jog velocity in screw or edge dislocations could be dominated by the irradiation-induced vacancies and interstitials. As a result (Fig. 22), the climb velocity becomes independent of stress and temperature.[34] Any stress and temperature dependence of the creep rate must result from their effects on the mobile dislocation density and the relative sink concentrations and effectiveness. On this basis Tesk et al.[19,20] have modified the Ansell-Weertman model[76] for climb over obstacles during irradiation creep so that the climb velocity is independent of applied stress, depending only on the excess flux of irradiation-produced interstitials (Fig. 23). Vacancies are clustered at voids (swelling is an experimental verification of this), and interstitials are preferentially attracted to dislocations. The stress dependence of their model develops from the effect of

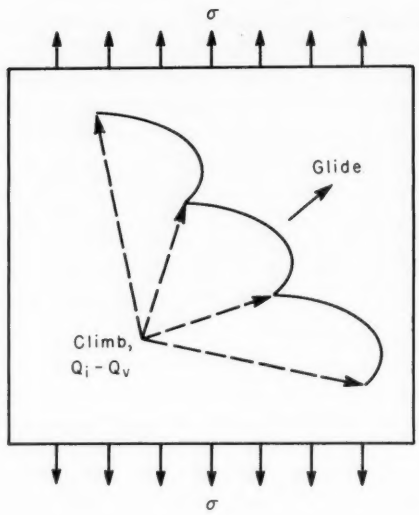

Fig. 22 Enhanced climb of jogged screw dislocations.

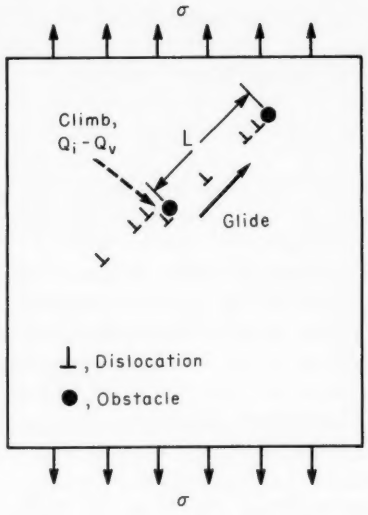

Fig. 23 Enhanced dislocation climb.

stress on decreasing the distance a dislocation must climb to get over the obstacles. The resulting relation is given as

$$\dot{\epsilon} = \frac{A_6 \sigma^2 L}{\mu^2 bd} \left(2D_{th} \frac{\sigma^2 bL}{\mu kT} + \frac{Q_{i,\mathrm{dis}} - Q_{v,\mathrm{dis}}}{L} b^2 \right) \quad (21)$$

where A_6 = a constant
L = spacing between obstacles
μ = elastic shear modulus
b = Burgers vector
d = obstacle height
D_{th} = thermal-diffusion coefficient
k = Boltzmann constant
T = absolute temperature
$Q_{i,\mathrm{dis}}$ = interstitial flux to dislocations
$Q_{v,\mathrm{dis}}$ = vacancy flux to dislocations

The first term on the right represents thermally activated climb and is important at high temperatures where D_{th} is large. The second term represents the irradiation-enhanced climb and is important when the interstitial flux to dislocations is large. This equation,[76] for moderately high stresses where piled-up dislocations climb over obstacles, has the flexibility of containing terms which represent microstructural features of the specimen such as the spacing between obstacles and the obstacle size. These microstructural features depend on neutron fluence and temperature. The excess interstitial flux-generating climb is related to the excess vacancy flux causing void nucleation and growth, thus allowing assessment of the interstitial flux from studies on voids.[10,20] Because the strain is generated by dislocation glide, creep by this mechanism proceeds under constant volume and contributes only to curves E and F in Fig. 2.

An estimate of the relative contributions of the various mechanisms is given in Table 3. Since dislocation climb is characterized by a second or higher order stress dependence, it becomes most important at high stress levels. For this general evaluation of the mechanisms, the dislocation climb model and jogged screw models are considered equivalent. Likewise, the spike- and loop-orientation mechanisms were treated together since loop orientation is a special case of the more general spike mechanism. Some of these mechanisms may switch in order of importance as a function of fluence and other variables, but there is insufficient data to allow a more precise estimate at this time.

A complex dependence of irradiation creep on stress[25,74,75] has been predicted as a result of multi-mechanisms operating simultaneously to produce creep. This predicted behavior (Fig. 24) includes stress-independent irradiation growth,* loop alignment, and climb control as the stress increases. These

*Although irradiation growth had commonly been regarded as a peculiarity of anisotropic crystal structures, Buckley[42] found irradiation growth to occur in fcc and bcc metals if the specimens had been cold worked. Therefore, the stress-independent irradiation-growth strain contribution (Fig. 24) applies to cold-worked stainless steels.[42]

Table 3 Estimated Importance of Irradiation-Creep Mechanisms (in Order of Decreasing Importance)

	Low Stress	High Stress
Low temperature <0.3 Tm	Volume creep (small clusters)	Dislocation climb
	Dislocation climb	Volume creep (small clusters)
	Loop orientation	Loop orientation
	Transient climb	Transient climb
	Loop diffusion creep	Loop diffusion creep
	Yielding creep (fcc and bcc materials require cold work)	Yielding creep (fcc and bcc materials require cold work)
High temperature ~0.3 to ~0.5 Tm	Volume creep (voids)	Dislocation climb
	Dislocation climb	Loop unfaulting
	Loop unfaulting	Volume creep (voids)
	Loop diffusion creep	Loop diffusion creep
	Loop orientation	Transient climb
	Transient climb	Loop orientation
	Yielding creep (fcc and bcc materials require cold work)	Yielding creep (fcc and bcc materials require cold work)

mechanisms operate either independently or sequentially[83] and the creep rates are added similar to conductances of resistive elements connected in parallel and in series in an electrical circuit.

The mechanisms of stress-free growth, stress-oriented loops, dislocation climb, and cutting of Seegar zones are treated as if contributing independently to irradiation creep. Thus the creep rate is the sum of Eqs. 7, 10, and 19. However, the dislocation-climb mechanism is composed of two sequential elements. At low stresses, irradiation-enhanced dislocation climb is so rapid that the creep rate is limited by the glide velocity $\dot{\epsilon}_{int}$, and a strong stress dependence is observed. At higher stresses the dislocation glide velocity becomes so rapid that the deformation is limited by the climb of individual dislocations and the irradiation enhanced creep rate is linear with stress. At higher stress levels the creep rate is controlled by climb over obstacles (Eq. 19) and the cutting of Seegar zones characterized by a very strong stress dependence. The operation of these mechanisms (Fig. 24) is represented over the complete range of stresses by the following expression:

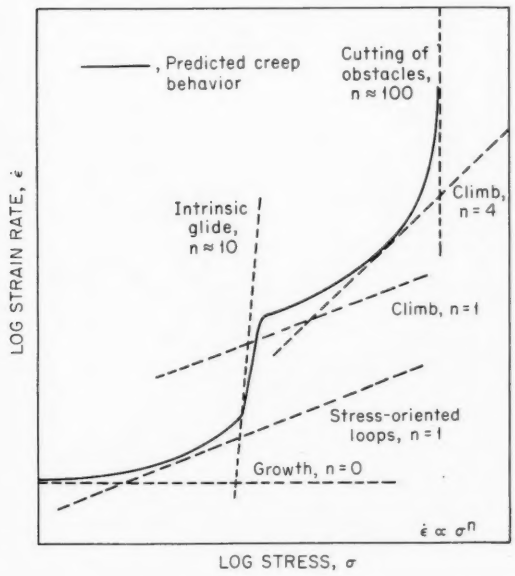

Fig. 24 Schematic representation of creep controlled by an assembly of mechanisms.[25]

$$\dot{\epsilon} = \dot{\epsilon}_{growth} + \dot{\epsilon}_{loop} + \left(\frac{1}{\dot{\epsilon}_{int}} + \frac{1}{\dot{\epsilon}_{climb} + \dot{\epsilon}_{cut}}\right)^{-1} \quad (22)$$

Cyclotron irradiations performed on uniaxial tensile specimens of austenitic stainless steels with 22-MeV deuterons[84] have shown significant irradiation-induced creep in the range of 300 to 450°C. This test simulates approximately twice the displacement rate in EBR-II. These results show a weak dependence of creep rate on temperature, and a stronger than linear stress dependence. Prior irradiation in EBR-II to a total fluence of 8×10^{21} neutrons/cm^2 at 460°C was found to significantly reduce the irradiation-induced creep rate.[85] These tests are conducted at high stress

levels in the range of 50,000 to 70,000 psi and therefore lie in the high stress domains (Fig. 24). The results[20] are attributed to irradiation-enhanced dislocation climb in accordance with the model of Eq. 21.

The stress dependence of irradiation creep of zirconium alloys, Zircaloy-2 and Zr-2.5 Nb, has recently been summarized by Fidleris.[86] These data (Fig. 25) show a striking resemblance to the complex stress dependence described by Nichols (Fig. 24).

Structural Mechanisms

Structural mechanisms may cause an increase of creep rate (softening) or a decrease of creep rate (hardening).

Softening. Dissolution of solution-strengthening elements results in softening or a reversal of solution strengthening. This may be enhanced by irradiation and cause a faster creep rate both in-reactor and in postirradiation creep tests. Obstacle coarsening, sometimes called overaging, can be influenced by irradiation, rendering increased dislocation mobility. Standring, Bell, and Tickle[87] have observed softening processes in 316 stainless steel at 525°C in the DFR.

Irradiation may increase the mobile dislocation density through the generation of dislocation loops. Unfaulting of Frank loops may increase the creep rate in postirradiation creep tests by increasing the mobile dislocation density. Gilbert and Holmes[88] have observed induced creep in postirradiation creep tests conducted in torsion on EBR-II safety-rod thimble material, 304 stainless steel, which contained ~10^{16} faulted loops/ cm^3 after being irradiated to 5.5 x 10^{22} neutrons/ cm^2 ($E > 0.1$ MeV) at 415°C. About 0.3%

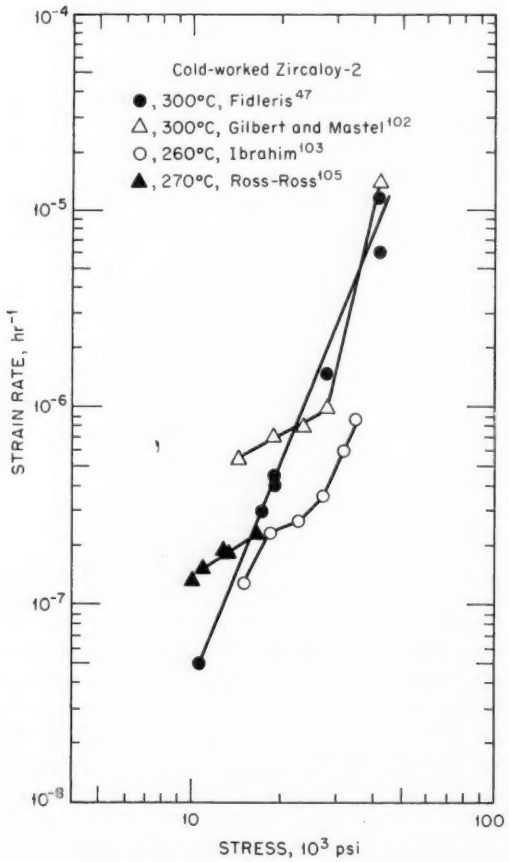

Fig. 25*a* Stress dependence of irradiation creep[86] for cold-worked Zircaloy-2.

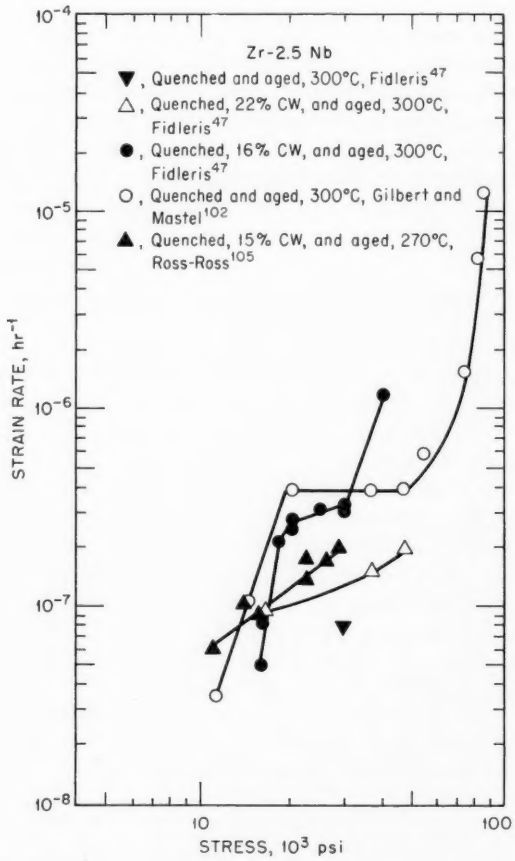

Fig. 25*b* Stress dependence of irradiated creep[86] for cold-worked Zr-2.5 Nb.

excess strain was observed at a maximum shear stress of 5000 psi at 550°C. This excess strain is attributed to the mobile dislocations released when the loops unfaulted.[71]

Clusters of point defects may break up due to thermal annealing and cause enhanced dislocation climb in postirradiation creep tests, or, if the clusters were pinning points, the dislocations would be released upon cluster breakup. A uniaxial tensile specimen prepared from a longitudinal section of a 15% cold-worked Zircaloy-2 pressure tube stress relieved for 72 hr at 400°C was irradiated to ~2 x 10^{19} neutrons/ cm^2 ($E > 1$ MeV) at 300°C and then stressed at 300°C to 45,000 psi.[89] In contrast to irradiation hardening[47] that occurs after an exposure of 3 x 10^{20} neutrons/ cm^2 ($E > 1$ MeV) (Fig. 26), a large enhancement of creep rate was observed (Fig. 27). This appears similar to a large creep-rate enhancement observed in molybdenum irradiated to a similar level of neutron fluence and stressed at 0.3Tm in a postirradiation creep test.[90] The enhanced creep rate was attributed to the decomposition of point-defect clusters upon stress application, allowing enhanced climb and dislocation mobility. The disappearance of swelling by point-defect accumulation at 0.3Tm is evidence for decomposition of small clusters at this temperature (Fig. 16). Kulcinski[91] showed that the application of pressure decreases the temperature for annealing of irradiation-produced defect clusters. This phenomenon[47] is limited to very low fluences, and, after somewhat larger fluences, the defect clusters become stable and irradiation hardening is observed instead of creep-rate enhancement (Fig. 26). This phenomenon could not be produced in Zr-2.5 Nb, emphasizing the role of Nb in stabilizing the defects.[92]

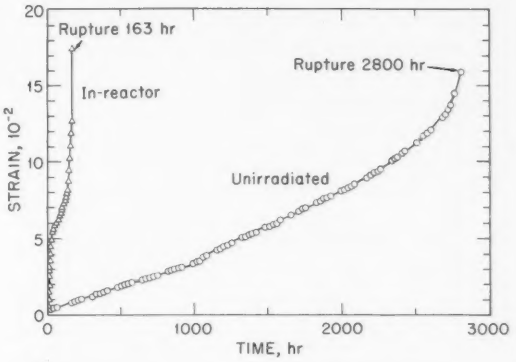

Fig. 27 Creep of cold-worked Zircaloy-2 at 300°C and 45,000 psi stress unirradiated and after a preexposure of 2 x 10^{19} neutrons/cm^2 ($E > 1$ MeV).[89]

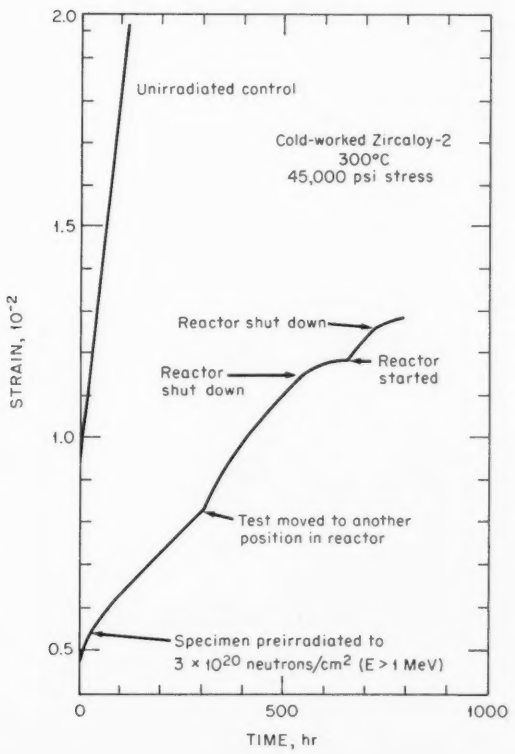

Fig. 26 Irradiation hardening and enhancement of creep in cold-worked Zircaloy-2.[47]

Other low-fluence in-reactor creep data at high stress levels in Zircaloy-2 also show some interesting results. A larger temperature dependence of in-reactor creep rates was found during neutron irradiation than during reactor outages.[93] Figure 28 shows the creep rates at 25,000 and 35,000 psi plotted vs. reciprocal temperature.[94] Similar behavior was also observed at stress levels of 30,000 and 20,000 psi, but overlapping of the curves made it simpler to show only two stress levels (Fig. 28). Due to the different slopes, depending on whether the neutrons were off or on, both creep-rate increases and decreases were observed when the reactor shut down. The observation of an increase or decrease was very sensitive to the test temperature and stress level.

One method by which irradiation may cause diffusion creep can be visualized in terms of a single crystal that would not be expected to display a significant creep rate by the Nabarro-Herring mecha-

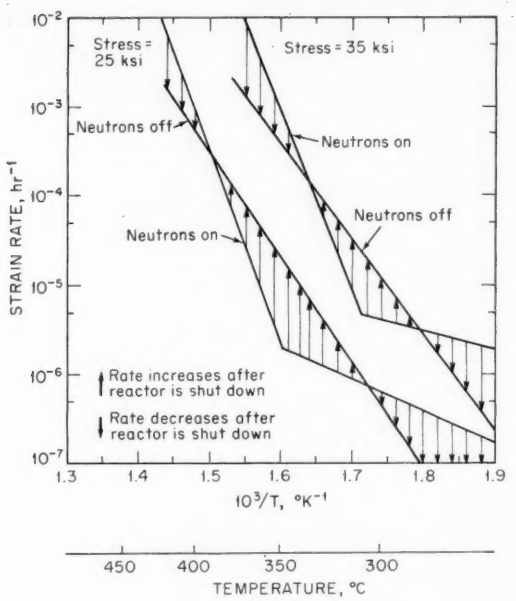

Fig. 28 In-reactor creep of cold-worked Zircaloy-2 showing effect of reactor shutdown on creep rate at low fluence level.[93,94]

nism.[72] If irradiation were to cause a development of grain structure, then Nabarro–Herring creep would occur. As the grain structure became more refined with increasing neutron fluence, diffusion creep would increase owing to its dependence on grain size. The argument could be applied to generation of dislocations due to irradiation in a polycrystalline material that initially had a low dislocation density. Irradiation could thereby initiate diffusion creep by the Coble mechanism.[95]

Although irradiation is not necessarily expected to cause a single crystal to change into a polycrystal, this concept of irridiation-induced microstructure developing to initiate a particular creep mechanism applies to the interstitial loop structure which develops in close-packed crystals. These loops do not form entirely on parallel planes but tend to form on all four orientations of the (111) type planes in fcc crystals. Tensile stress causes loops normal to the tensile stress to grow at the expense of those parallel to the tensile stress (Fig. 29) through thermally activated diffusion.[96] Consequently a form of diffusion creep occurs which could not have occurred had the loops not been generated. A mechanism of this type has been formulated by Ashby.[97] His result is given as

$$\dot{\gamma} = \frac{N_i \Omega}{\mu_R} \sigma \Omega \tag{23}$$

where N_i is the number of interstitials per cubic centimeter per second absorbed by loops, μ_R is the chemical potential of defects midway between dislocations, and Ω is the atomic volume of the defect. The creep rate is linear in flux, linear in stress, and varies in a complicated way with temperature. N_i is derived from models that treat the number of vacancies going to voids such as found in Refs. 10 and 20. Although creep by this mechanism will continue, if the irradiation ceases, creep would be transient and would eventually stop. Continuous irradiation is necessary for this mechanism to produce steady-state creep. The mechanism would eventually cease to operate as loops parallel to the tensile stress were consumed.

Piercy[34] discussed the case where solute atoms have a lower energy when associated with a region of irradiation damage than when associated with a dislocation. In this case solutes leave the dislocations during irradiation, thus increasing the dislocation mobility. Suppression of strain aging[98] due to irradiation may be an important factor in the creep-rate enhancement in zirconium alloys around 0.3 Tm. However, this probably is not applicable at strain rates below 7×10^{-7} hr^{-1}. Steady-state creep behavior[99] in Zr–2.5 Nb was shown to be consistent with a disloca-

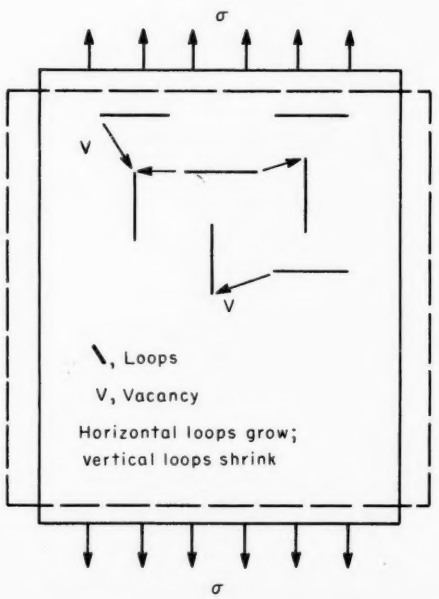

Fig. 29 Nabarro–Herring diffusional creep of loops.

tion climb model at strain rates below 7×10^{-7} hr^{-1} at 0.3 Tm. Strain–aging suppression at 0.3 Tm may be important at higher strain rates.

Irradiation may enhance the recovery of cold work, thus leaving cold-worked specimens less creep resistant. The specimen is in a particularly low creep-resistant state during cold-work recovery because dislocations released from their pinning points are mobilized.

The preceding discussion has introduced a few of the structural mechanisms that may cause a material to be less creep resistant as a result of irradiation. These mechanisms may affect creep during or after irradiation.

Hardening. Irradiation-produced defects, such as small vacancy and interstitial clusters, loops, and voids, may interact with dislocations to produce irradiation hardening or retarded creep. Irradiation may enhance precipitation of supersaturated constituents and result in precipitation hardening. Whereas theories of hardening are well developed for the yield phenomenon,[4,100] the Ansell–Weertman model[76] is one of the few models that account for hardening during plastic flow.

Irradiation can simultaneously produce hardening of thermal creep and inducement or enhancement of creep. Irradiation creep of Zr–2.5 Nb is shown[89] in Fig. 30. Whereas the in-reactor creep rate is lower than the creep rate for unirradiated control tests, further reduction of creep rate is observed when the reactor is turned off. A similar observation of coexisting hardening and enhancement is observed in Zircaloy-2 (Figs. 11 and 26).

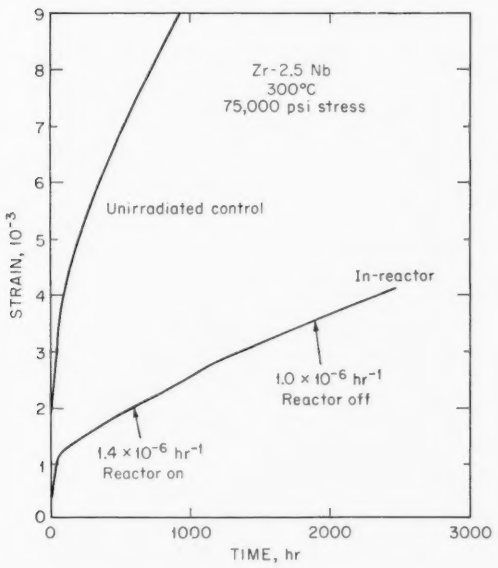

Fig. 30 Irradiation hardening and enhanced creep in quenched and aged Zr–2.5 Nb.[89]

Holmes[101] found both irradiation hardening and creep inducement during cyclotron irradiation of thorium. The thermal creep was suppressed, whereas irradiation induced creep in excess of thermal creep in an unirradiated specimen. The irradiation-induced creep strains at the low levels of fluence were completely recovered after turning off the 35-MeV proton beam. Holmes indicated that the concepts advanced by Konobeevsky[38] and Hesketh[39] seemed applicable. Point defects formed in the fission spike agglomerate in a manner tending to partially relax the elastic strain associated with the applied stress. The defect aggregates are unstable and disappear after completion of the irradiation so that the creep strain is recovered. The aggregates interfere with the motion of glide dislocations and suppress operation of the normal creep mechanisms.

CONCLUSIONS

Irradiation creep has been reported in many materials, both metals and nonmetals of cubic and noncubic crystal systems. Irradiation creep is a general phenomenon. There are numerous mechanisms by which irradiation creep may occur, and some of these are also important in postirradiation creep tests owing to the alterations in microstructure caused by irradiation. Irradiation creep has been observed to be sensitive to microstructure, providing encouragement that desired irradiation creep properties can be achieved by microstructural control. Solution-treated PE16 is an excellent example of this.

Irradiation creep is not well characterized over broad ranges of stress, temperature, neutron flux, and fluence, and theories for irradiation creep are not sufficiently developed or proven to provide reliable predictions of behavior to high neutron fluences as required in the design of LMFBR structural components. Considering that irradiation creep is probably composed of an assortment of mechanisms, many sensitive to microstructure, considerable study is still required in characterizing irradiation-creep behavior in terms of microstructure and test parameters before reliable extrapolations can be performed. Experimental programs are being conducted in the United States and other nations to develop an understanding of irradiation creep.

ACKNOWLEDGMENTS

Appreciation is expressed to many colleagues at the Hanford Engineering Development Laboratory and elsewhere for their helpful discussions, to J. J. Holmes for encouragement and contributions, to C. P. Cabell for dedicated assistance and contributions in technical editing, and to the Division of Reactor Development and Technology of the U. S. Atomic Energy Commission for supporting this work.

REFERENCES

1. G. W. Wensch, Introductory Remarks on Material Problems in Sodium-Cooled Reactors, in *Nuclear Metallurgy, Vol. IX, A Symposium on Materials for Sodium-Cooled Reactors, 1963 Winter Meeting of the American Nuclear Society, New York,* p. vii, L. R. Kelman and Sherman Greenberg (Eds.), American Institute of Mining, Metallurgical, and Petroleum Engineers, Metallurgical Society, New York, 1963.
2. G. W. Cunningham, Development of Fuel Cladding for Fast Reactor, in *Irradiation Effects in Structural Alloys for Thermal and Fast Reactors,* American Society for Testing and Materials, Special Technical Publication No. 457, p. 329, 1969.
3. C. E. Weber, Introduction—Fuels III—Special Session on Integral Fuel Element Performance Models, *Nucl. Appl. Technol,* **9:** 287 (1970).
4. A. L. Bement, Jr., Fundamental Materials Problems in Nuclear Reactors, in Second International Conference on Strength of Metals and Alloys, Pacific Grove, Calif., Aug. 30–Sept. 4, 1970, Report CONF-700819(Vol. 2), pp. 693–728, American Society for Metals, 1970.
5. C. Cawthorne and E. W. Fulton, Voids in Irradiated Stainless Steel, *Nature,* **216:** 515 (1967).
6. S. D. Harkness and Che-Yu Li, A Model for Void Formation in Metals Irradiated in a Fast Neutron Environment, in *Radiation Damage in Reactor Materials,* Symposium Proceedings, Vienna, 1969, pp. 189–214, International Atomic Energy Agency, Vienna, 1969 (STI/PUB/230)(Vol. 2).
7. R. Bullough, B. L. Eyre, and R. C. Perrin, The Growth and Stability of Voids in Irradiated Metals, *Nucl. Appl. Technol.,* **9:** 346 (1970).
8. T. T. Claudson, J. J. Holmes, J. L. Straalsund, and H. R. Brager, Fast-Reactor Radiation-Induced Changes in Cladding and Structural Materials, in *Radiation Damage in Reactor Materials,* Symposium Proceedings, Vienna, 1969, pp. 165–187, International Atomic Energy Agency, Vienna, 1969 (STI/PUB/230)(Vol. 2).
9. E. E. Bloom and J. O. Stiegler, The Effect of Helium on Void Formation in Irradiated Stainless Steel, *J. Nucl. Mater.,* **36:** 331 (1970).
10. H. W. Wiedersich, On Void Formation During Irradiation, in Second International Conference on Strength of Metals and Alloys, Pacific Grove, Calif., Aug. 30–Sept. 4, 1970, Report CONF-700819(Vol. 2), pp. 784–791, American Society for Metals, 1970.
11. H. R. Brager, J. L. Straalsund, J. J. Holmes, and J. F. Bates, Irradiation Produced Defects in Austenitic Stainless Steel, USAEC Report WHAN-FR-16, WADCO Corporation, a subsidiary of Westinghouse Electric Corporation, 1970.
12. T. T. Claudson, R. W. Barker, and R. L. Fish, The Effects of Fast Flux Irradiation on the Mechanical Properties and Dimensional Stability of Stainless Steel, *Nucl. Appl. Technol.,* **9:** 10 (1970).
13. S. Oldberg, D. Sandusky, P. E. Bohaboy, and F. A. Comprelli, Analysis of Swelling of Austenitic Stainless Steels in Fast Reactors, *Trans. Amer. Nucl. Soc.,* **12:** 588 (1969).
14. J. L. Straalsund and J. F. Bates, A Note on the Interdependency of Swelling, Void Diameter and Void Number Density in Annealed AISI Type 304 Stainless Steel, USAEC Report WHAN-FR-15, WADCO Corporation, a subsidiary of Westinghouse Electric Corporation, 1970.
15. H. J. Busboom, Cladding Development, Sodium-Cooled Reactor Fast Ceramic Reactor Development Program, Quarterly Report No. 30, February–April 1969, USAEC Report GEAP-10028, p. 63, General Electric Company, 1969.
16. E. L. Gilbert and L. D. Blackburn, Irradiation-Induced Creep in Austenitic Stainless Steels, in Second International Conference on Strength of Metals and Alloys, Pacific Grove, Calif., Aug. 30–Sept. 4, 1970, Report CONF-700819(Vol. 2), pp. 773–777, American Society for Metals, 1970.
17. W. N. McElroy, R. E. Dahl, Jr., and E. R. Gilbert, Neutron Energy-Dependent Damage Function for Analyses of Austenitic Steel Creep Data, *Nucl. Eng. Des.,* **14:** 319 (1970).
18. D. Mosedale, G. W. Lewthwaite, G. O. Leet, and W. Sloss, Irradiation Creep in the Dounreay Fast Reactor, *Nature,* **224:** 1301 (1969).
19. J. A. Tesk and Che-Yu Li, Some Considerations of Radiation-Enhanced Creep, *Trans. Amer. Nucl. Soc.,* **12:** 133 (1969).
20. S. D. Harkness, J. A. Tesk, and Che-Yu Li, An Analysis of Fast Neutron Effects on Void Formation and Creep in Metals, *Nucl. Appl. Technol.,* **9:** 24 (1970).
21. R. J. Jackson, W. H. Sutherland, and I. L. Metcalf, Metal Swelling and Irradiation Creep Effects upon the Fast Test Reactor Core Component Performance, USAEC Report BNWL-1430, Battelle–Northwest, 1970.
22. B. Watkins and D. S. Wood, The Significance of Irradiation-Induced Creep on Reactor Performance of a Zircaloy-2 Pressure Tube, in *Applications-Related Phenomena for Zirconium and Its Alloys,* American Society for Testing and Materials, Special Technical Publication No. 458, p. 226, 1969.
23. R. V. Hesketh, Irradiation Creep in Graphite at 40°C, *Phil. Mag.,* **11:** 917 (1965).
24. J. C. Bokros, G. L. Guthrie, R. W. Dunlap, and A. S. Schwartz, Radiation-Induced Dimensional Changes and Creep in Carbonaceous Materials, *J. Nucl. Mater.,* **31:** 25 (1969).
25. F. A. Nichols, Evidences for Enhanced Ductility During Irradiation Creep, to be published in *Mater. Sci. Eng.*
26. C. M. Walter, J. P. Bacca, and W. N. Beck, Comparison

Between BEMOD Modelling Code Predictions and Observed Performance of EBR-II Driver Fuel, *Trans. Amer. Nucl. Soc.*, **13:** 125 (1970).
27. A. J. Lovell and R. W. Barker, WADCO Corporation, a subsidiary of Westinghouse Electric Corporation, unpublished, 1971.
28. A. Boltax, P. Murray, and A. Biancheria, Fast Reactor Fuel Performance Model Development, *Nucl. Appl. Technol.*, **9:** 329 (1970).
29. J. S. Perrin, R. A. Robinson, and S. J. Basham, In-Pile Creep Experiments, in Progress on Development of Fuels and Technology for Advanced Reactors During July–September 1970, Progress Report, USAEC Report BMI-1893, Battelle Memorial Institute, 1970.
30. D. Brucklacher and W. Dienst, Continuous Measurement of Creep of UO_2 During Irradiation, *J. Nucl. Mater.*, **36:** 244 (1970).
31. J. L. Routbort and A. A. Solomon, Irradiation Effects in Creep of Oxide Fuels, in Reactor Development Program Progress Report, USAEC Report ANL-7758, p. 78, Argonne National Laboratory, 1970.
32. C. D. Williams, Development Potential of Zirconium Alloys for High-Temperature Applications, *Reactor Technol.*, **13:** 153 (1970).
33. P. A. Ross-Ross and C. E. L. Hunt, The In-Reactor Creep of Cold-Worked Zircaloy-2 and Zirconium–2.5 Wt.% Niobium Pressure Tubes, *J. Nucl. Mater.*, **26:** 2 (1968).
34. G. R. Piercy, Mechanisms for the In-Reactor Creep of Zirconium Alloys, *J. Nucl. Mater.*, **26:** 18 (1968).
35. E. N. daC. Andrade, Effect of Alpha-Ray Bombardment on Glide in Metal Single Crystals, *Nature*, **156:** 113 (1945).
36. O. A. Troitskii and V. A. Kalinn, Effect of γ-Quanta Irradiation on the Creep of Zinc Single Crystals, *Fiz. Metal. Metalloved.*, **27:** 327 (1969).
37. J. A. Brinkman and H. Wiedersich, Mechanisms of Radiation Damage in Reactor Materials, in *Flow and Fracture of Metals and Alloys in Nuclear Environments*, American Society for Testing and Materials, Special Technical Publication No. 380, p. 3, 1965.
38. S. T. Konobeevsky, Relaxation of Elastic Stresses Under Neutron Irradiation, *At. Energ. (USSR)*, **9:** 194 (1960).
39. R. V. Hesketh, A Possible Mechanism of Irradiation Creep and Its Reference to Uranium, *Phil. Mag.*, **7:** 1417 (1962).
40. J. S. Perrin, Creep of Reactor Fuel Materials, in Progress on Development of Fuels and Technology for Advanced Reactors During October–December 1968, USAEC Report BMI-1857, Battelle Memorial Institute, 1969.
41. R. V. Hesketh, Nonlinear Growth in Zircaloy-4, *J. Nucl. Mater.*, **30:** 219 (1969).
42. S. N. Buckley, Irradiation Growth and Irradiation-Enhanced Creep in fcc and bcc Metals, in The Interactions Between Dislocations and Point Defects, Part III, Dislocation Climb, proceedings of a symposium held at Harwell, July 4–12, 1968, B. L. Eyre (Ed.), Report AERE-R-5944(Vol. 2), pp. 547–565, 1968.
43. A. C. Roberts and A. H. Cottrell, Creep of Alpha Uranium During Irradiation with Neutrons, *Phil. Mag.*, **1:** 711 (1956).
44. W. S. Blackburn, Effect of Irradiation Growth on the Creep of Uranium Under a Uniaxial Load, *Phil. Mag.*, **6:** 503 (1961).
45. R. G. Anderson and J. F. W. Bishop, The Effect of Neutron Irradiation and Thermal Cycling on Permanent Deformation in Uranium Under Load, in Symposium on Uranium and Graphite, London, 1962, Monograph and Report Series No. 27, pp.17–23, Institute of Metals, 1962.
46. R. V. Hesketh, Application of the Generalized Theory of Yielding Creep to Irradiation Creep in Zirconium Alloys, *J. Nucl. Mater.*, **26:** 77 (1968).
47. V. Fidleris, Uniaxial In-Reactor Creep of Zirconium Alloys, *J. Nucl. Mater.*, **26:** 51 (1968).
48. E. R. Gilbert, Presentation at the Seventy-first Annual Meeting of ASTM Symposium on Irradiation Effects in Structural Alloys for Thermal and Fast Reactors (June 1968).
49. R. V. Hesketh, J. E. Harbottle, N. A. Waterman, and R. C. Lobb, Irradiation Growth and Creep in Zircaloy-2, in *Radiation Damage in Reactor Materials*, Symposium Proceedings, Vienna, 1969, p. 365, International Atomic Energy Agency, Vienna, 1969 (STI/PUB/230)(Vol. 1).
50. D. S. Billington and J. H. Crawford, Jr., *Radiation Damage in Solids*, p. 162, Princeton University Press, Princeton, N. J., 1961.
51. R. V. Hesketh, A Transient Irradiation Creep in Nonfissile Metals, *Phil. Mag.*, **8:** 1321 (1963).
52. G. W. Lewthwaite, D. Mosedale, and I. R. Ward, Irradiation Creep in Several Metals and Alloys at 100°C, *Nature*, **216:** 472 (1967).
53. P. H. Kreyns and M. W. Burkart, Radiation-Enhanced Relaxation in Zircaloy-4 and Zr–2.5 Wt.% Nb/0.5 Wt.% Cu Alloys, *J. Nucl. Mater.*, **26:** 87 (1968).
54. R. A. Wolfe, Kinetics of In-Pile Stress Relaxation, *Trans. Amer. Nucl. Soc.*, **12:** 589 (1969).
55. R. V. Hesketh, Collapse of Vacancy Cascades to Dislocation Loops, in Proceedings of the International Conference on Solid-State Physics Research with Accelerators, USAEC Report BNL-50083, pp. 389–401, Brookhaven National Laboratory, 1967.
56. R. V. Hesketh, Irradiation Creep in Nonfissile Metals, in 10th Symposium on Special Metallurgy, "Brittleness and Irradiation Effects," Saclay, France, June 23–24, 1966, Report CONF-660656, p. 185, 1967.
57. J. L. Kaae, On Irradiation-Induced Creep of Pyrolytic Carbon in a General State of Stress, *J. Nucl. Mater.*, **34:** 206 (1970).
58. A. J. Perks and J. H. W. Simmons, Radiation-Induced Creep in Graphite, *Carbon*, **1:** 441 (1964).
59. W. N. Reynolds, The Mechanical Properties of Reactor Graphite, *Phil. Mag.*, **11:** 357 (1965).
60. W. V. Green, J. Weertman, and E. G. Zukas, High-Temperature Creep of Polycrystalline Graphite, *Mater. Sci. Eng.*, **6:** 199 (1970).
61. J. G. Merkle, An Ellipsoidal Yield Function for Materials that can both Dilate and Compact Inelastically, *Nucl. Eng. Des.*, **12:** 425 (1970).
62. R. J. Price and J. C. Bokros, Mechanical Properties of Neutron-Irradiated Pyrolytic Carbons, *J. Nucl. Mater.*, **21:** 158 (1967).
63. H. E. Kissinger, Battelle Memorial Institute, Pacific Northwest Laboratory, unpublished, 1971.
64. E. R. Gilbert and J. L. Straalsund, A Relationship for

Nonconservative-Volume Creep Under Different States of Stress, *Nucl. Eng. Des.*, **12:** 421 (1970).

65. G. E. Dieter, *Mechanical Metallurgy*, p. 66, McGraw-Hill Book Company, Inc., New York, 1961.
66. J. W. Joseph, Jr., Stress Relaxation in Stainless Steel During Irradiation, USAEC Report DP-369, E. I. du Pont de Nemours & Co., Inc., 1959.
67. R. E. Schreiber, Relaxation of Torsional Stresses in Stainless Steel During Irradiation, USAEC Report DP-669, E. I. du Pont de Nemours & Co., Inc., 1962.
68. L. C. Walters, C. M. Walter, M. A. Pugacz, J. A. Tesk, and R. Carlander, EBR-II In-Pile Creep Experiments on Stainless-Steel Tubing, *Trans. Amer. Nucl. Soc.*, **13:** 145 (1970).
69. L. C. Walters, M. A. Pugacz, and C. M. Walter, In-Reactor Creep Experiments with Stainless-Steel Tubing, Reactor Development Program Progress Report, January 1971, USAEC Report ANL-7776, Argonne National Laboratory, 1971.
70. D. P. Hines, S. Oldberg, and E. L. Zebroski, Nonsteady-State Factors in Models for Swelling of Oxide Fuels, *Nucl. Appl. Technol.*, **9:** 338 (1970).
71. E. R. Gilbert and J. J. Holmes, Irradiation Creep by Loop Unfaulting, *Trans. Amer. Nucl. Soc.*, **13:** 609 (1970).
72. F. R. N. Nabarro, Deformation of Crystals by the Motion of Single Ions, in *Bristol Conference on Strength of Solids*, p. 75, The Physical Society, London, 1948.
73. G. Schoeck, Influence of Irradiation on Creep, *J. Appl. Phys.*, **29:** 112 (1958).
74. F. A. Nichols, Theory of the Creep of Zircaloy During Neutron Irradiation, *J. Nucl. Mater.*, **30:** 249 (1969).
75. F. A. Nichols, On the Mechanisms of Irradiation Creep in Zirconium-Base Alloys, *J. Nucl. Mater.*, **37:** 59 (1970).
76. G. S. Ansell and J. Weertman, Creep of a Dispersion-Hardened Alloy, *Trans. AIME, Met. Soc.*, **215:** 838 (1959).
77. D. Mosedale, Influence of Irradiation on Creep, *J. Appl. Phys.*, **33:** 3142 (1962).
78. D. Mosedale, Dislocation Climb and Irradiation, *J. Nucl. Mater.*, **35:** 250 (1970).
79. R. V. Hesketh, Diffusion Creep Under Neutron Irradiation, *J. Nucl. Mater.*, **29:** 217 (1969).
80. R. V. Hesketh, Dislocation Climb: First Catch Your Poisson, *J. Nucl. Mater.*, **35:** 253 (1970).
81. J. L. Straalsund, Comments on "Climb" or "Growth" Forces Exerted by Nonconservable Defects, *Scr. Met.*, **4:** 459 (1970).
82. G. W. Lewthwaite and D. Mosedale, The Analysis of Relaxation Tests on Specimens with Inhomogeneous Stresses, *Brit. J. Appl. Phys.*, **17:** 821 (1966).
83. C. Crussard and R. Tamhanker, High-Temperature Deformation of Steels, A Study of Equicohesion, Activation Energies, and Structural Modifications, *Trans. AIME, Met. Soc.*, **212:** 718 (1958).
84. S. D. Harkness, F. L. Yaggee, and W. F. Burke, A Simulation of In-Reactor Test Conditions Using Cyclotron Bombardment, Reactor Development Program Progress Report, p. 74, November 1970, USAEC Report ANL-7758, Argonne National Laboratory, 1970.
85. S. D. Harkness, F. L. Yaggee, and J. Styles, A Simulation of In-Reactor Test Conditions Using Cyclotron Bombardment, Reactor Development Program Progress Report, p. 65, December 1970, USAEC Report ANL-7765, Argonne National Laboratory, 1970.
86. V. Fidleris, The Stress-Dependence of the In-Reactor Creep Rate of Heat-Treated Zr–2.5 Wt.% Nb and Cold-Worked Zircaloy-2, *J. Nucl. Mater.*, **36:** 343 (1970).
87. J. Standring, I. P. Bell, H. Tickle, and A. Glendinning, Effects of Neutron Irradiation on Creep-Rupture Properties of Type 316 Stainless-Steel Tubes, in *Irradiation Effects in Structural Alloys for Thermal and Fast Reactors*, American Society for Testing and Materials, Special Technical Publication No. 457, pp. 414–428, 1969.
88. E. R. Gilbert and J. J. Holmes, WADCO Corporation, a subsidiary of Westinghouse Electric Corporation, unpublished, 1971.
89. E. R. Gilbert, WADCO Corporation, a subsidiary of Westinghouse Electric Corporation, unpublished, 1971.
90. J. Moteff, Radiation Damage in Body-Centered Cubic Metals and Alloys, in *Radiation Effects*, p. 727, Gordon and Breach Science Publishers, Inc., 1967.
91. G. L. Kulcinski, H. E. Kissinger, and B. Mastel, Annealing of Defects in Neutron-Irradiated Molybdenum—Effect of External Pressures to 70 kbars, in *Radiation Damage in Reactor Materials*, Symposium Proceedings, Vienna, 1969, p. 33, International Atomic Energy Agency, Vienna, 1969 (STI/PUB/230) (Vol. 1).
92. C. R. Cupp, The Effect of Neutron Irradiation on the Mechanical Properties of Zirconium 2.5% Niobium Alloy, *J. Nucl. Mater.*, **6:** 241 (1962).
93. J. J. Holmes, J. A. Williams, D. H. Nyman, and J. C. Tobin, In-Reactor Creep of Cold-Worked Zircaloy-2, in *Flow and Fracture of Metals and Alloys in Nuclear Environments*, American Society for Testing and Materials, Special Technical Publication No. 380, p. 385, 1965.
94. E. R. Gilbert and N. E. Harding, Comparison of In-Reactor Creep and Postirradiation Creep Tests of Structural Materials for Nuclear Applications, in *Irradiation Effects in Structural Alloys for Thermal and Fast Reactors*, American Society for Testing and Materials, Special Technical Publication No. 457, pp. 17–37, 1969.
95. R. L. Coble, A Model for Boundary Diffusion Controlled Creep in Polycrystalline Materials, *J. Appl. Phys.*, **34:** 1679 (1963).
96. A. M. Kosevich, Z. K. Saralidze, and V. V. Slezov, Effect of Irradiation on the Diffusional Dislocation Flow of Crystals, *Sov. Phys.-Solid State (Engl. Trans.)*, **9:** 697–703 (Sept. 1967).
97. M. F. Ashby, *On Radiation-Enhanced Creep*, Technical Report No. 4, Harvard University, 1971.
98. K. Veevers and W. B. Rotsey, Effect of Irradiation on Strain Aging in Annealed Zircaloy-2, *J. Nucl. Mater.*, **27:** 108 (1968).
99. E. R. Gilbert, *Steady-State Creep of Alpha Zirconium*, Ph. D. Dissertation, Washington State University, 1970.
100. M. F. Ashby, The Mechanical Effects of a Dispersion of a Second Phase, in Second International Conference on Strength of Metals and Alloys, Pacific Grove, Calif., Aug. 30–Sept. 4, 1970, Report CONF-700819(Vol. 2), pp. 507–541, American Society for Metals, 1970.
101. J. J. Holmes and L. O. Petersen, Creep of Thorium During Fission, *Phil. Mag.*, **16:** 845 (1967).
102. E. R. Gilbert and B. Mastel, Stress Dependence of the

In-Reactor Uniaxial Creep of Zr-2 and Zr–2.5 Nb, *Trans. Amer. Nucl. Soc.*, **12:** 132 (1969).

103. E. F. Ibrahim, In-Reactor Creep of Zirconium-Alloy Tubes and Its Correlation with Uniaxial Data, in *Applications-Related Phenomena for Zirconium and Its Alloys,* American Society for Testing and Materials, Special Technical Publication No. 458, p. 18, 1969.
104. F. J. Azzarto, E. E. Baldwin, F. W. Wiesinger, and D. M. Lewis, Unirradiated, In-Pile and Postirradiation Low Strain Rate Tensile Properties of Zircaloy-4, *J. Nucl. Mater.*, **30:** 208 (1969).
105. P. A. Ross-Ross, American Society for Metals Technical Report No. P9-64, presented at Materials Engineering Congress and Exposition, Philadelphia, Pa., October 1969.

FIFTH SYMPOSIUM ON NEUTRON INELASTIC SCATTERING

Grenoble, France, March 6–10, 1972

In recognition of the increasing number of investigations on dynamics of solids and liquids and on magnetic, molecular, and biological systems, the International Atomic Energy Agency will convene its Fifth Symposium on Neutron Inelastic Scattering. Utilizing this powerful experimental technique, researchers in recent years have improved considerably the understanding of phenomena in different systems. The fast development of theoretical interpretation has resulted. Many research reactors in advanced and developing countries furnish the neutron beams for solid-state research, and, with the rising generation of high-flux reactors, new potentialities are emerging for neutron-scattering investigations. It is hoped that this symposium will provide useful indications for the most profitable future course of research using the technique of neutron inelastic scattering.

The following list of topics is being considered for discussion:

- New experimental methods
- Solids
- Liquids
- Dynamics of phase transitions
- Magnetism
- Chemistry and macromolecules

The number of contributed papers will be limited, and the nomination of a participant will be accepted only if it is presented by the government of a member state of IAEA or by an international organization invited to participate. The working languages of the meeting will be English, French, Russian, and Spanish.

The Administrative Secretary of the symposium is H. H. Storhaug, Division of Scientific and Technical Information, International Atomic Energy Agency, Kärntner Ring 11, P. O. Box 590, A-1011 Vienna, Austria.

Interested people in the United States can obtain further information from John H. Kane, Special Assistant for Conferences, Division of Technical Information, U. S. Atomic Energy Commission, Washington, D. C. 20545.

EBR-II: An Experimental LMFBR Power Plant

By Leonard J. Koch*

Abstract: *Experimental Breeder Reactor II (EBR-II) is an experimental liquid-metal-cooled fast breeder reactor (LMFBR) power-generating station designed to operate on a utility-system network. It is the only operational pool-type LMFBR, and through 1970 it had produced more than 40,000 MWd(t) of power and had generated over 250 million kWh of electricity.*

The primary mission of the EBR-II has been shifted to an experimental irradiation facility for potential LMFBR fuels and structural materials. The experimental irradiation program has had a significant effect on operating schedules and on the amount and character of fuel-handling operations. Nevertheless, power operation of the EBR-II normally includes electric-power generation and relevant experience as an experimental power station.

Many difficulties arose during preoperational testing and the early operating phases of the EBR-II. These were corrected, and since 1967 the reactor and power system have operated very well, simultaneously increasing the number and variety of experimental irradiations conducted in the reactor. The EBR-II has demonstrated the technical feasibility of the pool-type LMFBR concept and provides a technological basis for the major commitments made to this concept.

On Aug. 21, 1957, Congress authorized $29,100,000 for the design and construction of the EBR-II. On Aug. 7, 1964, EBR-II first delivered power to the electrical-distribution system at the National Reactor Testing Station (NRTS) in Idaho. Since that time, the EBR-II has operated as an experimental base-load LMFBR power station, and through 1970 it had produced more than 40,000 MWd(t) of power and had generated over 250 million kWh of electricity. A chronology of EBR-II milestones is given in Table 1. The "capitalized" design and construction cost of the complete EBR-II facility, including reactor, power plant, fuel-cycle facility, and supporting facilities, was $32,285,430.

There are two basic concepts of LMFBR power stations: the loop concept and the pool concept. The loop concept consists in the traditional arrangement of primary-system components wherein the reactor vessel, pumps, and heat exchangers are separated from each other and interconnected by piping. Broad experience with loop-type systems exists since this concept has been used extensively for liquid- and gas-cooled reactors of all types. The pool concept consists in an arrangement wherein the primary-system components are contained in a large tank and operate submerged in sodium. Since this concept has been applied only to the LMFBR, and the EBR-II is the only reactor of this type which has been constructed and operated, experience with this concept is comparatively limited. However, pool-type LMFBR power stations ranging from 250 to 600 MW(e) are under construction in the United Kingdom, France, and the USSR. Two of the five U. S. reactor manufacturers involved in LMFBR development have selected the pool concept as the reference design for their LMFBR power-station studies.

The primary operating emphasis for the EBR-II has been shifted from experimental power generation to experimental irradiation of LMFBR fuels and structural materials. The major effect of this change in emphasis has been on the core loading, where more than 25% of the loading normally consists of experimental subassemblies that produce more than 10% of the total power, and on the fuel-handling system, which must make a large number of fuel-loading

*Argonne National Laboratory, 9700 South Cass Avenue, Argonne, Ill. 60440.

Table 1 EBR-II Milestones

Date	Event
July 11, 1955	Original authorization (Public Law 84-141)
Nov. 15, 1956	Award of architect–engineer contract; start of construction design
May 1957	Completion of preliminary safety-analysis report (ANL-5719)
Aug. 21, 1957	Revised authorization for increased scope and funding (Public Law 85-162)
Nov. 8, 1957	Award of first major construction contract for Reactor Containment Building
Sept. 30, 1961	Reactor made "dry critical" without sodium (critical mass, 230.16 kg of ^{235}U)
Jan. 29, 1963	Sodium filling of secondary system started
Feb. 18, 1963	Sodium filling of primary system started
Feb. 26, 1963	Sodium filling completed (10 railroad tank cars)
Nov. 11, 1963	Reactor made "wet critical" with sodium (critical mass, 181.2 kg of ^{235}U)
Apr. 9, 1964	Combined operation of primary and secondary sodium systems achieved
July 16, 1964	"Approach to power" started
July 29, 1964	Reactor power raised to 10 MW(t)
Aug. 5, 1964	Reactor power raised to 20 MW(t)
Aug. 7, 1964	Turbine generator synchronized and delivered power to NRTS loop (~1800 kW)
Aug. 13, 1964	Reactor power level raised to 30 MW(t) [~8000 kW(e)]
Oct. 13, 1964	Reactor power level raised to 37.5 MW(t) [~12000 kW(e)]
Mar. 27, 1965	Reactor power level raised to 45 MW(t) [~14000 kW(e)]
Aug. 26, 1968	Regular power operation begins at 50 MW(t) [~15000 kW(e)]
Sept. 25, 1970	Regular power operation begins at 62.5 MW(t) [~19000 kW(e)]

changes to accommodate requirements of the experimental irradiation program.

This review is concerned with the design, construction, and operation of the EBR-II as a 20-MW(e) experimental base-load LMFBR power station, with particular emphasis on those design aspects which apply to the pool concept.

DESIGN PHILOSOPHY

The EBR-II was designed to resolve as many technical problems as possible and to establish technical feasibility to the extent practicable with a 20-MW(e) experimental power plant. Another primary design objective was to make the largest practicable extrapolation from the EBR-I experience (the only experience available at the time) and to incorporate design features that could be extrapolated to large commercial reactors. However, these goals were established when a 150-MW(e) plant was considered "large."

The major design emphasis was on the reactor and primary system, with the remainder of the power system assigned somewhat of a "supporting role." As a result, the reactor and primary system represent a bold departure from system designs up to that time, and the balance of the plant represents a rather conservative design. The reactor and primary system were designed for a "stretch capability" even though feasibility of operating at the resulting power density would first require demonstration of feasibility by sustained operation at lower power levels. The balance of the power system was designed much more conservatively, with emphasis on reliability rather than on maximum advancement of technology. Thus it is not surprising that designers of the present series of LMFBR demonstration-type plants have adopted more of the EBR-II reactor and primary-system design features than those in the secondary and steam systems.

Within this framework the important design considerations were related to the following questions:

1. Was it feasible to achieve the thermal performance that appeared necessary for LMFBRs to achieve economic feasibility, i.e., power density in the range of 1 MW/liter of core volume, heat flux in the range of 1 million Btu/(ft^2)(hr), coolant velocity in the range of 25 ft/sec, and coolant-temperature rise in the range of 10°F/in. of core height?

2. Could reliable fission-product decay-heat removal be provided under all conceivable circumstances that might be encountered after reactor operation and during fuel handling?

3. Could the variety of mechanical requirements related to the compact core, control drives, and fuel handling be met?

4. Could total fuel inventory be held to acceptable levels with the high burnup rates and high specific activity of typical fast reactor fuel and the allowable burnup that appeared attainable?

5. Could reliable overall plant operation be achieved and plant maintenance performed consistent with commercial power-station requirements?

Thermal-performance considerations led to two basic design concepts that had a significant impact on reactor and plant design. The thermal performance required for power operation led to use of the fuel-subassembly concept, which permits the use of small-diameter fuel elements (fuel pins) to accommodate high power density, coolant-flow velocity, and pressure drop. The thermal performance required for

shutdown cooling led to the pool-type primary-system concept, which emphasizes the prevention of loss of coolant and reliability of heat removal under all normal and abnormal circumstances.

A major hurdle to be overcome in the early phases of any new concept involves its overall practicability or feasibility as a system. A major EBR-II design objective was to demonstrate the feasibility of the pool concept and to provide a technological base for large LMFBR plants of this type as well as for the LMFBR concept in general.

Although the EBR-II is relatively small, the experience is more relevant than a direct comparison of size would suggest because (1) some important plant features and characteristics are essentially independent of plant size or power and (2) most of the size-dependent features are less than linear with power in this dependency.

The EBR-II contains a full complement of instrumentation and control systems which measure and control the basic parameters involved in fast power-reactor operation. These operating variables are being measured and controlled under conditions and in an environment comparable to what will exist in a large commercial station. Perhaps more important, the variables interact with each other (including feedbacks) and exhibit characteristics similar to the larger plants. Similarly, the requirements for quality of design, fabrication, and construction are comparable and equally stringent; it is just as important that a 12-in. sodium pipe does not leak as a 24- or 36-in. pipe. The same is true for the performance of pumps, heat exchangers, steam generators, and fuel elements.

THE POOL CONCEPT

The basic EBR-II pool concept raised questions of feasibility of design, construction, and operation (including maintenance) and introduced unique design and construction problems. The EBR-II primary system is contained in a primary tank 26 ft in diameter and 26 ft deep (Fig. 1). The tank contains ~ 80,000 gal of sodium, and the total weight of the tank, sodium, and internals is ~ 900 tons. The normal operating temperature of the sodium (and tank) is 700°F, but the system was designed to accommodate occasional temperature changes from 250 to 750°F. Therefore the EBR-II primary system presents the typical structural–thermal design problems associated with this design concept.

Demonstration plants and large commercial LMFBRs will require a primary tank at least twice as large (40 to 60 ft in diameter) and probably containing about 10 times as much sodium (500,000 to 1,000,000 gal). Nevertheless, the EBR-II experience is pertinent because (1) the EBR-II required an inordinate proportion of field erection relative to its size because of its isolated location and the requirements of truck transport of components to the site and (2) the EBR-II demonstrated principles of construction, assembly, and installation which can be directly extrapolated to larger-size systems and components.

The EBR-II primary tank was field assembled and erected except for the cover assembly, which was shop fabricated in two halves (Fig. 2). The upper supporting structure was installed after the tank was completed, totally enclosing the tank and providing the support for the tank, which is hung from six radial beams on roller hangers (Fig. 1). Note that none of the larger plant designs use the EBR-II hanger arrangement, and it is quite probable that this concept is not practicable for supporting the very large tanks required. This concept does, however, illustrate the principle of accommodating thermal expansion while simultaneously controlling critical alignments. The design and construction, including detailed analyses and detailed quality-control procedures, have been described in detail.[1] Construction, erection, and testing of the primary tank and associated structures were completed on schedule, and, although this phase of the construction program was one of the most difficult, it was one of the most successful.

It is interesting to note that the construction of the Prototype Fast Reactor (PFR) in the United Kingdom has proceeded along similar lines, except that the upper structure was subdivided into six segments (for reasons of shipping) which were field assembled and erected. Encountered[2] in the roof structure were welding difficulties due to lamellar defects in the steel, and these difficulties delayed construction. The construction sequence adopted for the PFR was similar to that for the EBR-II and involved the construction of the supporting structure around the completed vessel. However, the technique used for the PFR was that of "floating" the tank to position it during erection.

Thermal tests were conducted on the EBR-II primary tank before and after it was filled with sodium to verify the thermal-expansion characteristics and to measure actual displacements of the tank and specific nozzles in the tank cover. These characteristics and displacements were generally in agreement with predictions but were smaller (20 to 40%) in magnitude than the calculated values. The roller-hanger supports provide adequately for thermal expansion while retain-

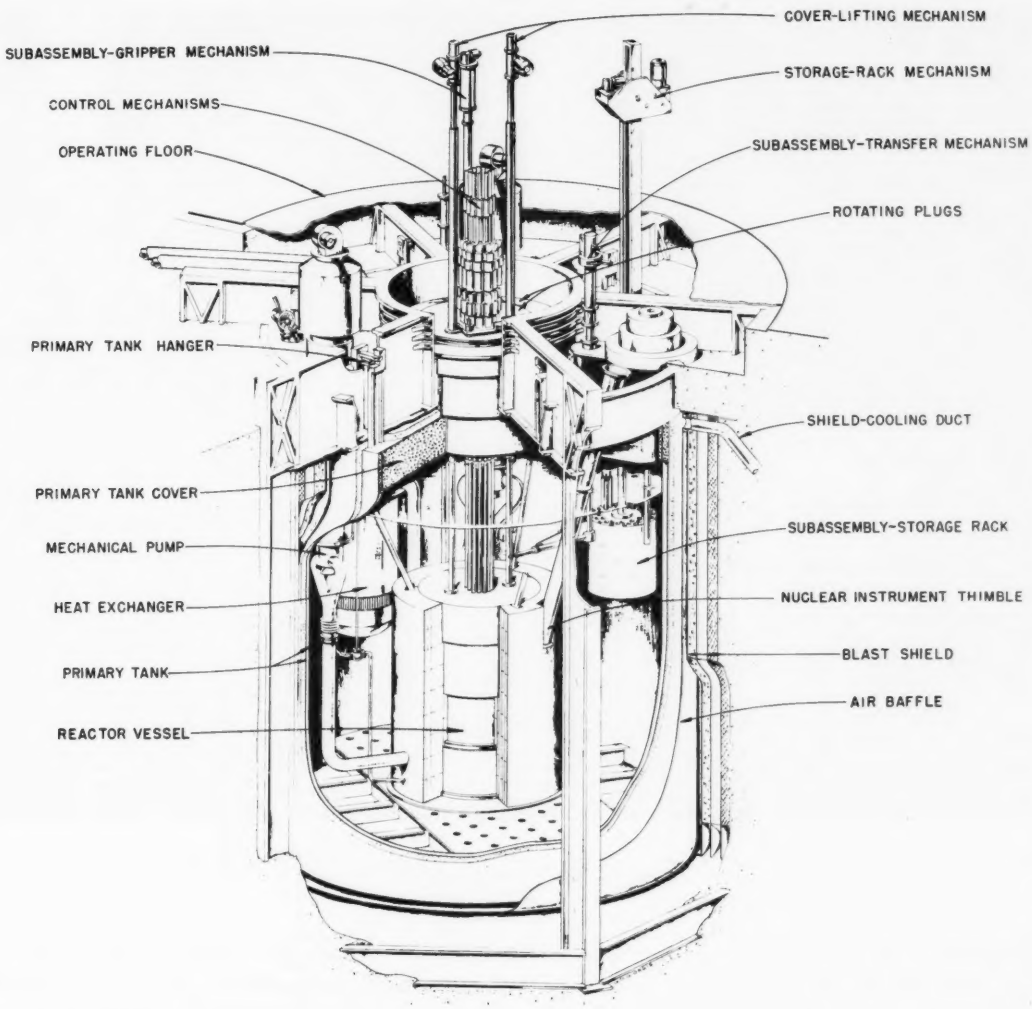

Fig. 1 Cutaway view of the EBR-II primary system.

ing alignment of critical components. The results of these tests and evaluations also have been reported in detail.[1]

The pool concept presents special problems and requirements related to the accessibility of components in the primary system. The EBR-II design utilizes a "plug-in" concept for the major components. This concept requires that each component be removable as a unit with direct personnel access to only the part of the component exposed to the building environment. All the components enter through and are supported from the top structure and cover of the primary tank. Each component includes an integral shield plug that is positioned within the corresponding nozzle in the top cover, thereby providing the "handle" for the component and simultaneously completing the top biological shield. The top cover contains 70 nozzles of various sizes and shapes, as shown in Fig. 2. These nozzles house components ranging from primary pumps, heat exchangers, fuel-handling components, sodium heaters, and instrumentation to spares.

Each of the components installed in these nozzles is removable as a unit. Some required a relatively unique design to achieve plug-in operation. The primary pumps and the intermediate heat exchanger are two such components.

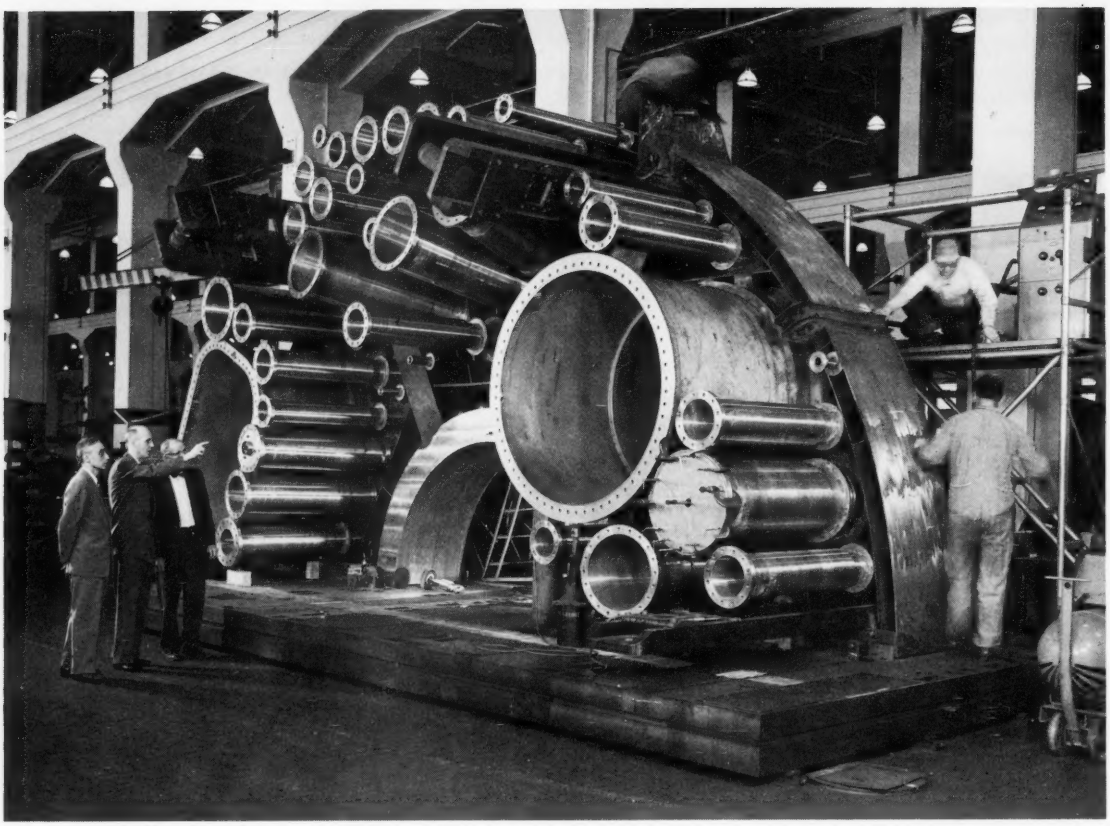

Fig. 2 Primary tank-cover half.

The EBR-II primary system uses two sodium supply loops, each containing a single-stage centrifugal pump driven by a variable-speed motor supplied by a motor-generator set that provides variable voltage and frequency. At full reactor power, each pump delivers ~4500 gal/min at 50 psig. The pump (Fig. 3) employs a radial hydrostatic bearing immediately above the impeller to which sodium is supplied directly from the impeller discharge. The pump is connected to the inlet piping by a spring-loaded ball-joint connector. This connection (Fig. 4) is automatically "broken" when the pump is removed and automatically "connected" when the pump is installed. Tests have shown that this connection leaks about 10 gal/min at rated operating conditions. The integral pump shield plug contains about 33 in. of carbon-steel balls and 34 in. of high-density concrete.

Both pumps failed during preoperational testing and were removed for repairs in early 1964. (The pump shafts had warped and "wiped out" labyrinth seals.) One pump was removed in late 1970 for scheduled inspection and maintenance after 32,000 hr of operation. Pump removal was accomplished by withdrawing the pump assembly into an argon-gas-filled caisson to avoid contaminating the sodium or cover gas (Fig. 5). The plug-in capability and reliable operation of the pumps have been adequately demonstrated.

The intermediate heat exchanger must also provide plug-in capability. The shell is permanent, but the tube bundle with attached shield plug is a removable unit. The tube bundle was made removable by bringing the secondary sodium inlet through the center of the unit to the lower header (Fig. 6). The heat exchanger has not been removed since the plant went into operation, but its plug-in capability was demonstrated during initial construction since it was the last major component installed and closed off the last means of access into the tank. Consequently the heat exchanger was

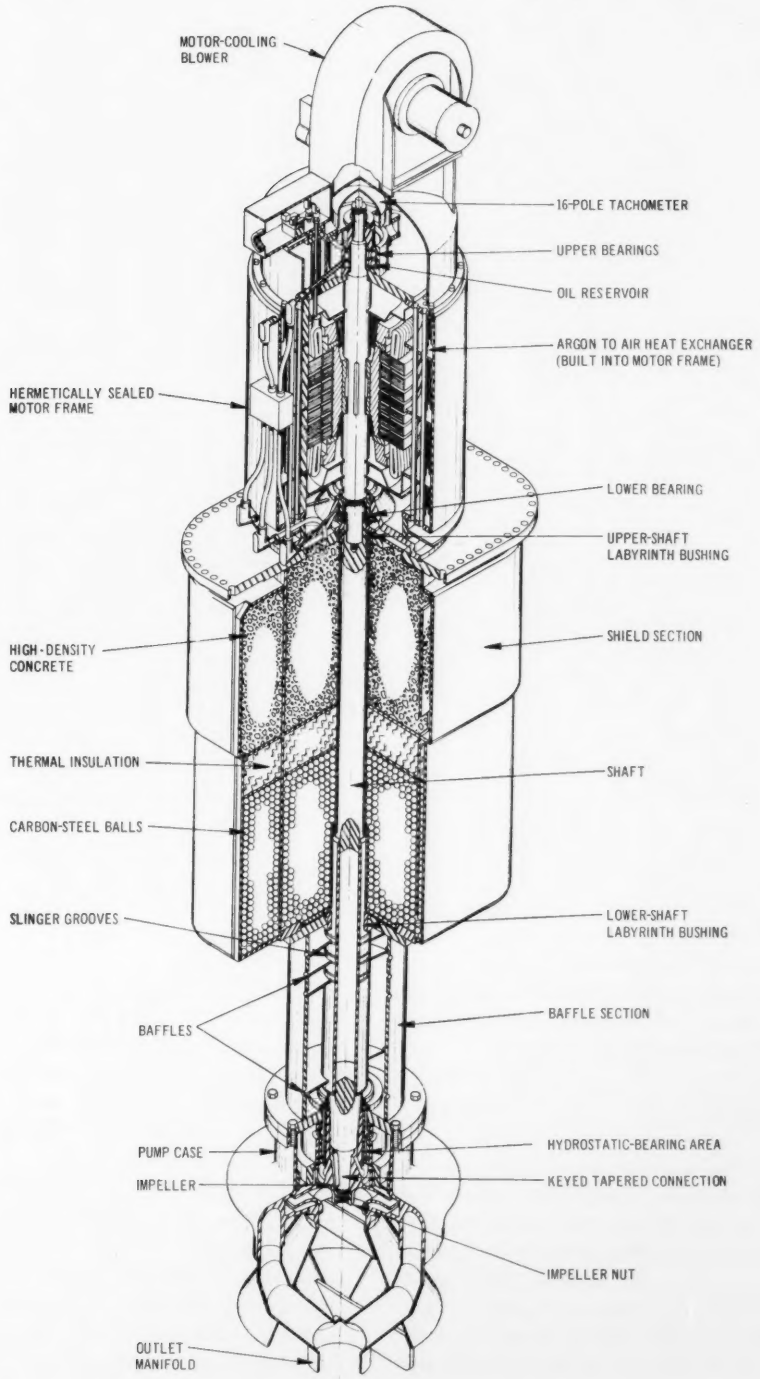

Fig. 3 The EBR-II primary pump.

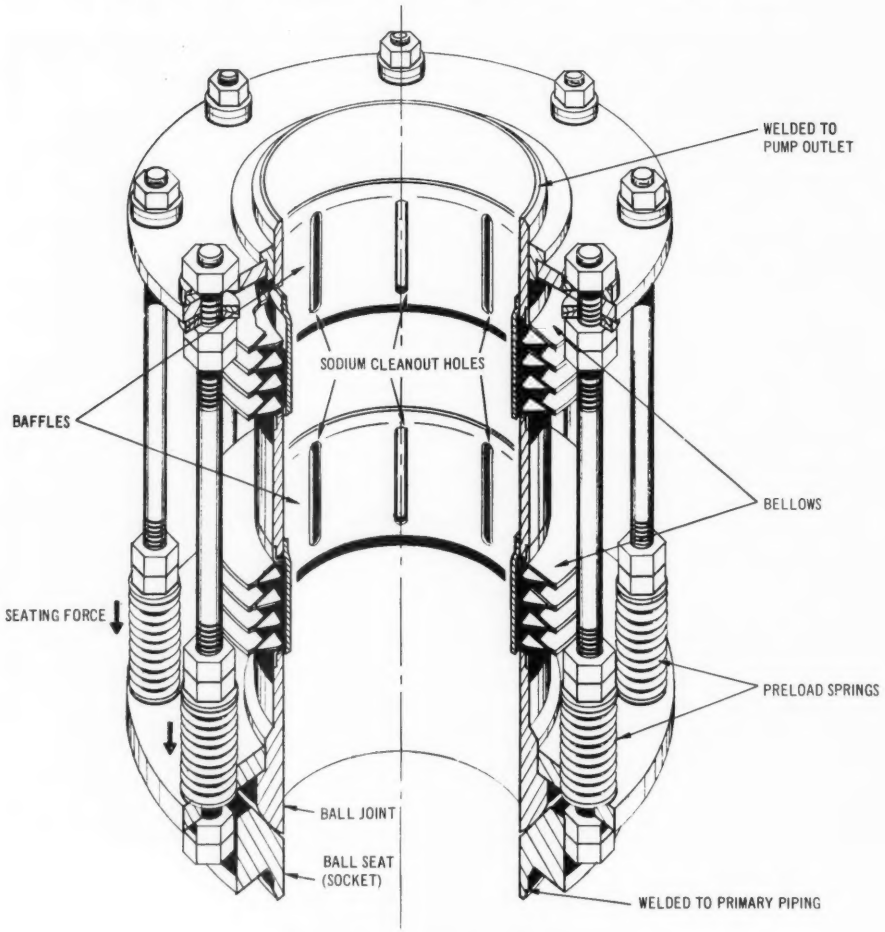

Fig. 4 Ball-joint pump connector.

the only major component to be installed in the primary tank "blind," i.e., no observers were in the tank during this final installation.

THE REACTOR

The EBR-II reactor design employs freestanding, close-packed subassemblies of hexagonal cross section (Fig. 7). They are positioned and supported in a combination grid–inlet coolant plenum, as shown in Fig. 8. Because of the large coolant pressure drop through the subassembly, they are subjected to a hydraulic lifting force. The EBR-II design provides a "hydraulic hold-down force" produced by the high-pressure coolant in the subassembly acting across the closed bottom end of the subassembly. This piston-like effect, coupled with the weight of the subassembly, counteracts the lifting force and eliminates the need for mechanical hold-down methods. The feasibility of this concept has been established by EBR-II, and it has been adopted for several commercial reactor designs (including the French Phenix reactor under construction and the USSR BOR-60 in operation and BN-350 under construction).

The EBR-II subassembly is reasonably typical of large reactor subassemblies appropriately scaled down in size. In each case the size is determined mainly by the desire for "manageable packages" of fuel elements (fuel pins). A comparison of pertinent data for the EBR-II and a typical 1000-MW(e) LMFBR is given in Table 2. Note that the EBR-II contains a larger total number of subassemblies than anticipated in a large reactor as a result of the very large number of blanket subassemblies in the EBR-II. (A thick blanket was

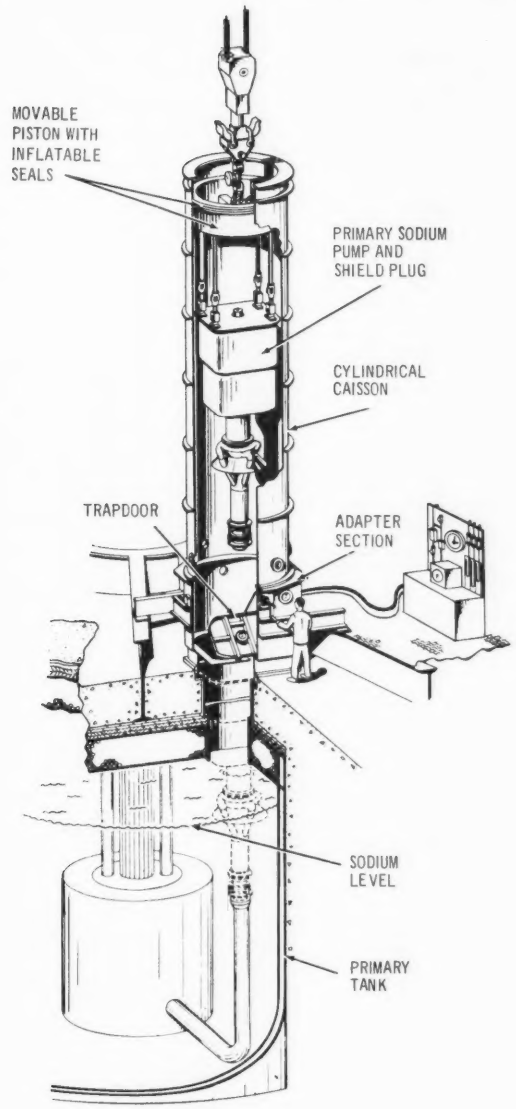

Fig. 5 Primary pump removal.

provided to permit blanket optimization studies.) Also, note that the EBR-II employs a relatively small-diameter fuel element, which is consistent with the use of metal-alloy fuel and a high power density. In each case, however, the subassembly must meet the same stringent requirements and perform the same functions.

The EBR-II was designed to achieve a maximum power density in excess of 1 MW/liter, which is somewhat higher than the design basis for large reactors. There has been no evidence of overheating or marginal thermal performance, providing assurance that large reactors will have a reasonable performance margin.

Table 2 Fuel Element and Subassembly Comparison

	EBR-II	1000 MW(e)*
Power, MW(t)	62.6	2500
Core height	15	30
No. of core subassemblies	67	275
No. of blanket subassemblies	570	125
Total subassemblies	637	400
Subassembly pitch, in.	2.320	6.0
Subassembly clad thickness, in.	0.040	0.100
Fuel elements per subassembly	91	271
Fuel element diameter, in.	0.174	0.275
Overall length of subassembly, ft	~7½	~12

*Representative parameters for comparative purposes—not optimized.

In the EBR-II coolant flow is orificed in each row of subassemblies to approximately match the power generated in that row. This is accomplished by a series of steps in the lower grid plate that covers the appropriate coolant-inlet holes in the subassembly. This arrangement is shown in Fig. 9 (see also Fig. 8), where the stepped construction can be seen for the five rows of the core and the two rows of the inner blanket. (The outer blanket utilizes low-pressure coolant and only two zones of orificing because of the very low power generation.) With this arrangement, all core subassemblies are identical and are correctly orificed automatically by position in the reactor. The same is true of the two rows of inner blanket subassemblies. Operating experience has been entirely successful and has demonstrated the feasibility of avoiding orificing-loading errors. This experience is applicable to large reactors where proper flow-power matching is much more important.

The EBR-II subassemblies are supported only in and by the two parallel plates comprising the lower grid structure. The subassemblies are freestanding and are permitted to move (horizontally) within the confines of the close-packed geometry. The EBR-II core and subassembly design was predicated on free but predictable movement of the subassemblies in response to the forces acting upon them. In addition, major emphasis was placed on minimizing the bowing of subassemblies inward toward the center of the core to minimize the positive bowing coefficient observed in

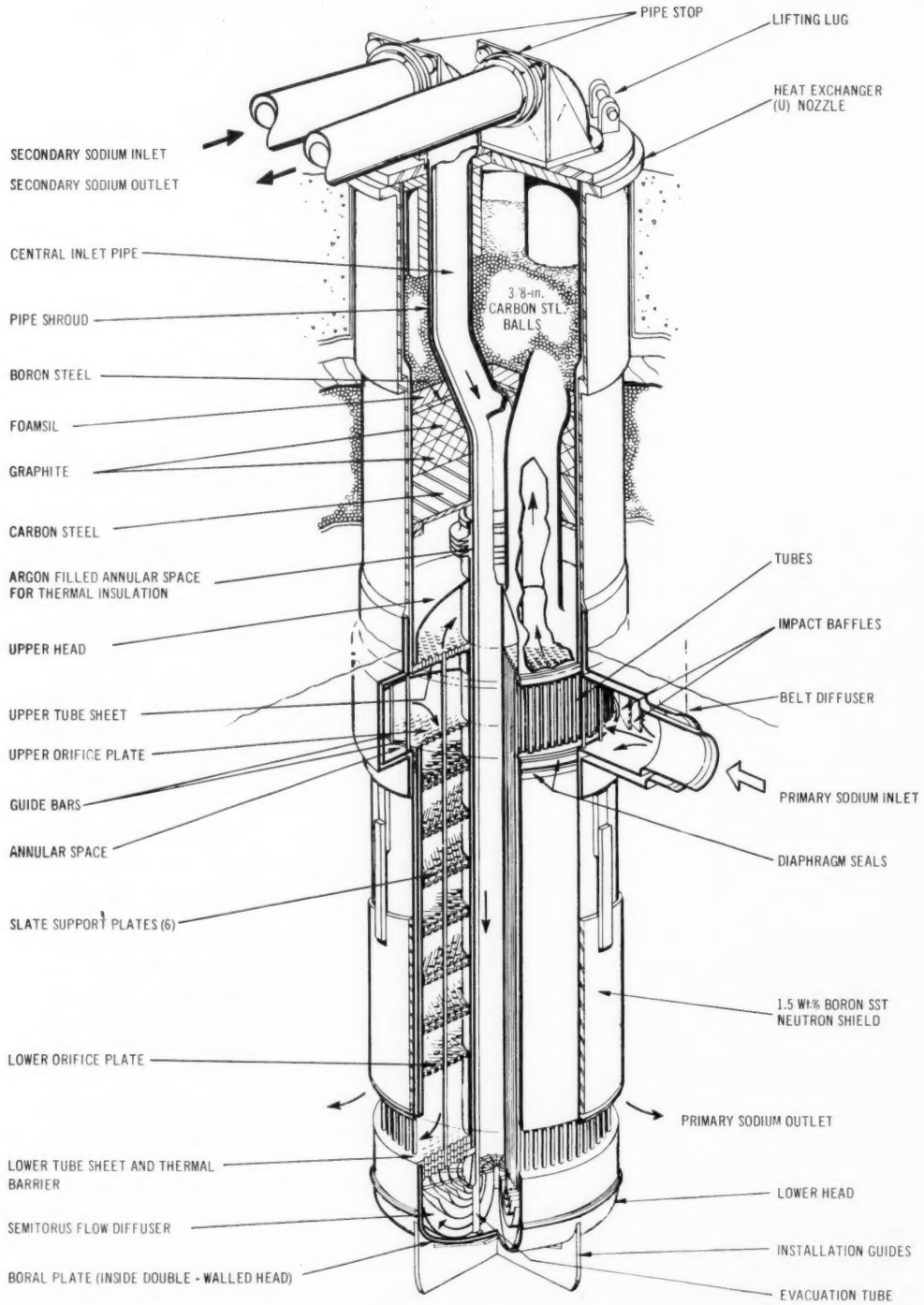

Fig. 6 Intermediate heat exchanger.

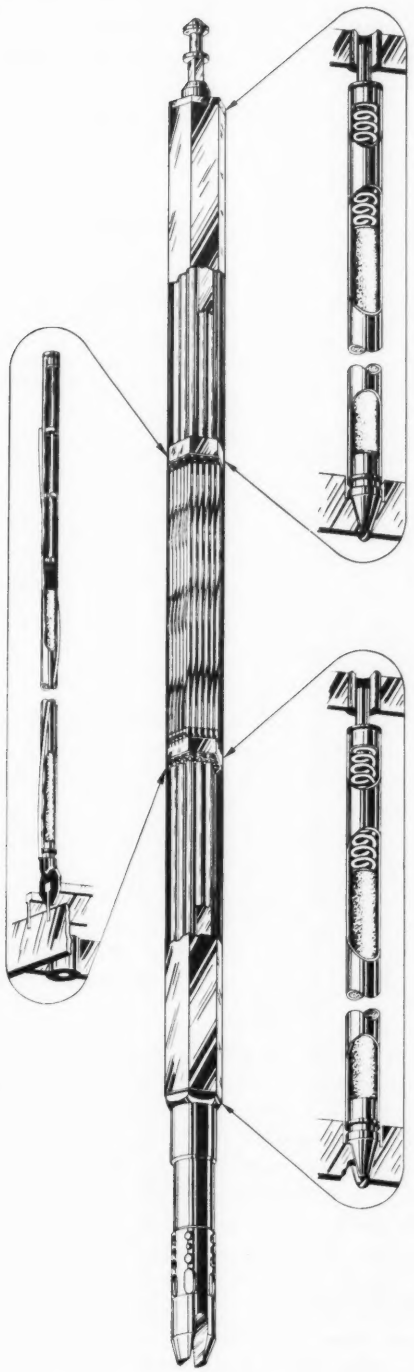

Fig. 7 The EBR-II fuel subassembly.

the EBR-I. This was accomplished by the use of spacer buttons on each subassembly placed at the approximate midplane of the core (Fig. 10). The nominal spacing of subassemblies is 2.320 in.; this provides a nominal 0.030-in. clearance between the subassemblies, which are 2.290 in. across flats. At isothermal conditions the nominal clearance between the 0.014-in.-high buttons is 0.002 in. At power, this clearance is taken up by thermal expansion of the hexagonal tube due to the temperature rise in the coolant to the button elevation. As a result, there is nominal metal-to-metal contact between subassemblies at the buttons to minimize inward bowing. The EBR-II power-coefficient measurements[3] were consistent with predictions,[4] including the bowing coefficient permitted by the small clearances at the grid support and spacer buttons and the relatively large clearances at the top of the subassemblies.

At the time the EBR-II was designed, fast-neutron irradiation-induced swelling in stainless steel had not been discovered (or produced to a measurable extent). A nominal clearance of 0.030 in. was provided between subassemblies (except at the spacer buttons) to accommodate some distortion and still permit fuel handling. Experience has shown that this clearance will accommodate a significant amount of stainless-steel swelling, probably at least in part because irradiation-induced creep tends to partially offset the swelling.

Figure 11 shows an experimental subassembly after a fuel burnup of ~ 100,000 MWd/ton and exposure to a fast-neutron fluence of $\sim 8 \times 10^{22}$. As can be seen, the subassembly expanded to the extent that significant scoring occurred during fuel handling. Also, note that the spacer button has taken a permanent set in a compressed configuration. This is a typical pattern for highly irradiated subassemblies and thimbles in the EBR-II. The buttons have compressed their full 0.014-in. height flush with the subassembly wall, and the hexagonal cans have expanded up to 0.050 in. across flats. Although a considerably better understanding is needed of both irradiation-induced swelling and irradiation-induced creep, the EBR-II experience demonstrates, at least qualitatively, that these phenomena can be accommodated to a considerable extent. As will be described later, the EBR-II fuel-handling system contributes significantly to this capability to accommodate stainless-steel swelling.

FUEL HANDLING

The design of the EBR-II fuel-handling system was determined largely by the requirements resulting from

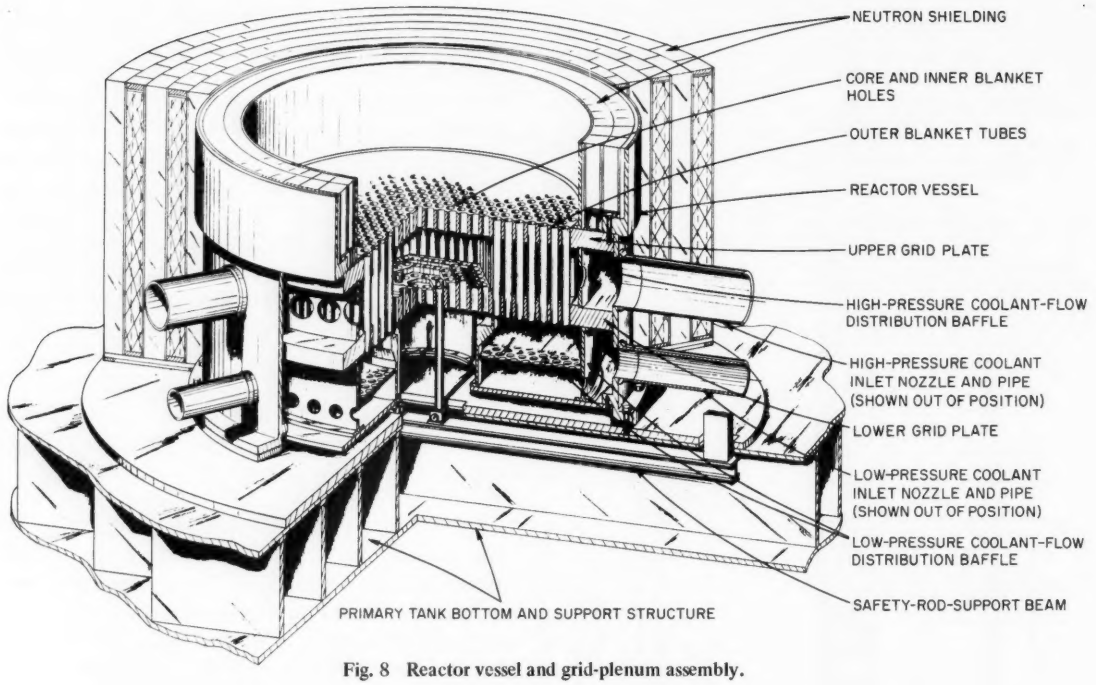

Fig. 8 Reactor vessel and grid-plenum assembly.

the following basic assumptions relative to LMFBR fuel cycles:

1. The high burnup rate would result in a relatively short fuel-residence time in the reactor.

2. The desirability of partial core reloading coupled with short fuel-residence time in the reactor would require frequent refueling shutdowns.

3. Since achievable burnup in (water-cooled) power reactors at that time was (conservatively) estimated to be between 5000 and 10,000 MWd/ton, fast reactor refueling systems should be based on an assumed burnup of not more than 10,000 to 20,000 MWd/ton.

Fuel handling is a critical function in an LMFBR power station because

1. It involves complex mechanical operations performed in high-temperature sodium.

2. The operation must be performed blind under sodium, and the equipment must be capable of handling distorted core components.

3. Fission-product decay-heat removal requires a very high degree of reliability of cooling.

4. The economics of the fuel cycle demand that the fuel-handling operations be performed with minimum reduction of plant availability.

The EBR-II fuel-handling design criteria were based on the assumption that the plant would be shut down every few weeks for a partial refueling. It was assumed that such a fuel-handling schedule would be acceptable only if such partial reloadings could be accomplished quickly to minimize reactor shutdown in a power system. As a result, a "quick-frequent" fuel-handling system was developed to conform to on-site fuel-processing requirements and to exploit the characteristics of the pool concept. Many of the design features are applicable to large commercial LMFBR power stations and are being adopted for the next-generation plants.

The EBR-II fuel-handling system (Fig. 12) employs two basic steps. The first consists in a transfer of subassemblies between the reactor and the storage basket with the reactor shut down. The second consists in a transfer of subassemblies between the storage basket and the Fuel-Cycle Facility via the interbuilding coffin (or to a shipping facility) while the reactor is operating. The first step (called "unrestricted" fuel handling) is performed quickly to minimize reactor shutdown time and is accomplished by preloading the storage basket with the required new subassemblies. Also, since these operations are performed with the subassembly entirely submerged in sodium, they can be performed immediately after reactor shutdown with completely reliable fission-product decay-heat removal.

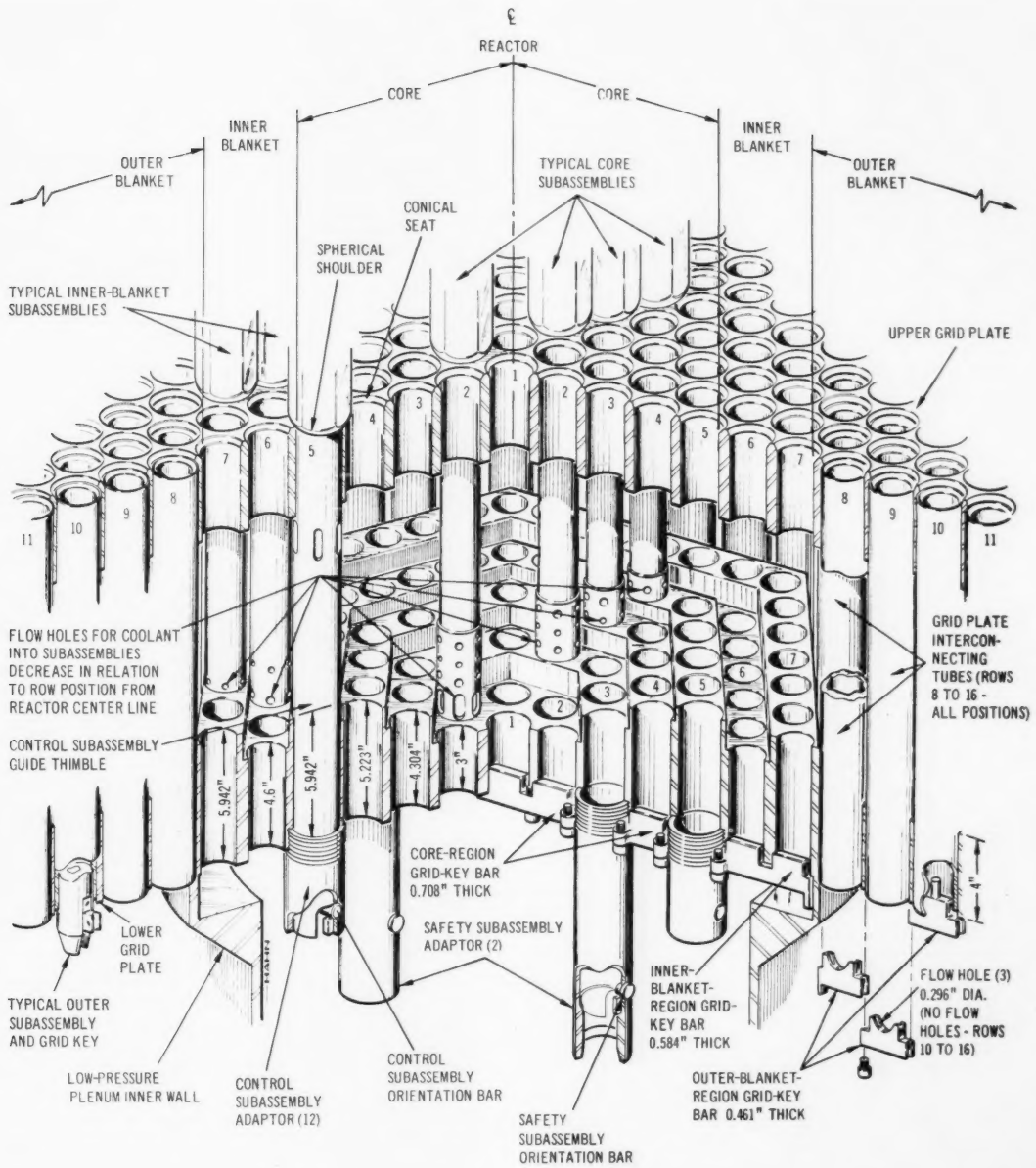

Fig. 9 Bottom view of grid-plenum assembly.

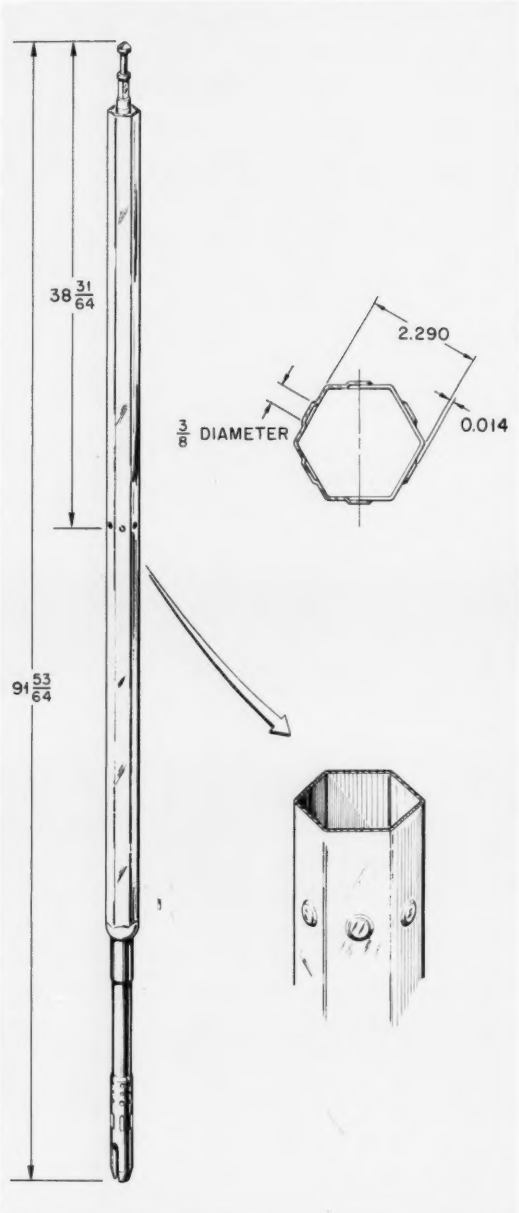

Fig. 10 The EBR-II subassembly–spacer button details.

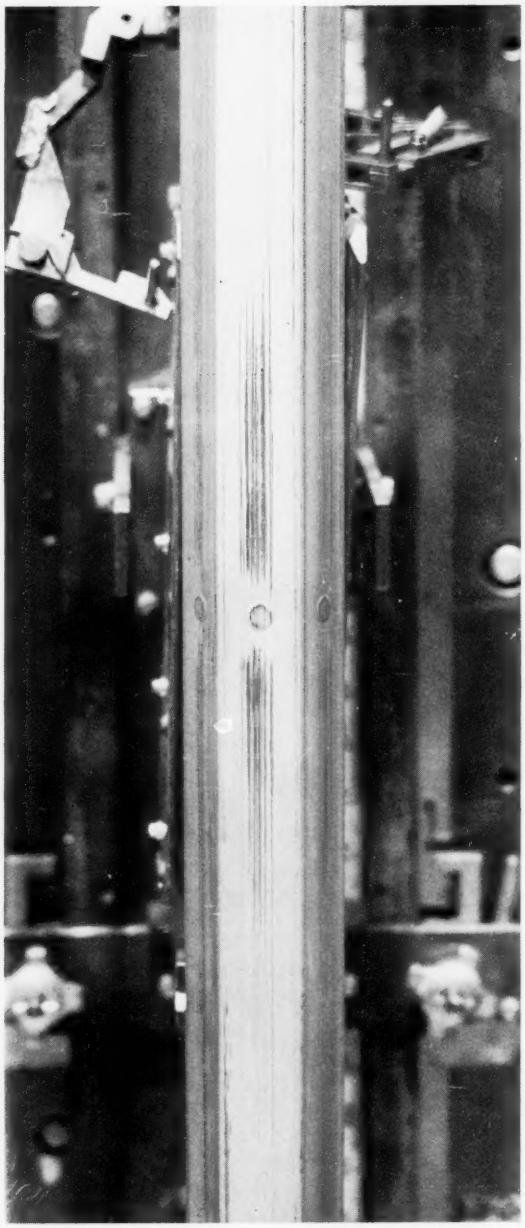

Fig. 11 High-burnup subassembly.

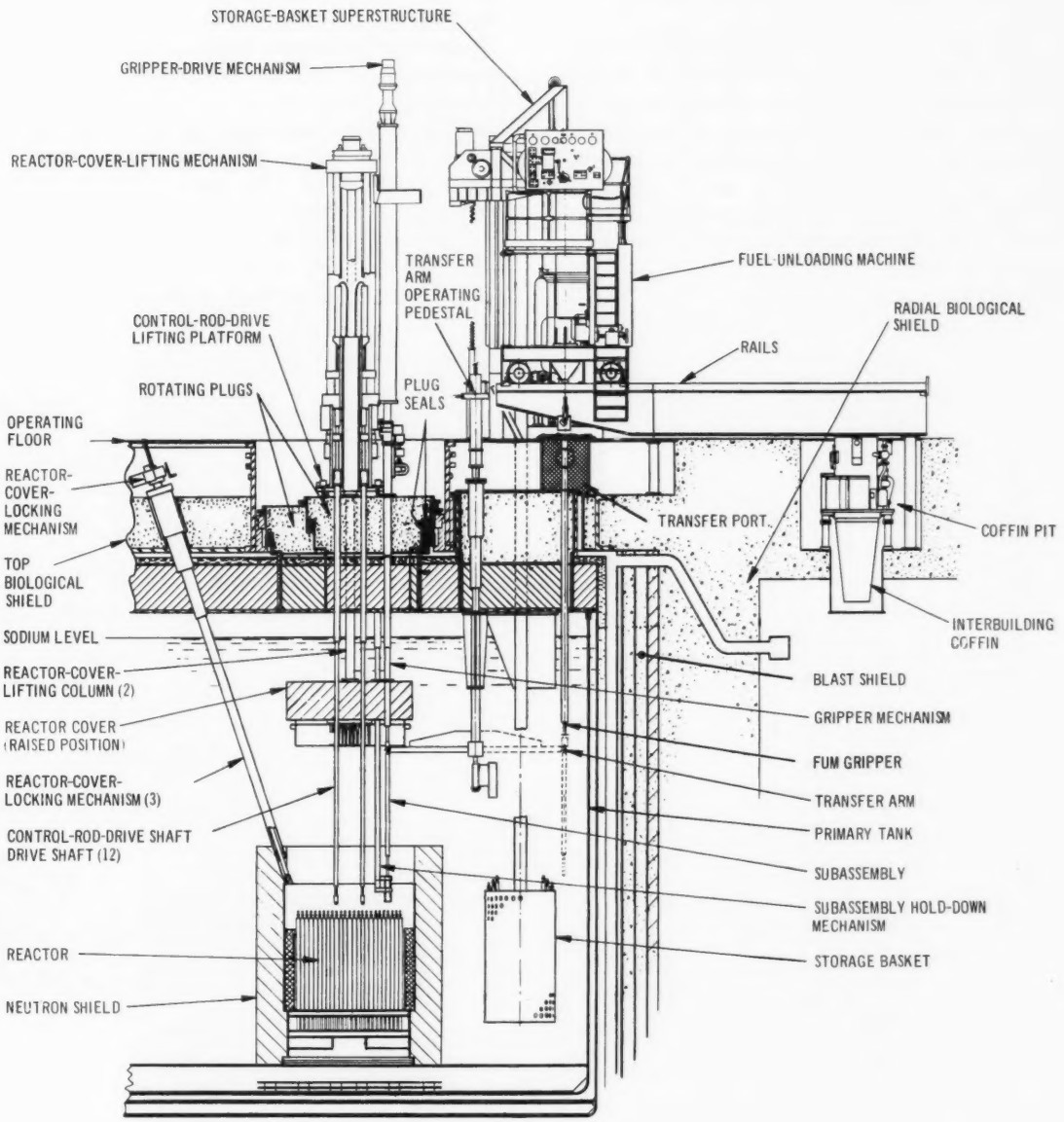

Fig. 12 The EBR-II fuel-handling system.

The design basis for unrestricted fuel handling was to accomplish partial reactor loading (about 25% of the core) in less than 2 days to correspond with periods of low power demand such as would occur over a weekend.

Although the EBR-II refueling schedules are established primarily by the requirements of the experimental irradiation program, the refueling shutdowns have been characteristically short, and the feasibility of weekend-type refueling has been demonstrated many times. Almost 5000 subassembly transfers have been made between the reactor and storage basket, which is several times the number that would have been required to support power operation only. Many of these transfers involved rearrangement of the core to accommodate experimental irradiation subassemblies or to relocate these subassemblies.

These subassembly transfers have included low burnup and high burnup fuels, control- and safety-rod thimbles, and a variety of experimental irradiations. The fuel-handling system has been capable of accommodating all the swelling and distortion that have occurred. This capability is undoubtedly due in large measure to the hold-down tube (Fig. 13), which spreads the six surrounding subassemblies ~ 0.060 in. on the diameter and holds them in place while the gripper removes a subassembly.

The second step (called "restricted" fuel handling) involves the removal of the subassembly from the primary tank and therefore a change in (cooling)

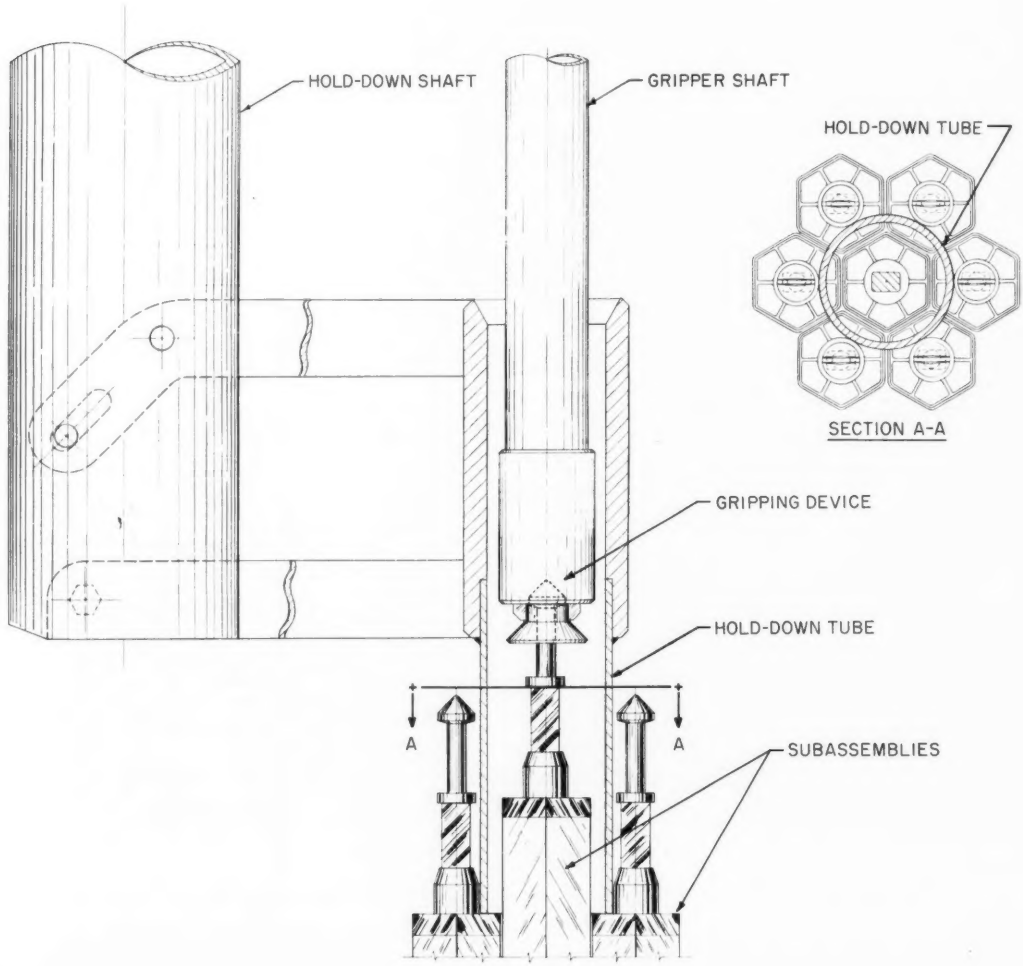

Fig. 13 Subassembly hold-down and gripper.

environment. In the EBR-II this involves a change from sodium cooling to argon-gas cooling and the transition occurs in the fuel-unloading machine. These transfers can be scheduled when the fission-product decay-heat rate has decreased to more manageable levels. The nominal cooling period in the EBR-II is 15 days, but this can be tailored to the processing or shipping schedule. Figure 14 shows the configuration of the reactor plant during restricted fuel handling and the path of the interbuilding coffin through the equipment air lock to the Fuel-Cycle Facility. Reactor building containment is maintained, and the reactor may remain in operation during fuel transport. More than 2000 such transfers have been made in EBR-II, again reflecting the added load imposed by the irradiation program.

The EBR-II experience has amply demonstrated that frequent fuel-handling operation involving short shutdowns are entirely feasible and that plant unavailability for fuel handling can be scheduled for periods of low power demand—periods as short as those which normally occur on weekends. The United Kingdom is planning to operate its PFR on such a schedule, and the PFR design incorporates a quick-frequent fuel-handling system that will permit fuel handling to be performed on weekends.

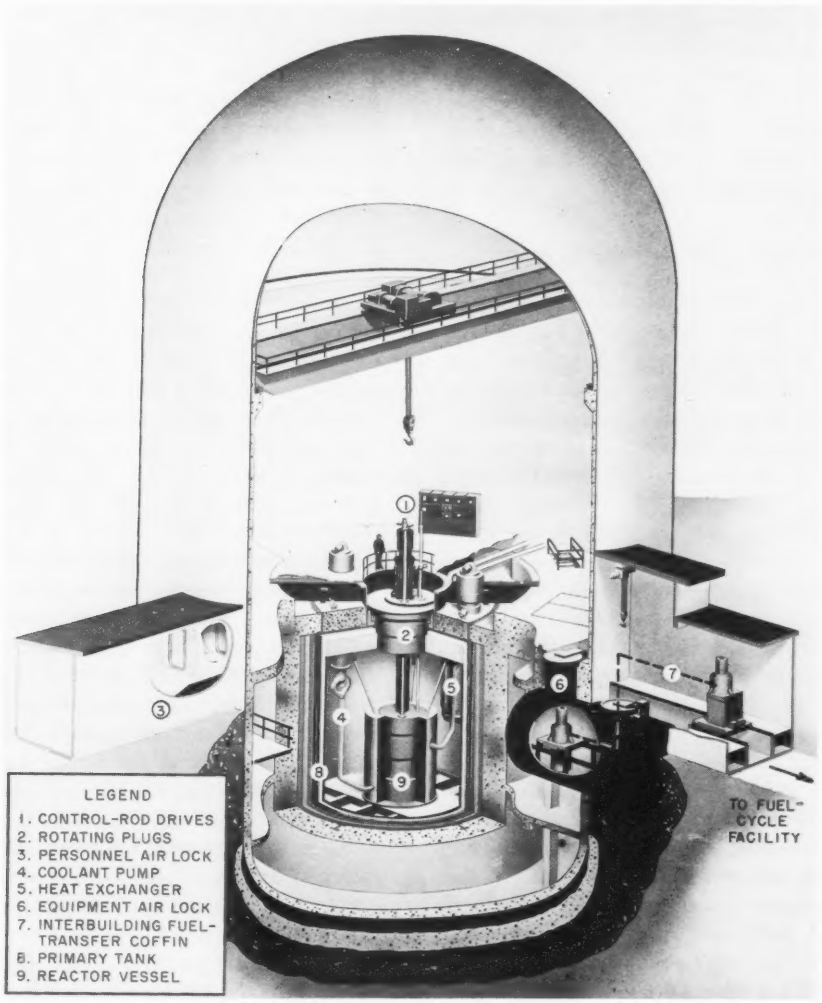

Fig. 14 Reactor plant–interbuilding fuel transfer.

Note that the low-burnup assumption that strongly influenced the EBR-II fuel-handling design is no longer valid. It is well established that fuel burnup of 50,000 to 100,000 MWd/ton is achievable and shutdown for fuel handling can be scheduled less frequently. This makes it feasible to consider other fuel-handling systems,[5] such as the hot-cell type that requires a significant change from the operating conditions and configuration to effect fuel handling. Reactor shutdown of probably at least a week will be required for even a partial reloading, and the refueling schedules and duration could tend to be more comparable to light-water-cooled power reactors. However, even with higher burnup fuel, the EBR-II type of quick-frequent fuel-handling system has many advantages. More frequent reloading or core-loading rearrangement to optimize fuel burnup is possible. Also permitted is such special operation as periodic rotation of subassemblies 180°, and this rotation will produce more uniform neutron exposure across the subassembly, will minimize differential stainless-steel or fuel swelling, and will thereby minimize warpage or distortion.

THE SECONDARY AND STEAM SYSTEMS

The operating conditions for the primary, secondary, and steam systems are shown in Fig. 15. The secondary sodium system and the steam system were conservatively designed to achieve maximum reliability and, in particular, to minimize the possibility of failure of the steam generator. This sodium-to-water/steam heat exchanger is one of the most critical components in the LMFBR.

A primary requirement of the EBR-II design was to achieve reliable operation of the steam generator because no alternate "heat sink" was provided for the power generated by the reactor. (Provisions were made to accept full-power delivery of superheated steam to the condenser and thereby operate the reactor at power without operation of the turbine generator, but this option requires that the steam system be operable.) Several relatively conservative design features were incorporated into the plant to satisfy this requirement. The flow sheet shows how the No. 4 feedwater heater utilizes superheated-steam extraction to heat the feedwater to 550°F (~30°F below the saturation temperature) to minimize the possibility of thermal shock to the system. Separate evaporators and superheaters are used in a natural-circulation system with a drum. The individual evaporator and superheater units are of shell-and-tube design with double tubes and double tube sheets.

Details of an evaporator assembly are shown in Fig. 16. The superheaters are essentially identical, except that a "core tube" is included inside each tube to reduce the cross-sectional area of the tube to increase the steam velocity in the resulting $\frac{1}{8}$-in. annulus.

The steam generators and the secondary sodium system were designed to favor the water/steam side of the system. Chloride stress corrosion was of major concern, and the evaporators and superheaters were arranged to avoid all crevices in the water side—the crevices were placed on the sodium side. The steel used for the steam system was $2\frac{1}{4}$ chrome–1 moly because of its superior chloride stress-corrosion resistance as compared to 304 stainless steel, which was preferred for the sodium systems. As a result, the primary sodium system is all 304 stainless steel, including the intermediate heat exchanger; the steam system is all chrome–moly steel, including the steam generator; and the secondary sodium system is a mixture of the two. Experience with these materials has been excellent and is applicable to large LMFBRs (with appropriate consideration of operating temperatures).

The EBR-II was designed to operate without valves in the main primary and secondary sodium systems because very little experience was available with large sodium valves. This resulted in the use of an a-c electromagnetic pump in the secondary system to achieve the necessary fine flow control directly with the pump and without flow-control valves. Note that flow rate in the primary system is not critical (provided, of course, that it is high enough for the power level) and normally is set at the full-power flow level for all significant reactor power levels. The secondary flow rate, however, must match the power level in the reactor to maintain the systems in balance. (The bulk sodium in the primary tank will change temperature if a mismatch exists.) The EBR-II system design meets these requirements but does so by avoiding the problem of achieving fine flow control with more conventional centrifugal pumps and flow-control valves. In this respect the EBR-II has not provided experience that would apply directly to future commercial LMFBRs.

Also note that the EBR-II does not contain check valves on the two primary pumps, and reverse flow will occur through a pump if it fails during plant operation. The reactor will scram, of course, due to low flow in the affected sodium circuit, and the flow from the operating pump (which will increase because of the reduced pressure drop) will be divided between the reactor and the nonoperating pump circuit. In the

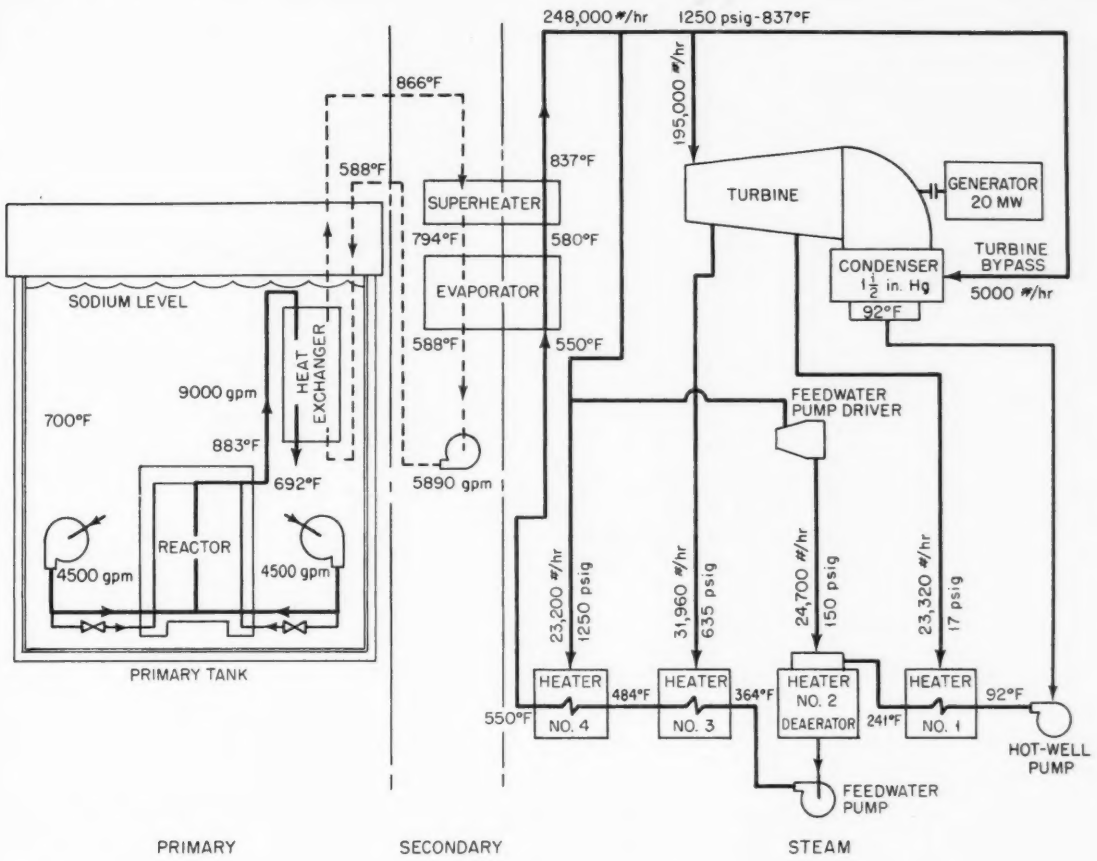

Fig. 15 Simplified flow diagram of EBR-II.

pool-type system, this reverse flow returns to the pool and causes no difficulty. In the loop-type system, such reverse flow would pass through the heat exchanger and hot-leg piping and cause rapid temperature changes. Loop-type systems incorporate check valves to avoid such an ocurrence.

The EBR-II design incorporates both resistance heating and 60-cycle induction heating to provide trace heating on sodium pipes and tanks. All these systems (including the outdoor piping) operate well and demonstrate that the reactor designer has considerable lattitude in the design of these systems (including primary sodium piping for loop-type reactors).

SHUTDOWN COOLING

Although the EBR-II was designed to satisfy the requirements for power production, the system posture at shutdown actually controlled many of the design details. A primary design criterion was to ensure that fission-product decay heat would be reliably removed from the fuel under all conceivable circumstances. The pool concept provided an optimum starting point by reducing the probability of loss of coolant to essentially zero. Shutdown cooling of the EBR-II, therefore, begins with assurance that the primary tank contains sodium.

Shutdown cooling of the EBR-II can be divided into two phases: (1) transfer of the fission-product decay heat in the fuel to the primary sodium and (2) removal of the heat from the primary sodium.

Heat removal from the fuel is accomplished by forced convection and natural convection. On normal shutdown of the reactor, either slow or scram, the main primary sodium pumps continue to operate. This flow is augmented by the auxiliary pump (Fig. 17),

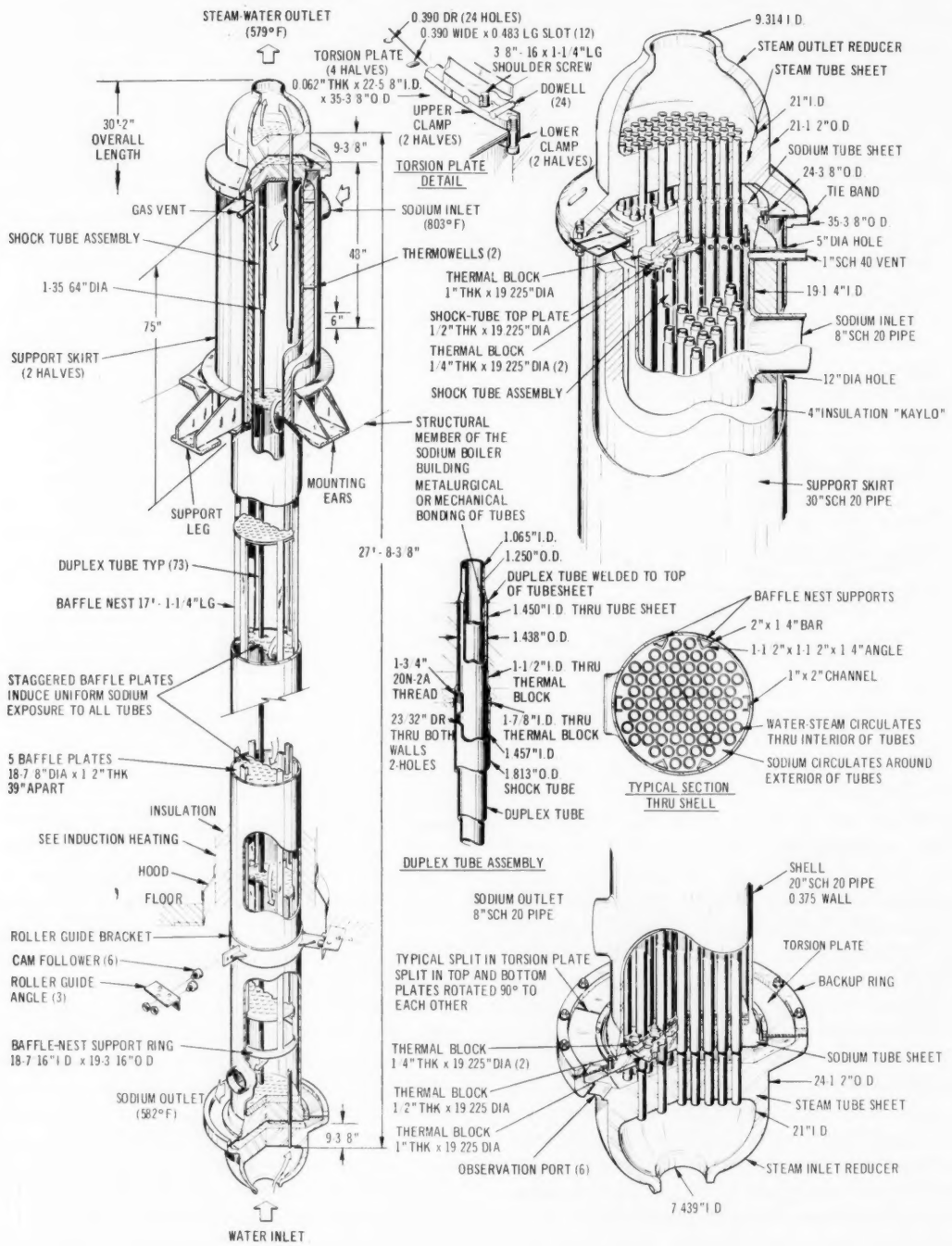

Fig. 16 The EBR-II evaporator unit.

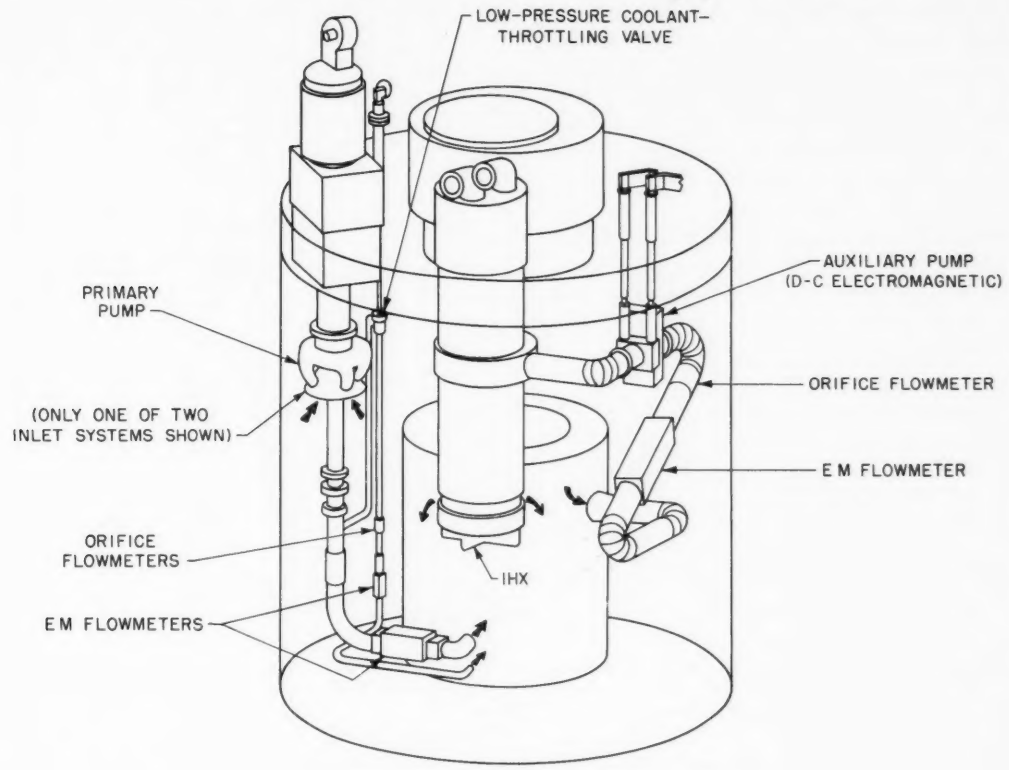

Fig. 17 Primary sodium circuit.

which is always "floating" on the system. This 500 gal/min d-c electromagnetic pump is connected to a rectifier and batteries. In the event of a total power failure, the batteries will supply current for about 30 min. The purpose of the auxiliary pump is to "smooth" the transition from forced convection to natural convection and eliminate the temperature transients (such as those shown in Fig. 18) which can occur under certain combinations of abnormal circumstances.[4] This transition period, if it were to occur, would exist for only a few minutes; therefore the auxiliary pump could easily serve its function under even the worst conditions.

Natural convection will occur very easily if heat is removed from the primary sodium in the intermediate heat exchanger but will also occur if heat is not removed. This was accomplished by positioning the heat exchanger above the reactor; the outlet is $\sim 7\frac{1}{2}$ ft above the horizontal center line of the core, as shown in Fig. 17. Therefore, even with no heat removal in the heat exchanger, thermal driving head in the primary circuit is sufficient to ensure natural circulation through the reactor.

If the heat is not removed from the primary tank, the primary sodium will gradually increase in temperature, as shown in the top curve of Fig. 19. Two shutdown coolers are provided for reliable removal of the heat from the primary sodium entirely by natural convection. Each cooler system consists of a bayonet-type exchanger (Fig. 20) which is immersed in the primary tank and utilizes eutectic NaK as the coolant.

The shutdown cooling systems are arranged as shown in Fig. 21. An NaK-to-air heat exchanger is mounted in a stack immediately outside the containment building. The stack housing is provided with dampers and is well insulated so that very little heat is lost from the system during normal operation. There are no valves in the NaK system, and a small amount of natural circulation occurs continually because of the small heat loss. When the dampers are opened, by either operator action or power failure, natural-air circulation is initiated in the stack, greatly increasing

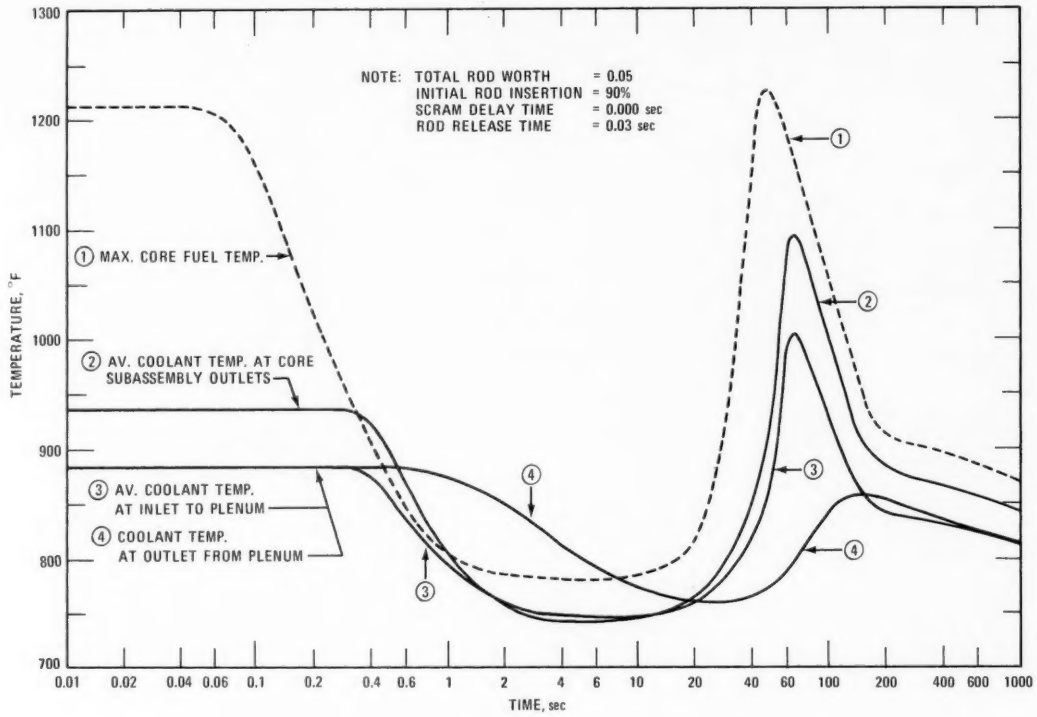

Fig. 18 Fuel and coolant temperature under abnormal shutdown conditions.

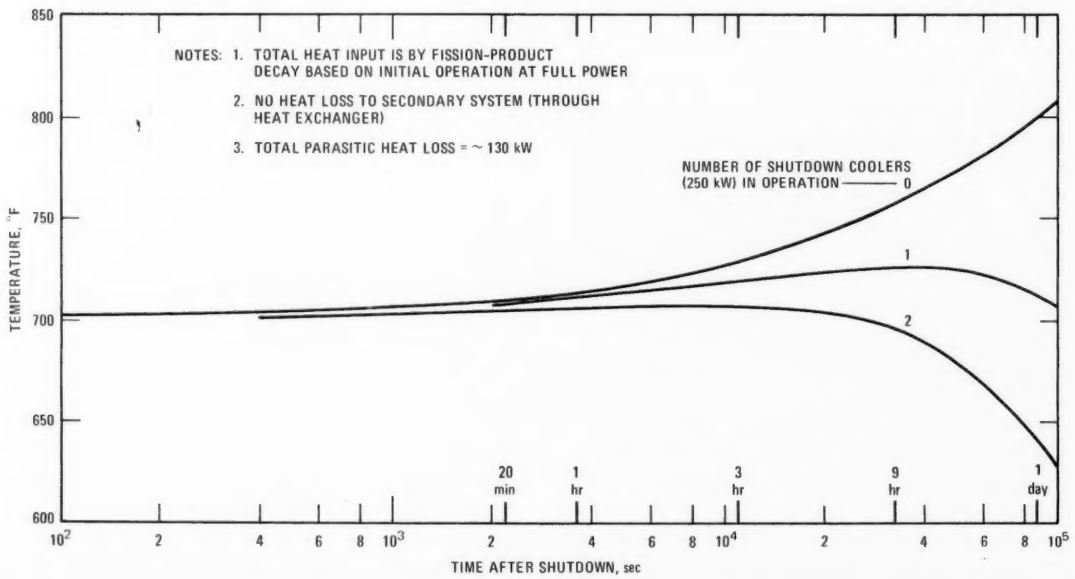

Fig. 19 Primary tank bulk-sodium temperature vs. time after shutdown.

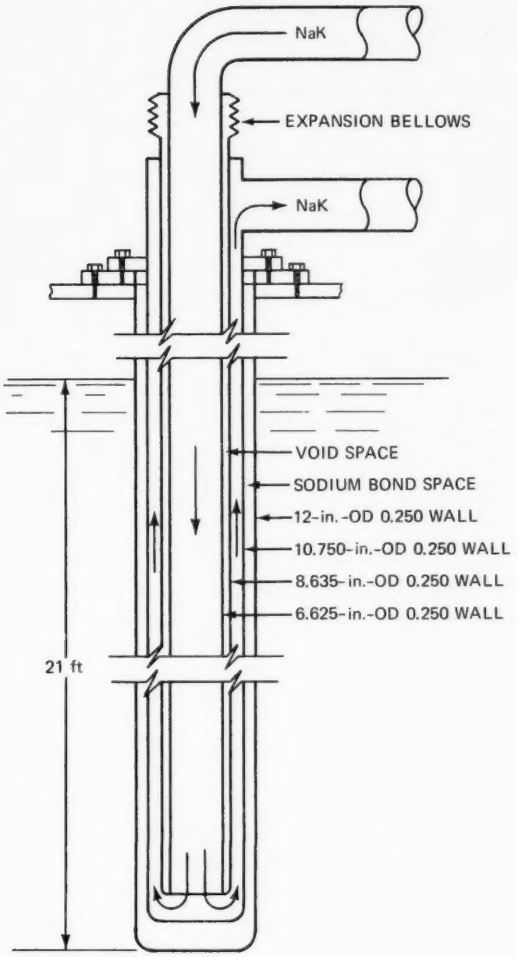

Fig. 20 Shutdown cooler.

heat removal in the heat exchanger and causing increased natural circulation of the NaK. Each shutdown cooler was designed to remove 250 kW of heat, and the effect of this heat removal on the primary tank temperature is shown in Fig. 19 (for both one and two coolers). The primary tank bulk-sodium temperature is maintained within 50°F of normal without auxiliary power of any kind.

Detailed safety studies in the United Kingdom[6] concluded that fission-product decay-heat removal through the normal systems to produce steam from which the heat is then dissipated cannot be accomplished with the reliability demanded by their probability analyses (a frequency of 10^7 reactor-years). These studies conclude that a backup system transferring heat directly to the atmosphere by natural convection potentially is capable of achieving the required reliability. Operating experience with EBR-II has shown the shutdown cooling system to be feasible and practicable as well as reliable (even though it has contributed only 6 years to the 10^7 years statistics). Perhaps more important, a pool-type LMFBR that can operate unattended and without external energy supply can be provided with reliable fission-product decay-heat removal. This may be a unique attribute of this concept.

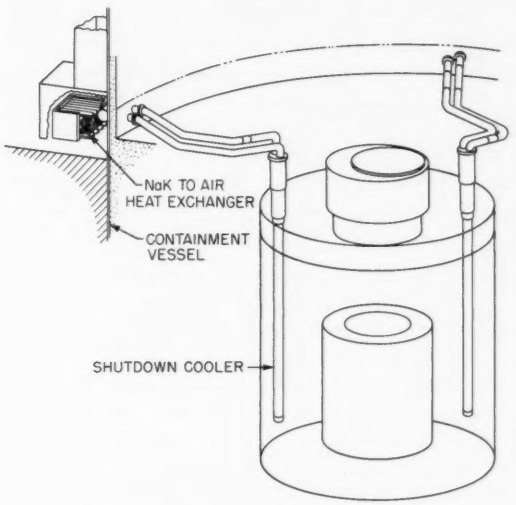

Fig. 21 Shutdown cooling system.

OVERALL PLANT OPERATION

An LMFBR generating station includes a large number of components and systems new to the utility industry. The use of sodium as a high-temperature heat-transfer fluid represents a significant departure from established power-plant practice, and the EBR-II operating experience with sodium systems and components is pertinent to future LMFBR plant operation.

The EBR-II was designed to operate at power levels up to 62.5 MW(t), but, because thermal performance at that power represented such a large extrapolation from existing experience, extensive operation at 45 MW(t) was planned to verify performance and performance margins. Extensive analyses of predicted performance at 45 MW(t)[4] indicated that reliable performance could be achieved at that power level. As a result, the initial approach to power (August 1964) scheduled operations in steps to 45 MW(t). Operation at 50 MW(t) was

authorized in 1968 and at 62.5 MW(t) in 1970. These power increases were carefully scheduled to be compatible with requirements of the experimental irradiation program.

Overall plant operation provides a good measure of the operability of all the plant systems (concurrently) and provides a good measure of the reliability of each. The EBR-II annual power production is shown in Table 3 and provides a convenient indication of overall plant operations. It should be emphasized that the plant factor shown is based on the most conservative method of computation, and no allowance is made for the loss of power operation necessitated by the experimental irradiation program and supporting activities. Also, the EBR-II generates electricity virtually all the time the reactor operates at significant power levels. (Note: The thermal efficiency varies slightly, depending on power level and mode of operation, i.e., amount of steam bypass and steam-turbine-driven vs. electric-motor-driven boiler feed pump, but 30% is a representative average.)

In 1967, two problems resulted in prolonged shutdowns and low plant factor because sufficient information was not available to solve the problems. The first involved copper corrosion of two bus bars in the primary sodium system and consequent uncertainty as to the disposition of the copper in the system. Few data were available relative to the behavior of copper in sodium, and it was necessary to develop such information. It was subsequently concluded that the copper probably had deposited in the cold trap because of the temperature dependence of copper solubility in sodium. The second problem involved a change in power coefficient which followed the substitution of stainless steel for depleted uranium in part of the radial blanket (to improve reflector characteristics and experimental irradiation capability). The change was found to have caused a change in radial temperature distribution and resultant bowing of core subassemblies. The physical changes were estimated to be very small, but final verification that the partial stainless-steel blanket had caused the change in power coefficients could only be provided by returning to an all-uranium blanket. Both these problems resulted in significant reactor shutdowns while various hypotheses to explain the observed conditions were evaluated.

Table 3 EBR-II Annual Power Production

Year	Authorized power level, MW(t)	MWd(t)	Plant factor* (thermal), %	MWh(e)	Plant factor† (electric), %
1964	45	705		3,480	
1965	45	4,345	26	29,532	94
1966	45	7,195	43	44,311	86
1967	45	3,296	19	19,348	82
1968	45, 50	7,162	42	47,913	93
1969	50	7,800	43	51,291	91
1970	50, 62.5	11,313	58	69,177	85

$$*\text{Plant factor (thermal)} = \frac{\text{MWd of power produced}}{\text{authorized power level (MW)} \times 365}$$

$$\dagger\text{Plant factor (electric)} = \frac{\text{MWh of electricity produced}}{\text{thermal power} \times 30\% \text{ thermal eff.}}$$

All the original systems and components are still in operation. Problems have been encountered and corrected. Improvements have been made, but the basic plant remains essentially unchanged. A brief summary of experience with major systems and components follows.

Primary Sodium System

The two primary sodium pumps have performed satisfactorily since the modified shafts and labyrinth seals were installed in February 1964. Through 1970, each pump had operated ~32,000 hr—most of this operation at full-power design conditions of ~4500 gal/min at 50 psi. The scheduled inspection and maintenance in late 1970 was relatively routine, and no significant difficulties were encountered or deficiencies found in the pump.

Secondary Sodium System

The linear a-c electromagnetic sodium-pump duct developed small cracks that were ascribed to vibration induced by reduced pressure in the duct due to pressure drop in the inlet transition section of the

pump. The cracks were repaired by welding small "patches" into the duct wall, and the adverse pressure differential was corrected by operating the pump casing at reduced pressure. This operation resulted in a net positive internal pressure in the duct, tending to force the duct out against the pump stator and eliminating the potential for vibration in the thin duct. The pump has performed satisfactorily since this correction was made in June 1964. (A new pump of improved design was procured and is available on standby if the original pump again experiences difficulty.)

Steam System

In February 1965 a very small steam leak to the atmosphere occurred at a weld of an upper tube to a steam tube sheet. The steam outlet pipe was removed at the steam outlet reducer (see upper right-hand view of Fig. 16), and the leak was repaired in place. This leak, apparently due to a small inclusion in the weld, is the only leak that has occurred in these units. The units have performed extremely well in all respects and in accordance with design.

Reactor Components

Very early in the operating program (October 1964) a linear ball bearing in an experimental oscillator-rod drive failed, and some of the loose balls caused jamming of the two adjacent control rods and drives. It was necessary to remove the two control drives for repair and to replace the oscillator drive. This was an extremely difficult repair operation because the control rods had jammed in their thimbles, and special procedures were required to remove them. This was perhaps the most difficult correction encountered and resulted in the reactor being shut down for almost 4½ months. Although some of the balls from the failed bearing were not retrieved, no additional difficulties have arisen due to this failure.

Control- and safety-rod thimbles have been replaced utilizing the fuel-handling system and the special tools designed for this purpose. Stainless-steel swelling has proved to be the determining consideration for scheduling thimble replacement when adjacent subassemblies become difficult to remove.

Fuel Handling

As described previously, the EBR-II fuel-handling system probably has performed more operations than would be required to support operation of the reactor for its normal lifetime as a power plant. Some difficulties have been encountered with the mechanisms, but they have been repairable without significant difficulty. Improvements have been made to the force-limiting drives and to the position-indication systems to minimize the probability of maloperation.

The most difficult repair involved the transfer arm (Fig. 12), which required removal in February 1966 to repair an improperly welded bell crank in the locking-pin linkage. The shape of this unit required removal of a relatively large shield plug (with the arm attached). The inert-gas-filled plastic-bag technique was used to remove the arm and plug to avoid contaminating the primary sodium. This method of removal proved to be very satisfactory and considerably easier than the caisson system used for removing the primary pumps. The entire operation was completed in less than 3 weeks, and the unit has operated satisfactorily since that time. The plug-in capability of this unit was very adequately demonstrated.

A rather persistent sticking problem with the gripper unit in the fuel-unloading machine (FUM) can best be categorized as a "nuisance problem." The gripper operates in sodium (in the primary tank) and in argon gas (in the FUM); it must make the transition between these two environments each time a subassembly is transferred. Sodium oxide buildup occurs, and the gripper must be cleaned to remove this buildup. A new gripper, designed with increased clearances between the moving parts, has operated much better and requires cleaning much less frequently. Since the FUM is used for "restricted fuel handling," normally performed with the reactor operating, this problem has had very little effect on reactor operation.

A second sticking problem arose with the rotating plugs which was caused by oxidation of the Sn–Bi molten-metal seal. Oxide accumulation in the seal trough can hinder plug rotation. This can be avoided by a regularly scheduled program of oxide removal. Since this operation can only be performed with the reactor shut down to permit plug rotation, it must be carefully scheduled to minimize reactor downtime.

The overall experience with the fuel-handling system has been excellent; the system has proved to be extremely versatile as well as reliable and has performed a greater variety and number of operations than originally intended.

CONCLUSIONS

The EBR-II was designed as an experimental LMFBR power plant but has been used primarily as an

experimental irradiation facility for LMFBR fuels and structural materials. It has been extremely effective as an irradiation facility—more than 1400 experimental fuel elements and samples have been irradiated (including more than 900 oxide and 100 carbide elements); it has become relatively routine to have 30 to 40 experimental subassemblies in the reactor at one time with as much as 10 to 15% of the power being generated in the experimental fuel elements. The EBR-II has also operated very effectively as an LMFBR generating station—more than 250 million kWh of electricity have been produced.

A variety of problems have arisen during the EBR-II operation, but it is important to note that

1. The major problems occurred during the early phases of operation; in fact, several occurred during preoperational testing.

2. All these major problems were solvable and were corrected the first time. The original solution was satisfactory and provided a "permanent fix."

Many potential problems remain which cannot be solved directly by the EBR-II. The most important probably are those which relate to much larger size plants and higher temperature systems. A third category might include potential problems related to systems or concepts that are basically different and where the EBR-II experience is not directly relevant (for example, the hot-cell-type reactor refueling system).

Two factors should be considered in evaluating such potential future problems:

1. The experience to date with design of large plants and the construction of demonstration-size plants in Europe have not identified any basic problems that have discouraged the designers of pool-type LMFBRs. The British have said:[2] "No information has arisen either in the PFR design process or during its construction to lead us to change from the single tank concept for the first 1300-MW(e) commercial reactor." [The schedule for this 1300-MW(e) LMFBR calls for construction to begin early in 1974.] The French state:[7] "No important difficulty due to the choice of a pool reactor was found during the design and construction of Phenix, and the same choice will be made for the next reactor." [They plan to begin construction of a 1000-MW(e) pool-type reactor in 1974.]

2. Experience with the EBR-II suggests that the early commercial plants (prototypes and full-size plants) should be able to accommodate a reasonable amount of experimentation and still achieve reliable performance as generating stations. This indicates that some allowance should be made for self-improvement or "bootstrapping" in these early plants.

A major consideration related to the adoption of commercial LMFBR power stations involves economics, the overall economic feasibility of the LMFBR system, and the comparative economics of the various options within the system. The EBR-II can contribute to establishing "economic feasibility" of the system or specific options only to the extent that it demonstrates that the system is amenable to normal engineering development and the problems encountered can be solved by normal engineering methods. The EBR-II has demonstrated this degree of "technical feasibility," even where first-of-a-kind engineering was required. Experience with the EBR-II also affirms that LMFBR technology is complex and difficult. The EBR-II probably represents another level of technical sophistication for the utility industry in its progression from fossil-fueled plants to thermal reactors to LMFBRs. Furthermore, the EBR-II experience provides a basis for confidence that such a level of sophistication can be achieved by the industry.

REFERENCES

1. R. W. Seidensticker, Design, Analysis, and Construction of EBR-II Primary Tank and Associated Structures, USAEC Report ANL-6922, Argonne National Laboratory, September 1970.
2. R. H. Campbell, Current Status of the British Fast Reactor Construction Programme, presented at ASME Conference on Fast Reactors, Palo Alto, Calif. March 8–10, 1971.
3. H. O. Monson, EBR-II Initial Operation—Highlights, British Nuclear Energy Society Conference on Fast Breeder Reactors Vol. 103, pp. 135–152, May 1966.
4. L. J. Koch et al., Hazard Summary Report, Experimental Breeder Reactor-II (EBR-II), USAEC Report ANL-5719, May 1957; also, Addendum to Hazard Summary Report, Experimental Breeder Reactor-II (EBR-II), USAEC Report ANL-5719(Addendum), June 1962.
5. L. J. Koch, Fast Reactor Fuel Handling, USAEC Report ANS-100, pp. 333–347, American Nuclear Society, April 1965.
6. F. R. Farmer et al., An Appreciation of Fast Reactor Safety, USAEC file No. NP-18487, pp. C. 7. 1–8, 1970.
7. Y. G. Adda, J. P. Crette, B. Geffroy, and J. R. Leduc, Phenix Design and Preliminary Studies on 1000-MW(e) Fast Reactor, presented at ASME Conference on Fast Reactors, Palo Alto, Calif., March 8–10, 1971.

BIBLIOGRAPHY

A. H. Barnes et al., The Engineering Design of EBR-II, A Prototype Fast Neutron Reactor Power Plant, *in Proceedings of the International Conference on the Peaceful Uses of Atomic Energy, Geneva, 1955,* Vol. 3, pp. 330–344, United Nations, New York, 1956.

L. J. Koch et al., Construction Design of EBR-II: An Integrated Unmoderated Nuclear Power Plant, in *Proceedings of the Second International Conference on the Peaceful Uses of Atomic Energy, Geneva, 1958,* Vol. 9, pp. 323–347, United Nations, New York, 1958.

T. R. Bump and H. O. Monson, Predicted Dynamic Behavior of EBR-II, in *Proceedings of the Second International Conference on the Peaceful Uses of Atomic Energy, Geneva, 1958,* Vol. 11, pp. 404–419, United Nations, New York, 1958.

H. O. Monson and M. M. Sluyer, Containment of EBR-II, in *Proceedings of the Second International Conference on the Peaceful Uses of Atomic Energy, Geneva, 1958,* Vol. 11, pp. 124–138, United Nations, New York, 1958.

L. J. Koch et al., EBR-II Dry Critical Experiments, USAEC Report ANL-6299, Argonne National Laboratory, February 1961.

W. B. Loewenstein, Physics Design of EBR-II, USAEC Report ANL-6383, Argonne National Laboratory, July 1961.

R. L. McVean et al., EBR-II Dry Critical Experiments, USAEC Report ANL-6462, Argonne National Laboratory, February 1962.

L. J. Koch, Experimental Breeder Reactor No. 2 and Transient Test Reactor Facility, in *Proceedings of Symposium on Sodium Reactors Technology, Lincoln, Nebr., May 24–25, 1961,* USAEC Report TID-7623, pp. 9–32, June 1962.

H. H. Hummel et al., Stability Analysis of EBR-II, USAEC Report ANL-6484, Argonne National Laboratory, January 1962.

L. J. Koch et al., Sodium Cooled Fast Breeder Reactors, in *Proceedings of the Third International Conference on the Peaceful Uses of Atomic Energy, Geneva, 1964,* Vol. 6, pp. 33–44, United Nations, New York, 1965.

F. S. Kirn and W. B. Loewenstein, EBR-II Wet Critical Experiments, USAEC Report ANL-6864, Argonne National Laboratory, October 1964.

M. Novick et al., EBR-I and EBR-II Operating Experience, Report ANS-100, pp. 25–40, American Nuclear Society, April 1965.

M. Novick et al., EBR-II Operating Experience, Report ANS-101, pp. 1–1 to 1–20, American Nuclear Society.

G. E. Deegan et al., Operating Experience with EBR-II, USAEC Report ANL-7520, Part II, pp. 24–38, Argonne National Laboratory, November 1968.

L. J. Koch, System and Component Design for Fast Reactors, presented at the International Conference on Constructive Uses of Atomic Energy, November 10–15, 1968, Washington, D. C., Vol. 11, 343–360; reprinted in *Reactor Technol.,* **13**(1): 36–53 (Winter 1969–1970).

W. E. Ruther, Factors Influencing Dross Formation in the Fusible Seals of the EBR-II Rotating Plugs, USAEC Report ANL-7653, Argonne National Laboratory, January 1970.

J. K. Long and W. R. Wallin, A Documentation of Criticality Data for EBR-II with a Stainless Steel Radial Reflector, USAEC Report ANL-7541, Argonne National Laboratory, April 1970.

A. V. Campise, A Study of the Response of the EBR-II Plant Protective System to Hypothetical Malfunctions in the Reactor System, USAEC Report ANL-7665, Argonne National Laboratory, June 1970.

AEC Critical Review Series

ATMOSPHERIC TRANSPORT PROCESSES, Part 2: Chemical Tracers

Elmar R. Reiter, Colorado State University

January 1971

The use of trace constituents of the atmosphere in estimating the effects of the general circulation has opened into a wide field of research. This book focuses on the large-scale aspects of the atmospheric circulation and on the effect of this circulation on tracer distributions. Future research in this fertile field should produce more cooperation between the chemists, atmospheric dynamicists, and synopticians and thus provide better returns from the intricate and complex experiments necessary in exploring the many aspects of our global atmosphere and of the atmospheres of other planets. (388 pages, 7 x 9¾ inches, Library of Congress Catalog Card Number: 76-603262)

Contents

This book is available for $6.00 as TID-25314 from National Technical Information Service, U. S. Department of Commerce, Springfield, Virginia 22151

Announcing the publication of

Public Safety
& Underground Nuclear Detonations

Samuel Glasstone

June 1971

(6 X 9; 286 pages; 109 illustrations)

Available for $3.00 as TID-25708 from
National Technical Information Service
U. S. Department of Commerce
Springfield, Virginia 22151

The United States program for testing nuclear explosive systems has two main objectives: first, to maintain the nation's security and, second, to develop peaceful applications of nuclear explosives for the benefit of all mankind.

To meet the national objective of developing nuclear explosives for peaceful applications, the Atomic Energy Commission in 1957 established the Plowshare Program. For such applications as stimulating the flow of natural gas and petroleum, mining and quarrying and other earth-moving projects, and cracking high-temperature rocks to utilize their natural geothermal energy, the Plowshare Program will require the design and testing of special nuclear explosives.

This book describes the comprehensive safety program carried out by the Atomic Energy Commission and the methods through which those responsible for ensuring safety in underground nuclear detonations implement their basic philosophy, which has been summarized as follows: A nuclear device can be detonated safely only when it is ascertained that the operation can be accomplished without injury to people and domestic animals, directly or indirectly, and without an unacceptable damage risk to ecological systems and to natural and man-made structures.

Published by the Atomic Energy Commission, the book was prepared through the coordinated effort of government agencies and contractors; the work of many competent scientists in a number of related disciplines is presented.

AEC Symposium Series

neutron standards and flux normalization

Proceedings of a symposium held at Argonne National Laboratory, Argonne, Illinois, October 21–23, 1970

Coordinator: Alan B. Smith, Argonne National Laboratory

August 1971
540 pages, 6 x 9
Library of Congress Catalog Card: 77-611328

This symposium, sponsored by the European–American Nuclear Data Committee, emphasizes the need for precise nuclear quantities of critical importance to nuclear-energy programs, primarily reactor development. The symposium (1) quantitatively assesses the status of the field, (2) defines available precisions, (3) identifies outstanding problems, (4) formulates recommendations, and (5) provides guidance for future work.

The areas covered include

- Neutron and flux standards, rationale and applications
- Light elements, experiment and interpretation
- Fission and capture standards
- Techniques and methods for flux, fluence, and cross-section measurement
- Special topics
- Reports and recommendations of the working groups

Published as No. 23 in the AEC Symposium Series,
this book is available as CONF-701002 for $6.00 from
National Technical Information Service, U. S. Department of Commerce,
Springfield, Virginia 22151

NUCLEAR SCIENCE ABSTRACTS

The U. S. Atomic Energy Commission, Division of Technical Information, publishes *Nuclear Science Abstracts (NSA)*, a semimonthly journal containing abstracts of the literature of nuclear science and engineering.

NSA covers (1) research reports of the U. S. Atomic Energy Commission and its contractors; (2) research reports of government agencies, universities, and industrial research organizations on a worldwide basis; and (3) translations, patents, books, and articles appearing in technical and scientific journals.

Complete indexes covering subject, author, source, and report number are included in each issue. These indexes are cumulated and sold separately.

Availability

SALE *NSA* is available on subscription from the Superintendent of Documents, U. S. Government Printing Office, Washington, D. C. 20402, at $42.00 per year for the semimonthly abstract issues and $38.00 per year for the cumulated-index issues. Subscriptions are postpaid within the United States, Canada, Mexico, and all Central and South American countries, except Argentina, Brazil, Guyana, French Guiana, Surinam, and British Honduras. Subscribers in these Central and South American countries, and in all other countries throughout the world, should remit $52.50 per year for subscriptions to semimonthly abstract issues and $47.50 per year for the cumulated-index issues. The single-copy price for the abstract issues is $1.75 postpaid, with this exception: Add one-fourth of $1.75 for mailing to the countries to which the $52.50 subscription rate applies.

EXCHANGE *NSA* is also available on an exchange basis to universities, research institutions, industrial firms, and publishers of scientific information. Inquiries should be directed to the Division of Technical Information Extension, U. S. Atomic Energy Commission, P. O. Box 62, Oak Ridge, Tennessee 37830.

Subscription Information

Technical Progress Reviews may be purchased from Superintendent of Documents, U.S. Government Printing Office, Washington, D.C. 20402. *Nuclear Safety* at $3.50 per year (six issues) for each subscription or $0.60 per issue; *Reactor Technology* at $3.00 per year (four issues) for each subscription or $0.75 per issue; *Isotopes and Radiation Technology* at $2.50 per year (four issues) or $0.70 per issue.

Postage and Remittance

Postpaid within the United States, Canada, Mexico, and all Central and South American countries except Argentina, Brazil, Guyana, French Guiana, Surinam, and British Honduras. For these Central and South American countries and all other countries: add, for each annual subscription, $1.00 for *Nuclear Safety* and $0.75 for each of the other journals; for single issues, add one-fourth of the single-issue price. Payment should be by check, money order, or document coupons, and MUST accompany order. Remittances from foreign countries should be made by international money order or draft on an American bank payable to the Superintendent of Documents or by UNESCO book coupons.